Cosmological simulations with disformally coupled symmetron fields

Robert Hagala

Thesis submitted for the degree of
Master of Science in Astronomy

Institute of Theoretical Astrophysics
University of Oslo

June, 2015

Abstract

In this thesis, we investigate statistical properties of the redshift zero matter distribution in disformal gravity through N-body simulations. The disformal model studied here is a conformally coupled field in a symmetron potential, but with an additional exponential disformal term. First, important concepts about general relativity, modified gravity, and simulations are presented. The equation of motion for the disformal scalar field is found, along with the modified geodesics of dark matter particles in this model. We implement the resulting differential equations into the N-body code Isis/Ramses. The results of tests, which compare results from the disformal code to simulations done with earlier symmetron-only codes, are shown; and the code reproduces the symmetron results fairly well. Finally, we perform cosmological simulations with 256^3 particles, for five different parameter sets, for which the matter power spectrum and the halo mass function are shown. We also present the average field profile, the field oscillation amplitude, and the magnitude of the fifth forces around a massive halo. The conformally coupled symmetron increases both the power spectrum and the mass function noticeably, compared to ΛCDM. The main result of this study is that adding a strong disformal term can mask some of the increase in clustering, thereby bringing both the power spectrum and the mass function closer to general relativity. Furthermore, we found that the disformal term gives rise to oscillations of the scalar field in high density regions. Such oscillations can lead to increased magnitudes of the fifth forces, compared to the symmetron alone.

Acknowledgements

Thanks to my supervisors **David Mota** and **Claudio Llinares** for their excellent advice, discussions, and feedback. It was exciting to be allowed to be the main author of a paper based on this thesis. Without my supervisors, neither this thesis nor the paper would have existed.

Thanks to **Miguel Zumalacárregui** for valuable input following the publication of the paper.

Many thanks to my parents **Margareta** and **Yngvar**, and my sister **Lillian**. You have been very supportive of my academic ambitions for as long as I can remember.

Also, warm thanks to each of my friends. You helped me muster the willpower to write this thesis by being generally cool, and hanging out with me whenever I was not working.

A special thanks to my girlfriend **Eirin Arnesen**, who did a lot of proofreading. She has also put up with living with me for several years, which is an admirable achievement on its own.

The cosmological simulations were performed on the NOTUR cluster HEXAGON, the computing facilities at the University of Bergen. So thanks to NOTUR, even though their FORTRAN compilers were really strict, and I had to wrestle with the *already working* code and makefile for days before it finally compiled on the cluster.

Contents

Chapter 1

Introduction

1.1 Motivation

The Einstein field equations were first introduced by Albert Einstein in 1915 [1]. These equations are used to calculate how matter curves space, and in turn how the curved space affects matter. In other words, these equations tell exactly how gravity works, and how stars and galaxies should move in the universe. The solutions to these equations implied either an expanding or a collapsing universe. However, at the time the field equations were introduced, the universe was believed to be static, neither collapsing nor expanding. Einstein knew the equations allowed for an additional constant term, so he introduced the *cosmological constant* – simply called Λ – two years later. This was done to achieve a static universe solution to the field equations [2]. Not many years after the introduction of Λ, Edwin Hubble discovered that the universe was in fact expanding [3], and the cosmological constant was largely forgotten.

Knowing that distant galaxies were expanding away from each other, it was logical to assume they had been closer together in the past. Lemaître came to this conclusion already in 1931 [4], but it was not until after the discovery of the cosmic microwave background radiation (CMB) in 1964 [5], that the Big Bang model was universally accepted as the theory for the early universe. In this model, the universe started out in an extremely hot and dense state. Adiabatic expansion cooled the universe, and allowed stars and galaxies to form under gravitational collapse.

In 1998 two separate groups studied distant type Ia supernovae and found the first observational evidence indicating that the universe not only expands, but expands at an accelerating rate. This is consistent with the existence of a cosmological constant Λ [6, 7]. The extra constant term was quickly reintroduced into the Einstein field equations, where it was taken to represent the density of the unknown *dark energy* that is pushing distant galaxies apart from each other.

Cold dark matter is an invisible, pressureless and frictionless form of matter that gives galaxies most of their mass. Dark matter was indirectly postulated in 1933 by Zwicky – he found from galaxy movements that the Coma cluster had a mass around 500 times larger than expected, compared to the amount of visible light it emitted

[8]. Recent measurements suggest that the universe in total contains over five times as much dark matter as normal baryonic matter [9]. The cosmological constant and cold dark matter are the main ingredients in the standard model for cosmology, called ΛCDM. The ΛCDM model seems to fit most modern precision observations of large scale structures and of the cosmic microwave background radiation [10, 11]. However successful in predicting observations, the model does not explain what the source of the dark energy Λ is. Attempts to calculate the energy density from the so-called vacuum energy in particle physics, yields answers of 60 or more orders of magnitude greater than the measured cosmological value of Λ. A cancellation of that many terms by whatever process is very improbable and would require an extreme fine-tuning. This is the *cosmological constant problem*, which is considered a severe issue in modern physics [12].

A viable solution to this problem might be that the particle physics vacuum energy is completely concealed on gravitational scales – for example due to the breaking of supersymmetry [13] – while other mechanisms than the vacuum energy are responsible for the measured cosmic expansion. One way to search for such mechanisms is by slightly modifying the equations for gravity in general relativity in such a way that the equations give rise to dark energy and expansion on large scales. There are innumerable models for modified gravity [14], some of which will be presented in this thesis.

An important property for viable modifications to gravity is that the equations should reduce to standard general relativity on solar system scales. This is needed because general relativity is experimentally tested in the solar system to extremely high precision. Consequently, any modifications to gravitational physics must give similar results within very tight constraints on these scales [15]. Recovery of general relativity in environments similar to the solar system is achieved through so-called *screening mechanisms*. Screening mechanisms usually work by making mathematical terms that are different from standard general relativity insignificant in high density regions, like inside a galaxy [16].

In the last decades, N-body simulations have become increasingly popular tools in cosmology. These are very computationally demanding applications, usually designed to run on supercomputers for several hours, or even days. The purpose of N-body codes is to trace the motion of millions of particles as they interact with each other, mainly through gravity, but any other forces – like friction and radiation pressure – can in theory be implemented. The simulated particles are not necessarily individual particles like atoms, quarks or electrons; In cosmological simulations, the mass of each "particle" is often several millions or billions times the mass of the sun. One example of a well-known cosmological N-body simulation is the Millennium run, which simulated the evolution of over 10 billion particles – each with a mass of a little over a billion suns – in a cube with sides spanning over 2 billion light years [17]. Such simulations generally retrieve large scale structures like galaxy clusters and filaments similar to the ones we observe in large scale surveys, like the Sloan Digital Sky Survey [18]. See figure 1.1 for a visual comparison of the Millennium simulation and the observed galaxy distribution on scales of some billion light years. Even though these simulations give impressive results on large scales, some evidence exists that they fail on sub-galaxy scales, for instance

in the prediction of dwarf galaxies orbiting the Milky Way [19, 20]. A common factor for some of these simulations is that they only include Λ and cold dark matter, but no baryons, neutrinos, or alternative dark energy theories. However, as computing power increases, more and more advanced simulations can be done.

Evidence suggests that one has to investigate and simulate physics beyond ΛCDM to understand the whole picture. Of course, including interacting baryons and other known physics might alleviate some of the problems with ΛCDM simulations [21], but the most daunting question still remains: What is the nature of the two main components of our universe, namely dark energy or dark matter? We will leave to the particle physicists to answer what dark matter is, allowing us to focus on investigating theories for dark energy. This thesis will focus on simply one model of modified gravity that has shown some promise, namely the disformal model. The disformal model has been studied extensively in the linear regime with applications to inflation, dark energy, and dark matter [22, 23, 24, 25, 26, 27, 28, 29, 30, 31, 32, 33, 34, 35, 36, 37, 38]. Still, this model has not been studied well on non-linear scales, which means on the scale of galaxy clusters and smaller. This study aims to begin filling this gap.

This thesis will first introduce the basic astrophysics and numeric computation background needed to understand the rest of the text. Calculations will be carried out to find equations that describe the disformal theory of gravity. Using these equations, we perform N-body simulations by altering the already existing non-static N-body code Isis [39, 40], which in itself is a modification of Ramses [41, 42], extended to simulate scalar field theories. The goal of this thesis is to investigate statistical properties of the simulated matter distribution on galaxy and galaxy cluster scales at redshift zero. In particular, the matter power spectrum and the halo mass function of particles affected by disformal gravity will be presented. These will be compared to the ones from standard ΛCDM simulations. These kinds of simulations have never been carried out for this model before. The results found in this study can be used to predict observational evidence for disformally coupled fields, and perhaps to inspire further theoretical research on the disformal screening mechanisms present in this theory.

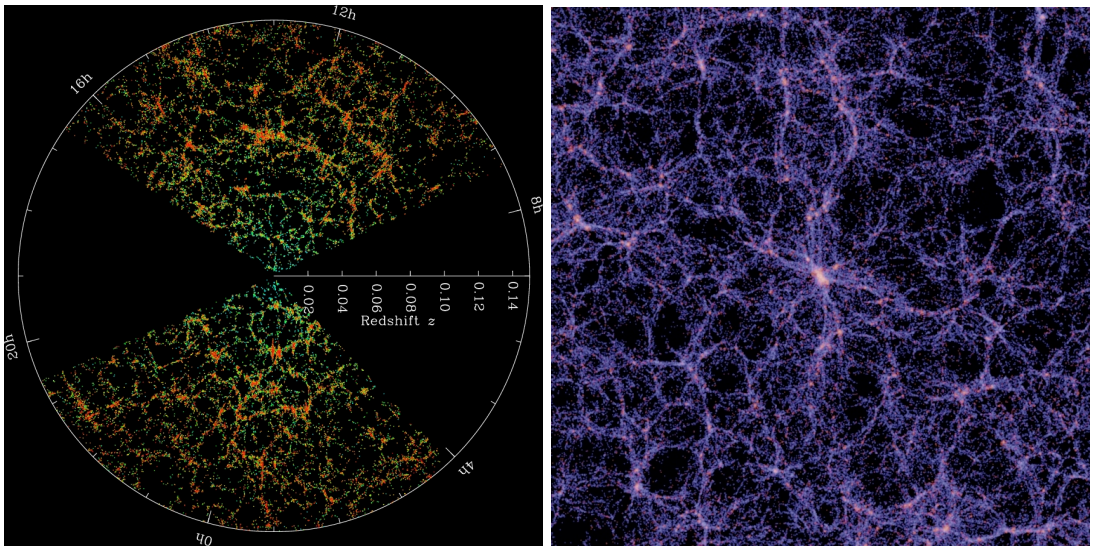

Figure 1.1: The distribution of galaxies on large scales.
The left panel is a slice of the observed galaxy distribution in our universe, gathered from the Sloan Digital Sky Survey [43]. Each dot represents a galaxy, and the slices are 2.5 degrees thick. The earth is at the centre, and a redshift of 0.15 is approximately a distance of 2 billion light years. The sectors to the left and right are excluded from the survey because dust in our own galaxy is obstructing much of the view. The right panel is a slice from the Millennium Simulation, which shows the computed galaxy distribution on large scales, assuming ΛCDM [44]. The width of the right image is a little under 2 billion light years, so the scales of the two images are comparable*. In both images one can clearly see galactic structures, which are often called *the cosmic web* due to the filaments resembling a spider's web.

*The concerned reader might notice that the observations have redshift as the distance scale, while the simulations use actual distances. For small redshifts ($z < 1$), the linear Hubble law is quite accurate. This means that there is approximately a one-to-one ratio between the redshift z and the distance in Mpc for the scales that are relevant here.

Symbol	Explanation	Numerical value
G	Newton's gravitational constant	$6.673 \cdot 10^{-11}\,\mathrm{N{\cdot}m^2kg^{-1}}$
$G_\odot$	Newton's gravitational constant in units of $\mathrm{pc}/M_\odot$ (when $c = 1$)	$4.780 \cdot 10^{-14}\ \mathrm{pc}/M_\odot$
$G_{\mu\nu}$	The Einstein tensor	
$g_{\mu\nu}$	The metric tensor in the Einstein frame, or in GR	
$\Gamma^\lambda_{\mu\nu}$	Christoffel symbols, see section 1.4	
R	The Ricci scalar, see section 1.4	
Λ	The cosmological constant	
$M_\odot$	The mass of the sun, a useful mass unit in cosmology	$1.989 \cdot 10^{30}$ kg
M_{Pl}	The Planck mass	$2.177 \cdot 10^{-8}$ kg
ρ	The density at some point	
ρ_0	The average density in the universe	
Ψ	The Newtonian gravitational potential	
ϕ	A real-valued scalar field in scalar-tensor theories	
ϕ_0	The vacuum expectation value of a scalar field	
$\chi{=}\frac{\phi}{\phi_0}$	A dimensionless scalar field, normalized to ϕ_0	
S	The action of a physical system	
$\mathcal{L}$	The Lagrangian density	
a	Expansion factor of the universe, $a = 1$ today	
z	Redshift, a measure of time/distance, $z = 0$ today	
$H = \frac{\dot{a}}{a}$	The Hubble parameter at a given time	
H_0	The Hubble parameter today	67.11 km/s/Mpc [9]
h	The dimensionless Hubble parameter today	0.6711 [9]
τ	Supercomoving time, useful in simulations	
$\hbar$	reduced Planck constant, used in quantum physics	
c	Speed of light	
c_s	Speed of waves in a wave equation	
$P(k)$	Matter power spectrum	
k	Wavenumber, inversely proportional to distance	

Table 1.1: Symbols used in this thesis, with a short explanation and the numerical value. Not all values given here are used in calculations, but are included for completeness.

1.2 Conventions

In this thesis, index notation is used for vectors and tensors, where Greek indices means any spacetime index 0, 1, 2 or 3, while latin indices means only some spatial index 1, 2 or 3. Upper indices are contravariant, while lower are covariant. Standard Einstein summation is assumed, which means that repeated indices – with one upper and one lower index – indicates a summation over all possible indices, specifically $x_\mu y^\mu \equiv \left(x_0 y^0 + x_1 y^1 + x_2 y^2 + x_3 y^3\right)$.

The comma notation for partial derivatives will be used throughout this thesis, where $\phi_{,\mu} \equiv \partial_\mu \phi = \frac{\partial \phi}{\partial x^\mu}$. Notice that physical vectors are contravariant, while derivatives with respect to vectors are covariant. A dot over a quantity is always a partial derivative with respect to cosmic time, $\dot{\phi} = \frac{\partial \phi}{\partial t} = \phi_{,0}$ (we will sometimes use the comma notation $\phi_{,0}$ in intermediate calculations, often to emphasize the origin of the time derivative). A prime denotes a partial derivative with respect to supercomoving time $x' \equiv \frac{\partial x}{\partial \tau}$.

The notation for the covariant derivative is nabla notation (e.g. $\nabla_\nu \phi$). A nabla without indices simply means the three-dimensional gradient, a vector which is in flat space defined as $\nabla\phi = \phi_{,x}\hat{\mathbf{x}} + \phi_{,y}\hat{\mathbf{y}} + \phi_{,z}\hat{\mathbf{z}}$. Here $\hat{\mathbf{x}}$ is a unit vector in the direction of the x-coordinate, and so on. All three-dimensional vectors in this thesis are denoted with boldface.

For simplicity, natural units where $c = \hbar = 1$ are used in the thesis, but in the code the units of c will be reintroduced because RAMSES has its own length and time unit system with $c \neq 1$. The metric signature $(-,+,+,+)$ is assumed.

Table 1.1 on the preceding page shows a key to most symbols that will be used.

1.3 Statistics in cosmology

When proposing or testing models in cosmology, it is imperative to have some way to statistically compare results from the model with the observed universe. When comparing the results, it is important to remember that we only have one observable universe, which may or may not be statistically close to the theoretical *average* universe with the exact same parameters and laws of physics.

The cosmological principle can be stated as follows: "At large enough scales, the universe is homogeneous and isotropic.". This principle implies that the universe follows strict mechanical rules, and that our position in the universe is not statistically different from any other vantage point. Without accepting the cosmological principle, there is no convincing way to compare models with observations, since what we observe around us could in some sense be specially tailored instead of evolved from physical laws.

The mapping of large scale structure in the local universe is done through redshift surveys, which are both time consuming and might have problems measuring distances accurately due to the peculiar motion of galaxies. The measurements can however be corrected quite well. After applying these corrections, one can find the observed power spectrum of overdensities $P(k)$ and the halo mass function $n(>M)$. Both of these quantities can also be found theoretically for a given model, hence the power spectrum

and mass function are good tests for cosmological models [45].

For many cosmological models, estimates for $P(k)$ and $n(>M)$ can be found analytically through linear perturbation theory. However, these results are only valid for large scales, and tell little or nothing about the formation of structures. To find $P(k)$ and $n(>M)$ that are valid for non-linear scales, one must extract them from simulated data.

1.3.1 The Fourier transform and the wavenumber

Fourier transformation is a method to extract wave information from a function $f(x)$. The Fourier transform $\tilde{f}(k)$ will contain the prevalence of repeated patterns with frequency k in the original function $f(x)$. The wavenumbers k are inversely proportional to the corresponding length in real space, $k \propto 1/L$. A large k therefore symbolizes *high* frequencies and *small* length scales, while a small k means large scales. It follows that $\tilde{f}(k)$ is a measure of the strength of waves with wavelength $L = 2\pi/k$ found in the function $f(x)$. In cosmology this is useful, for instance if we have the average density field in real space. By first Fourier transforming the density field, we can read out the presence of structures at specific length scales given by k. More on this in the next subsection about the power spectrum.

The definition of the three-dimensional Fourier transform and its inverse is [45]:

$$\tilde{f}(\mathbf{k}) = \int e^{-i\mathbf{k}\cdot\mathbf{x}} f(\mathbf{x}) \, \mathrm{d}^3x, \tag{1.1}$$

$$f(\mathbf{x}) = \frac{1}{(2\pi)^3} \int e^{i\mathbf{k}\cdot\mathbf{x}} \tilde{f}(\mathbf{k}) \, \mathrm{d}^3k. \tag{1.2}$$

Note that the conventions for where to have the factors of 2π vary, for example some books use the symmetric definition with $1/(2\pi)^{3/2}$ in front of both the Fourier and the inverse Fourier transform. The wavenumber k is the absolute value of the wave vector $\mathbf{k}$. In cosmology, the units of k are usually h/Mpc.

1.3.2 The power spectrum

After finding the mass density $\rho(\mathbf{x})$, and the mean mass density $\bar{\rho}$, the overdensity at some coordinate $\mathbf{x}$ is found from the definition $\delta(\mathbf{x}) = (\rho(\mathbf{x}) - \bar{\rho})/\bar{\rho}$. The power spectrum $P(k)$ is defined from the self correlation of the Fourier transform of the overdensity [45], specifically

$$\left\langle \tilde{\delta}(\mathbf{k}) \, \tilde{\delta}(\mathbf{k}') \right\rangle = (2\pi)^3 P(k) \, \delta^3(\mathbf{k} - \mathbf{k}'). \tag{1.3}$$

The power spectrum is a good measure of how prevalent lumps of size approximately $1/k$ are in the data set.

Transforming the power spectrum $P(k)$ back into real space with the inverse Fourier transform gives the two-point correlation function $\xi(r)$. The two-point correlation function is defined as the increase in probability of finding two overdense lumps (e.g. two

galaxies) at a distance r apart, over a completely random distribution. In other words $\xi(r) = 0$ for all r means that the matter is completely randomly distributed. $\xi(r) > 0$ for a specific r indicates that, because of some mechanism, the probability is larger for finding two overdensities separated by a distance r than it would be if the matter was randomly distributed. Similarly, a negative $\xi(r)$ for some r implies that at a distance r from an overdensity, there is an increased probability of finding an *underdensity*.

1.3.3 Cumulative halo mass function

Dark matter tends to gather in gravitationally stable lumps. These *dark matter haloes* are the seeds for the formation of galaxies and galaxy clusters.

The cumulative halo mass function

$$n(>M), \tag{1.4}$$

is a measure for how many dark matter haloes, with mass larger than M, that exist per cubic megaparsec.

Some times the mass function is presented not as the cumulative mass function, but as the number density of haloes with mass M within a logarithmic interval,

$$\frac{\mathrm{d}n(>M)}{\mathrm{d}\ln M}. \tag{1.5}$$

This definition is not used in this thesis.

1.4 Curvature in general relativity

In general relativity, gravity is considered to be a result of the curvature of spacetime. To calculate how particles interact through gravity, one must first calculate how space curves and then find the shortest possible paths – called geodesics – for the particles in this curved spacetime. In this section, quantities used in general relativity to describe curved spacetime will be presented briefly. This field of study is called Riemann geometry [46].

The basic quantity used to describe the geometry of space is the metric tensor $g_{\mu\nu}$. In a curved spacetime, one needs a Christoffel connection $\Gamma^{\lambda}_{\mu\nu}$, to describe covariant derivatives, which basically are directional derivatives that are independent of the choice of coordinates*. The definition of the covariant derivative is $\nabla_\mu x^\nu = x^\nu_{,\mu} + \Gamma^\nu_{\mu\lambda} x^\lambda$ for the contravariant x^ν, and $\nabla_\mu \omega_\nu = \omega_{\nu,\mu} - \Gamma^\lambda_{\mu\nu}\omega_\lambda$ for the covariant ω_ν. Note that for scalar quantities, the covariant derivative is equal to the partial derivative $\nabla_\mu \phi = \phi_{,\mu}$.

*Recall for example, that to find the gradient in flat three-dimensional space, one simply has that $\nabla = \hat{\mathbf{x}}\frac{\partial}{\partial x} + \hat{\mathbf{y}}\frac{\partial}{\partial y} + \hat{\mathbf{z}}\frac{\partial}{\partial z}$ in cartesian coordinates, while in spherical coordinates one has $\nabla = \hat{\mathbf{r}}\frac{\partial}{\partial r} + \frac{1}{r}\hat{\boldsymbol{\phi}}\frac{\partial}{\partial \phi} + \frac{1}{r\sin\phi}\hat{\boldsymbol{\theta}}\frac{\partial}{\partial \theta}$. Here the factors $1/r$ and $1/r\sin\phi$ appear because of choice of coordinates, and can be "hidden" inside the Christoffel symbols to create expressions independent of coordinate system. To regain the numerical values one has to extract the Christoffel symbols from the specific metric (coordinate system) that is used, for instance $g_{rr} = 1, g_{\theta\theta} = r^2\sin^2\phi, g_{\phi\phi} = r^2$ for spherical coordinates and simply $g_{xx} = 1, g_{yy} = 1, g_{zz} = 1$ for Cartesian coordinates.

The Christoffel symbols can be found from the definition

$$\Gamma^{\lambda}_{\mu\nu} = \frac{1}{2} g^{\sigma\rho} \left(g_{\nu\rho,\mu} + g_{\rho\mu,\nu} - g_{\mu\nu,\rho} \right). \tag{1.6}$$

The Riemann tensor quantifies the curvature, and can be found from the Christoffel symbols via the formula

$$R^{\rho}_{\sigma\mu\nu} = \Gamma^{\rho}_{\nu\sigma,\mu} - \Gamma^{\rho}_{\mu\sigma,\nu} + \Gamma^{\rho}_{\mu\lambda}\Gamma^{\lambda}_{\nu\sigma} - \Gamma^{\rho}_{\nu\lambda}\Gamma^{\lambda}_{\mu\sigma}. \tag{1.7}$$

A contraction of the Riemann tensor gives the Ricci tensor $R_{\mu\nu} = R^{\lambda}_{\mu\lambda\nu}$, and a further contraction of this (after raising an index) gives the Ricci scalar, $R = g^{\mu\nu}R_{\mu\nu}$. In general relativity one often sees the Einstein tensor $G_{\mu\nu} = R_{\mu\nu} - \frac{1}{2}Rg_{\mu\nu}$, the usefulness of which will be clear in the next section about Einstein's field equations.

To find how individual point particles move in the curved spacetime described by the metric $g_{\mu\nu}$, one uses the geodesic equation (which can be found from the action principle, but is defined geometrically through the curve along which the tangent vector is parallel-transported [46]). The geodesic equation in general relativity reads

$$\ddot{x}^{\mu} + \Gamma^{\mu}_{\alpha\beta}\dot{x}^{\alpha}\dot{x}^{\beta} = 0. \tag{1.8}$$

This equation follows from stating that gravity is not a force in the common sense, but rather just a result of the curvature of space; particles that are not affected by external forces, will move in a *locally* straight line relative to the curved space. The geodesic equation therefore is the equation of motion for a particle affected only by gravity.

1.5 The action principle and Einstein's field equations

A very important principle in all branches of physics is the principle of least action [47]. For any system, there exists an action which is the time integral of the Lagrangian. Mathematically, this action can be written $S = \int L \, \mathrm{d}t$. In classical mechanics, the Lagrangian is equal to the difference between the kinetic and the potential energy of a system $L = K - V$. If the system contains continuous matter or fields, it can be useful to write the action as the four-dimensional spacetime integral of a *Lagrangian density* $\mathcal{L}$, such that $S = \int \mathcal{L} \, \mathrm{d}x^4$ in Minkowski space. The Lagrangian density $\mathcal{L}$ will often simply be referred to as the Lagrangian in this thesis, when there can be no confusion.

The action principle states that, during any spacetime interval, the action should stay the same, $\delta S = 0$. In classical mechanics, consequences of the action principle include the Euler-Lagrange equation (which can be used to find the equations of motion for mechanical systems), and conservation of mechanical energy. A modified version of the action principle is important in quantum mechanics and quantum field theory.

Here follows an example of how to apply the action principle, which doubles as an introduction to Einstein's field equations. We will perform a variation of the Einstein-Hilbert action, and use the action principle to derive Einstein's field equations in general relativity. The Einstein-Hilbert action is given by [46]:

$$S_{\mathrm{EH}} = \int \sqrt{-g} R \, \mathrm{d}^4 x, \tag{1.9}$$

where $g = \det(g_{\mu\nu})$ is the determinant of the metric $g_{\mu\nu}$, and R is the Ricci scalar. This action is the integral of the simplest scalar invariant Lagrangian density that can be constructed from the metric, namely $\mathcal{L} = R$. The factor of $\sqrt{-g}$ is a geometric volume factor (the Jacobian) that is needed when taking the integral over the non-flat four-dimensional spacetime.

Adding the Einstein-Hilbert action and the matter action together, one finds the total "action of the universe":

$$S = \int \sqrt{-g}\left(\frac{R}{16\pi G}\right) \mathrm{d}^4x + \int \sqrt{-g}\mathcal{L}_M \, \mathrm{d}^4x. \tag{1.10}$$

Here, the constant factor of $1/16\pi G$ is included so that the resulting equation reduces to the usual Newtonean gravity in the nonrelativistic limit (this is common in e.g. [46]). This action should now be varied with respect to the inverse metric $g^{\mu\nu}$, meaning that one has to do a linear perturbation $g^{\mu\nu} \to g^{\mu\nu} + \delta g^{\mu\nu}$, such that $S \to S + \delta S$. This gives

$$\delta S = \int \left[\left(\frac{1}{16\pi G}\right) \delta\left(\sqrt{-g}R\right) + \delta\left(\sqrt{-g}\mathcal{L}_M\right)\right] \mathrm{d}^4x. \tag{1.11}$$

Here the notation $\delta(x)$ means a variation of some variable x. Using that $\delta\sqrt{-g} = -\frac{1}{2}\sqrt{-g}g_{\mu\nu}\delta g^{\mu\nu}$, and the definition of the Ricci scalar (see section 1.4), one eventually finds that

$$\delta S = \int \sqrt{-g}\left[\left(\frac{1}{16\pi G}\right)\left(R_{\mu\nu} - \frac{1}{2}Rg_{\mu\nu}\right) + \frac{\delta\mathcal{L}_M}{\delta g^{\mu\nu}} - \frac{1}{2}g_{\mu\nu}\mathcal{L}_M\right] \delta g^{\mu\nu} \, \mathrm{d}^4x. \tag{1.12}$$

Now, the action principle states that the action should stay unchanged no matter how the metric changes, meaning $\delta S = 0$ for any $\delta g^{\mu\nu}$. This can only be achieved if everything inside the square brackets of equation (1.12) is equal to zero. Which easily results in the equation

$$R_{\mu\nu} - \frac{1}{2}Rg_{\mu\nu} = 8\pi G\left(-2\frac{\delta\mathcal{L}_M}{\delta g^{\mu\nu}} + g_{\mu\nu}\mathcal{L}_M\right). \tag{1.13}$$

Here everything inside the parenthesis on the right hand side is defined to be the energy-momentum tensor $T_{\mu\nu}$. Using the definition of the Einstein tensor, $G_{\mu\nu} \equiv R_{\mu\nu} - \frac{1}{2}Rg_{\mu\nu}$, we now have the simplest form for Einstein's field equations, namely the tensor equation

$$G_{\mu\nu} = 8\pi G T_{\mu\nu}. \tag{1.14}$$

The field equations* tell all there is to know about how all the contents of the universe – on the right hand side of equation (1.14) – interact with the curvature of space – on

*The reason for the plural *equations*, is that the tensor equation (1.14) actually consists of $4 \times 4 = 16$ separate equations, when inserting all possibilities for μ and ν. Not all of these equations are independent, however.

the left hand side. This equation can be used to find the evolution of matter, radiation, and scalar fields in the universe.

There are many scalar invariant terms that are technically allowed to be added to the Lagrangian in addition to R. For example, simply adding a constant scalar term Λ such that

$$S = \int \sqrt{-g} \frac{1}{16\pi G} \left(R - 2\Lambda\right) \mathrm{d}^4x + \int \sqrt{-g} \mathcal{L}_M \, \mathrm{d}^4x, \tag{1.15}$$

will give rise to the Einstein field equations with a cosmological constant,

$$G_{\mu\nu} + \Lambda g_{\mu\nu} = 8\pi G T_{\mu\nu}. \tag{1.16}$$

This tensor equation allows for an exponentially expanding universe, and is the cornerstone of the standard model of cosmology, ΛCDM. The expressions general relativity (GR), standard gravity, and ΛCDM all refer to unmodified gravity in this thesis.

1.6 Modified gravity

Modifications to Einstein's general relativity were considered already a few years after his theory was first published. This was done by realizing that it is completely possible to include higher order invariant terms in the action (1.10), for example R^2 and so on [48]. Such higher order theories became more popular in the 1960s. When trying to quantize the classical theory of gravity, it was found that higher order counterterms in the action were necessary to make the quantized theory normalizable [49]. These theories were mostly interesting in high-energy physics.

The first generally popular modification of gravity to be applied on galaxy scales was modified Newtonian dynamics (MOND). MOND was introduced in 1983 to explain galaxy rotation curves and hence greatly reduce the amount of *dark matter* needed in the calculations [50]. The original idea in MOND is to modify Newtons second law such that the equation reads $F_\mathrm{N} \propto a^2$ for low accelerations, but reduces to $F_\mathrm{N} \propto a$ in the solar system and on earth. This theory is still studied, but has multiple problems, especially in systems that are not spherically symmetric [51, 52].

Today there exist a multitude of theories for modified gravity [14]. The starting point of most of these theories is to begin with another form for the Lagrangian than simply $\mathcal{L} = R$, or $\mathcal{L} = R + 2\Lambda$. For example one can take some scalar function of R instead of simply R, such that $\mathcal{L} = f\left(R\right)$. These kinds of theories are called $f\left(R\right)$-theories. One example that can lead to early cosmic inflation is $f\left(R\right) = R + \alpha R^2$ [53]. There are many other more or less justified terms that can possibly be constructed and inserted into $\mathcal{L}$, especially if one in addition to the tensor field $g_{\mu\nu}$, also allows for the existence of a scalar field ϕ. The general Lagrangian in these *scalar-tensor theories* is called the Horndeski Lagrangian [54], but writing down this complete Lagrangian requires multiple pages, and it is not very relevant for the rest of the thesis. The most important addition to the Lagrangian for our purposes is that of a *canonical scalar field* ϕ, namely

$$\mathcal{L}_\phi = -\frac{1}{2}\phi^{,\mu}\phi_{,\mu} - V\left(\phi\right). \tag{1.17}$$

The first and second term on the right hand side represent the kinetic energy density of the scalar field and the potential energy density respectively. These terms are known from classical field theory, and are therefore well motivated. Even more so after the confirmed existence of the Higgs boson, whose field obeys this very Lagrangian [55, 56].

The idea of a scalar field as the source of dark energy emerges because the potential energy of the scalar field can under certain conditions emulate a cosmological constant in the resulting field equations. Just adding the Lagrangian of a scalar field that rolls slowly down a potential can therefore give an accelerating expansion on large scales. Such models are called quintessence models [57]. However, quintessence models lack screening mechanisms and a coupling to matter. They have theoretical results that diverge from ΛCDM, which one should be able to measure in observations. Such divergences are not measured to this date.

As stated earlier, all valid theories of modified gravity must contain some screening mechanism for the theory to recover general relativity on solar-system scales. One large class of scalar-tensor theories are the ones that are screened in regions of high Newtonian gravitational potential Ψ – which usually happens in areas inside or close to high density galaxies and galaxy clusters. In these theories there needs to be a coupling between the scalar field ϕ, and the matter. This coupling is introduced through the *Jordan frame* metric $\bar{g}_{\mu\nu}$, which in general is some function of the field, the standard Einstein frame metric $g_{\mu\nu}$, and their derivatives. The Jordan frame metric enters in the matter section of the action, meaning that it must be used instead of the Einstein frame metric for calculating the matter Lagrangian, and the Jacobian $\sqrt{-g}$ factor. The general action for all of these density screened theories with a canonical field then reads

$$S = \int \left[\sqrt{-g} \left(\frac{R}{16\pi G} - \frac{1}{2}\phi^{,\mu}\phi_{,\mu} - V(\phi) \right) + \sqrt{-\bar{g}}\bar{\mathcal{L}}_{\mathrm{m}} \right] \mathrm{d}^4x. \tag{1.18}$$

Now, $\bar{\mathcal{L}_m}$ is the Lagrangian density of matter computed using the Jordan frame metric $\bar{g}_{\mu\nu}$ instead of $g_{\mu\nu}$, whenever applicable.

In section 1.5, we varied the Einstein-Hilbert action with respect to the metric to find how particles should behave in general relativity. Doing the same thing to the new scalar-tensor action (1.18), would result in a modified version of Einstein's field equations. One can now also vary the action with respect to the scalar field ϕ, which yields the equation of motion for the field value. Assuming Minkowski space, this equation of motion in the simplest case is a second order differential equation on the form

$$\ddot{\phi} = \nabla^2\phi - V_{\mathrm{eff},\phi}, \tag{1.19}$$

where V_{eff} is the *effective potential* felt by the scalar field, and is usually a function of ϕ and the matter density ρ [16]. This equation of motion is comparable to the Klein-Gordon equation in quantum field theory, which describes how the quantum field of a spin zero particle (e.g. the Higgs field) evolves.

To find out how point particles* move in the modified theory, we assume that the particles follow straight lines in the Jordan frame, thus we must calculate the geodesics

*In cosmology point particles often means galaxies.

using the Jordan frame Christoffel symbols $\bar{\Gamma}^{\mu}_{\alpha\beta}$ found from the Jordan frame metric $\bar{g}_{\mu\nu}$. The geodesic equation – at least in the models shown here – now takes a similar form to that in general relativity [58],

$$\ddot{x}^{\mu} + \bar{\Gamma}^{\mu}_{\alpha\beta}\dot{x}^{\alpha}\dot{x}^{\beta} = 0. \tag{1.20}$$

However, the Jordan frame Christoffel symbols are usually more difficult to calculate than the Einstein frame Christoffel symbols from general relativity. The acceleration of particles in the Jordan frame can be decomposed into the few terms originating from general relativity – which will always be present – and all the extra terms, arising from the modification to gravity. These extra terms in the acceleration of particles are called *fifth forces*, and are present in many alternative theories of gravity. The fifth forces should vanish in screened areas.

Two specific matter coupled scalar-tensor theories will be presented in the following subsections. First, the relatively simple and well-studied symmetron model with just a conformal coupling. Secondly, the disformally coupled model will be introduced.

1.6.1 The conformally coupled symmetron model

In conformally coupled theories, a scalar field ϕ interacts with matter and changes the Jordan frame metric $\bar{g}$ that matter recognizes. The relation between the Jordan frame metric and the Einstein frame metric is given by

$$\bar{g}_{\mu\nu} = A(\phi) \cdot g_{\mu\nu}, \tag{1.21}$$

where $A(\phi)$ is some function of the value of the scalar field, and is called the *conformal coupling term*.

The symmetron model is a specific conformally coupled theory which has been well studied, both in the background linear regime [59, 60], and in the non-linear regime through simulations [61, 62, 40, 63, 39]. The modified Einstein-Hilbert action for the symmetron model is given by equation (1.18). The Jordan frame metric $\bar{g}$ is related to the Einstein frame metric $g_{\mu\nu}$ according to

$$\bar{g}_{\mu\nu} = [A_{\text{sym}}(\phi)]^2 \cdot g_{\mu\nu}, \tag{1.22}$$

where the conformal coupling term A_{sym} is responsible for how the field interacts with the matter/energy content of the universe*. Note that if $A_{\text{sym}} = 1$, the Jordan and Einstein frame metrics are identical, and the field will not couple to matter. The symmetron screening mechanism – which will be explained soon – is designed to make $A_{\text{sym}} \to 1$ in high density areas. Particles in screened locations will behave like in general relativity.

*The definition of the conformal term in the Symmetron theory, where $A(\phi) \to [A_{\text{sym}}(\phi)]^2$, is purely practical.

In the symmetron model, one specifies the symmetron potential and the conformal coupling as

$$V(\phi) = -\frac{1}{2}\mu^2\phi^2 + \frac{1}{4}\lambda\phi^4 + V_0, \tag{1.23}$$

$$A_{\text{sym}}(\phi) = 1 + \frac{1}{2M^2}\phi^2, \tag{1.24}$$

where μ, λ, V_0, and M are free parameters of the model. It should be noted that the mass-scale M is always large compared to the scalar field value ϕ, so one often takes the approximation $A^2_{\text{sym}} = 1 + \left(\frac{\phi}{M}\right)^2$, ignoring terms to forth order of $\left(\frac{\phi}{M}\right)$. This specific choice of A_{sym} and V, after applying the action principle $dS = 0$ to equation (1.18), leads to an equation of motion for the scalar field where the field behaves as if it rolls on an effective potential of the form

$$V_{\text{eff}}(\phi, \rho) = \frac{1}{2}\left(\frac{\rho}{M^2} - \mu^2\right)\phi^2 + \frac{1}{4}\lambda\phi^4. \tag{1.25}$$

Figure 1.2 shows the effective symmetron potential for two different densities, specifically $\rho = 0$ (vacuum, comparable to the void between galaxy clusters) and $\rho = 4\mu^2M^2$ (a high density, comparable to the inside of a galaxy cluster). In high densities, the effective potential is parabola-like and has a single minimum at $\phi = 0$, $V = 0$. In low densities, the effective potential achieves the characteristic "Mexican hat" form with two minima that lie at a lower potential than $V = 0$. The specific density at which the potential switches from one to two minima is $\rho_{\text{SSB}} = M^2\mu^2$, where SSB is short for spontaneous symmetry breaking.

The early universe is dense, such that $\rho \gg \rho_{\text{SSB}}$, and the scalar field starts out at rest close to $\phi = 0$. As long as the field sits in the bottom of the high density potential, there is no coupling to matter, because when $\phi \to 0$, one finds that $A^2_{\text{sym}} \to 1$, and therefore $\bar{g}_{\mu\nu} \to g_{\mu\nu}$. This means that the theory is completely screened in the early universe. However, as the universe evolves and expands, the areas of lowest density – often called voids – will experience spontaneous symmetry breaking when $\rho < \rho_{\text{SSB}}$. The name symmetry breaking comes from the fact that the $\phi \to -\phi$ symmetry is broken when there no longer is an oscillation around $\phi = 0$, but rather around *either* $\phi = +\phi_0$ or $\phi = -\phi_0$. The quantity $\phi_0 \equiv \mu/\sqrt{\lambda}$ is called the *vacuum expectation value* of the field, and is the minimum of the effective potential, when we assume complete vacuum, specifically $\rho = 0$. In the voids where the symmetry is broken, the screening is no longer efficient and fifth forces will appear [64]. In galaxy clusters, the overdensities grow fast enough that the density has never dropped below ρ_{SSB}, and the model is still screened.

Whether the field falls to $+\phi_0$ or $-\phi_0$ after the symmetry breaking is a complex matter, and small differences in parameters or initial conditions could change the resulting sign of the scalar field. In the symmetron model, the physics are the same for a field that has fallen to a negative value and a field that has fallen to a positive value, but interesting features and physics appear in the *domain walls* between areas that have opposite signs of the scalar field [65, 66].

The geodesic equation in the symmetron model is given by [61]:

$$\ddot{x}^{\mu} + \Gamma^{\mu}_{\alpha\beta}\dot{x}^{\alpha}\dot{x}^{\beta} = -\frac{\partial \log A_{\rm sym}(\phi)}{\partial \phi}\left(\nabla^{\mu}\phi + \dot{\phi}\dot{x}^{\mu}\right), \tag{1.26}$$

which for $A_{\rm sym} = 1$ reduces to general relativity, as expected. This means that for a stationary particle (i.e. all $\dot{x}^{\mu} = 0$), one expects a fifth force proportional to both the value and the gradient of the scalar field. Specifically

$$\mathbf{F}_5 \propto (\log A_{\rm sym})_{,\phi}\,\nabla\phi \lesssim \phi\nabla\phi, \tag{1.27}$$

where in the last approximation, it was assumed that $1/A \approx 1^{*}$. The relation (1.27) confirms that the fifth force should be screened in areas where $\phi \to 0$, but also shows that there should be little of the fifth force when the gradient of the field is low (e.g. in large areas of relatively uniform matter density, far from massive haloes).

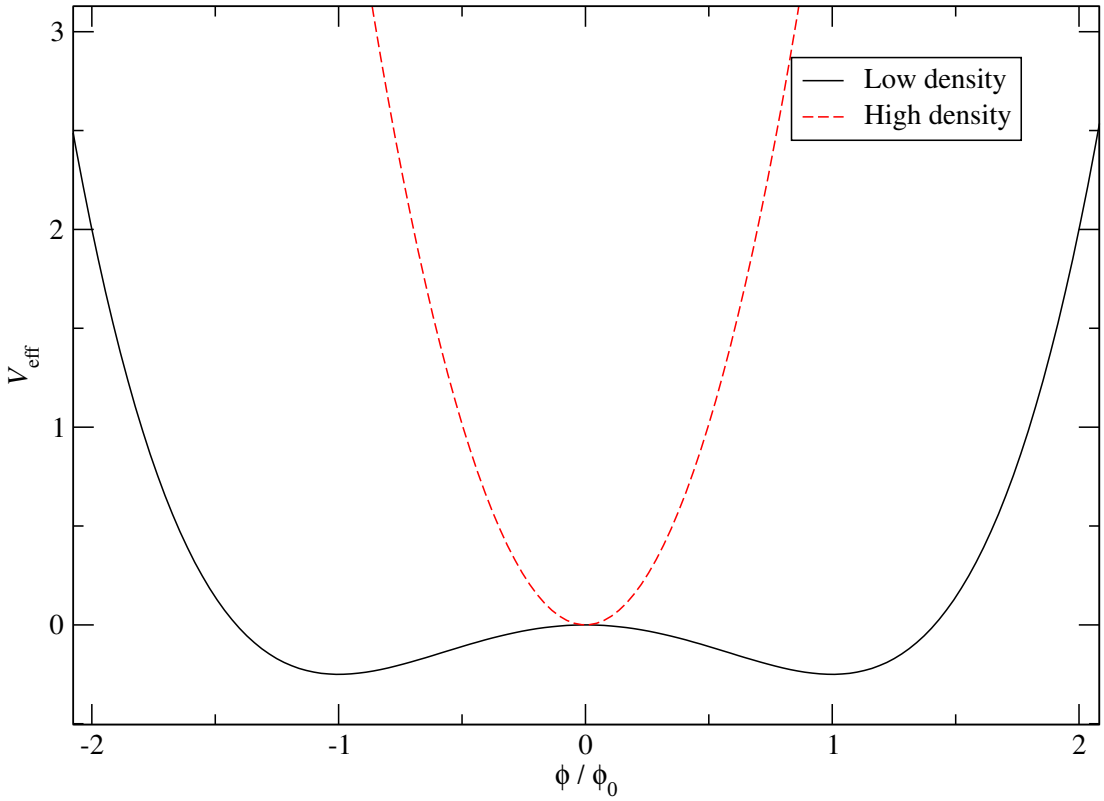

Figure 1.2: The figure shows the effective potential of the symmetron field in areas of low density (black line) and in areas of high density (red, dashed line).

*This approximation is valid when we have decided on a value of the parameter M such that $M \gg \phi$.

1.6.2 Disformally coupled models

In disformally coupled theories of gravity, the action is again given by equation (1.18). However, the expression for the Jordan frame metric $\bar{g}$ has an extra disformal term, which links the time and space derivatives of the field to matter,

$$\bar{g}_{\mu\nu} = A(\phi)\, g_{\mu\nu} + B(\phi)\, \phi_{,\mu}\phi_{,\nu}. \tag{1.28}$$

On the most general form, the conformal term $A(\phi)$, the disformal term $B(\phi)$, and the potential $V(\phi)$ are free functions. They are in some papers taken to be either constant or exponential functions of ϕ, which simplifies some analytic calculations [36]. In this thesis the symmetron form for the potential V and the conformal term A will be used, in addition to a simple exponential for the disformal term B (as will be seen in section 2.1). Now the variation of the action with respect to ϕ becomes much more complicated than in the symmetron case, because of cross terms from the two terms in the Jordan frame metric (1.28). The details on the calculation of the equation of motion will be given in section 2.3.

Matter particles will move in geodesics determined by the Jordan frame metric. Generally, the modified geodesic equation reads

$$\ddot{x}^{\mu} + \bar{\Gamma}^{\mu}_{\alpha\beta}\dot{x}^{\alpha}\dot{x}^{\beta} = 0, \tag{1.29}$$

where $\bar{\Gamma}^{\mu}_{\alpha\beta}$ are the Christoffel symbols for matter found from the relation [58]

$$\bar{\Gamma}^{\mu}_{\alpha\beta} = \Gamma^{\mu}_{\alpha\beta} + \frac{1}{2}\bar{g}^{\mu\nu}\left[\nabla_{\alpha}\bar{g}_{\beta\nu} + \nabla_{\beta}\bar{g}_{\alpha\nu} - \nabla_{\nu}\bar{g}_{\alpha\beta}\right]. \tag{1.30}$$

The detailed calculation of particle movements for the disformal model will be carried out in section 2.5.

In the case of a constant disformal coupling, $B = \text{const}$, and no conformal coupling, $A = 1$, the disformal fifth force is expected to be proportional to the second derivative of the field with respect to time, as well as the gradient of the field [25]. Specifically

$$\mathbf{F}_5 \propto \ddot{\phi}\nabla\phi. \tag{1.31}$$

From this, one would expect that oscillations of the field in areas with some field gradient will give rise to fifth forces. To screen these forces, the field needs to be at rest, or oscillate uniformly over large areas. In the general case where there is some conformal coupling, one can expect more terms in the fifth force. This possibility will be investigated further in this thesis.

1.7 N-body simulations

A computer simulation is a program that is made to behave like some physical system, so that one can study the result of the program instead of the actual physical system it imitates. In cosmology this is especially helpful, because doing a real-world experiment

on how stars and galaxies evolve would be unpractical, or indeed impossible. We only have access to one visible universe, so without simulations we would have no way to examine how the universe would behave if we rewinded it and allowed it to evolve with slightly different parameters or initial conditions.

With simulations, complex nonlinear systems of many particles – that are completely uncomputable by pen-and-paper methods – can be studied. For example, even finding the *exact* motion of three particles interacting through gravity is not possible analytically, but a good *approximate* solution can be found quite easily with a simple simulation. Any number N of particles can be simulated using such methods, hence the name N-body simulation.

When doing numerical simulations it is important to normalize the variables one uses, such that the values do not exceed unity by far. This is because numerical errors are more likely to occur when performing floating-point operations on two numbers of different orders of magnitude.

1.7.1 Newtons second law, algorithm

As a simplified example, it will be shown how to numerically compute the motion of particles affected by gravity, using Newton's gravity and Newton's second law [67]. Newton's second law states that the acceleration $\mathbf{a} = \ddot{\mathbf{x}}$ of a massive object i is proportional to the vector sum of all forces $\mathbf{F}_{i,j}$ acting on the object from all *other* objects $j \neq i$, and inversely proportional to the mass m_i of the object. Specifically

$$\mathbf{a}_i = \sum_{j \neq i} \frac{\mathbf{F}_{i,j}}{m_i}. \tag{1.32}$$

Assuming that the objects are point masses, and that Newtonian gravity is the only force acting between them, the magnitude of the gravitational force on a single object from another is given by Newton's law of universal gravitation,

$$|\mathbf{F}_{\mathrm{i,j}}| = G\frac{m_i m_j}{r^2}. \tag{1.33}$$

G is Newton's gravitational constant, and r is the distance between object i and j. The direction of the force is along the line connecting the two objects. The inertial mass of an object is incidentally equal to the gravitational mass of the object. From this follows that, when finding the total acceleration due to gravity, the mass of the object studied can be cancelled.

$$|\mathbf{a}_i| = \sum_{j \neq i} \frac{G}{\cancel{m_i}} \frac{\cancel{m_i} m_j}{r^2}. \tag{1.34}$$

To implement this equation into a code and track the positions and velocities of the particles, one has to make a system of first order differential equations; One equation for the position, and one for the velocity og each particle. The equations in this case

are:

$$\begin{aligned} \dot{\mathbf{x}}_i &= \mathbf{v}_i, \\ \dot{\mathbf{v}}_i &= \mathbf{a}_i = G \sum_{j \neq i} \frac{m_j}{|\mathbf{x}_j - \mathbf{x}_i|^3} \left(\mathbf{x}_j - \mathbf{x}_i \right). \end{aligned} \tag{1.35}$$

These equations must be discretized in time to be solved by a computer. The simplest way to do this is with the forward Euler integration, simply by letting the infinitesimals become finite, $\mathrm{d}t \to \Delta t$. We now find that the change in position, $\Delta \mathbf{x}_i$, at a given time t is given by $\mathbf{v}_i(t) \cdot \Delta t$. Similarly, the change in velocity during the same time interval, is given by $\Delta \mathbf{v}_i = \mathbf{a}_i(t) \cdot \Delta t$. Taking one time step forward, one gets the forward Euler algorithm for integration:

$$\begin{aligned} \mathbf{x}_i(t + \Delta t) &= \mathbf{x}_i(t) + \mathbf{v}_i(t) \cdot \Delta t, \\ \mathbf{v}_i(t + \Delta t) &= \mathbf{v}_i(t) + \mathbf{a}_i(t) \cdot \Delta t. \end{aligned} \tag{1.36}$$

In a three-dimensional implementation, the calculation will probably be split up into a separate set of equations for each of the three spatial components of $\mathbf{x}$ and $\mathbf{v}$. The calculation must be done for each particle i, summing over the forces from each other particle $j \neq i$. This iteration is then repeated for each new time step of size Δt, from a pre-decided initial state, at $t = t_0$, until some time $t = t_{\text{end}}$.

In theory, one can include as many particles as desired in this method, classifying it as an N-body simulation. However, this simple, brute-force algorithm quickly becomes computationally demanding when increasing the number of particles. When using forward Euler, the time step Δt must be chosen sufficiently small for the particles to not jump too far in each step. This is because in practice, the particles follow straight lines between each discrete calculation. If, for instance, two particles are supposed to orbit each other in stable, elliptical orbits, a too large time step will actually result in the particles spiralling outwards in the simulation. Consequently, forward Euler does not conserve mechanical energy.

Ways to improve the implementation is to use smarter schemes for the time integration – for example the leapfrog scheme, which conserves energy – and to collect particles in groups. Using these groups when calculating the gravity force on a distant particle, instead of summing over each particle individually, will drastically reduce the time needed for the computations.

1.7.2 The leapfrog scheme

The leapfrog method is a second order method for solving coupled differential equations, unlike forward Euler, which is only a first order method*. Nevertheless, the leapfrog algorithm uses the same amount of calculations per time step, and has the added benefit of conserving energy in a mechanical system.

*A second order method has an absolute error ϵ that goes as $\epsilon \propto (\Delta t)^2$, whereas a first order method has an error that goes as $\epsilon \propto \Delta t$. Forward Euler requires a power of two the amount of time steps in the same interval, to reach the same accuracy as the leapfrog scheme.

The scheme is some times called velocity Verlet, these schemes essentially consist of the same calculations. The principle is that the velocity is evaluated at each integer-and-a-half time step, while the acceleration and position are evaluated at each integer time step. Thus the velocity and the position evaluations will "leapfrog" over each other. One time step of the leapfrog method (for one particle with position $\mathbf{x}$, velocity $\mathbf{v} = \dot{\mathbf{x}}$ and acceleration $\mathbf{a} = \ddot{\mathbf{x}}$) can be written as

$$\begin{aligned} \mathbf{v}\left(t + \frac{1}{2}\Delta t\right) &= \mathbf{v}(t) + \mathbf{a}(t) \cdot \frac{1}{2}\Delta t \\ \mathbf{x}(t + \Delta t) &= \mathbf{x}(t) + \mathbf{v}\left(t + \frac{1}{2}\Delta t\right) \cdot \Delta t \\ \mathbf{v}(t + \Delta t) &= \mathbf{v}\left(t + \frac{1}{2}\Delta t\right) + \mathbf{a}(t + \Delta t) \cdot \Delta t. \end{aligned} \tag{1.37}$$

Here, the acceleration at time $t + \Delta t$ that is evaluated at the end of a time step is saved and re-used at the start of the next time step (where $t \to t + \Delta t$). In this way there is only one evaluation of the acceleration in each time step [68].

1.7.3 Cosmological simulations

There are many cosmological N-body codes that apply different methods to efficiently simulate the evolution of point particles in the universe. Examples of cosmological N-body codes are the particle mesh code Ramses [41] and the hierarchical tree code Gadget-2 [69]. This subsection will be focused on particle mesh codes, on which Isis is based.

The code has an initial, coarse particle mesh grid, on which particles are distributed from some given initial conditions. The initial random distribution of the particles must fulfil certain criteria, often constrained by observations of the cosmic microwave background. The initial distribution is usually computed in an external program through linear perturbation theory.

A common feature in particle mesh N-body codes is adaptive mesh refinement (AMR). First, the best approximation of the gravitational potential Ψ at the centre of each cell is calculated from the densities of particles in the other cells of the grid. The acceleration of a single particle is then found from the gradient of this estimated gravitational potential. In this way, the code saves a lot of computing power by treating all other particles as a density field instead of as point particles. As time passes, the particles start to gather in lumps due to gravity. When many particles are clustered in a few cells, the value of the estimated Ψ at the centre of each of these cells becomes unprecise. Furthermore, the large gravitational acceleration close to a dense lump of particles gives rise to numerical errors when the time step is too large. Both these problems are solved by refining the mesh structure – for grid cells where the particle density is high, the three-dimensional cell is divided into eight cells with half the width and half the time step of their parent cell. Such refinements can, if needed, be applied to already refined cells to further increase both the temporal and spatial resolution in

important areas. This recursive subdivision into octants results in a so-called *octree* grid structure.

The gravitational potential Ψ is found from the density field using the Poisson equation,

$$\nabla^2\Psi = 4\pi G\rho. \tag{1.38}$$

This equation can be solved numerically by doing a given amount of Gauss-Seidel iterations. In Gauss-Seidel iteration number $n+1$, the potential Ψ_i^{n+1} at each cell i is estimated from the density in the current cell ρ_i, and the potential of the surrounding cells at the previous iteration n. The simplified formula for such an iteration reads

$$\Psi_i^{n+1} = \frac{1}{6}\left(\sum_{\text{six adjacent}} \Psi_j^n\right) - A\rho_i, \tag{1.39}$$

where A is some constant including $4\pi G$ and the width of the grid cell. This method converges very slowly, but the equation (1.38) is in RAMSES solved quite efficiently on a level-by-level basis with a *multigrid scheme* [42]. This scheme uses Gauss-Seidel iterations on each grid, but with added corrections from the coarser grids.

The absolute size of the simulation box is limited. The length of each of the edges of the box is often 64, 128, or 256 Mpc/h*. To ensure that the simulation behaves as if there was infinite space, and not just a box of particles with nothing outside, one usually applies periodic boundary conditions. In this way, particles on the far left side of the simulation are gravitationally affected by particles on the far right side, and particles that disappear out of the box will warp over and reappear on the other side. In short, the simulation behaves as if the simulation box was copied and placed on each side of the original box.

1.7.4 Scalar fields in simulations

When simulating conformally coupled scalar fields, it is normal practice to assume the field is quasistatic, which means one takes $\ddot{\phi} = \dot{\phi} = 0$. This is usually justified by the fact that the fifth force is $\mathbf{F}_5 \propto \phi\nabla\phi$, and therefore the motion of the particles is not affected by temporal oscillations of the field. The resulting equation of motion for the scalar field, when removing all time derivatives, is a Poisson equation on the form

$$\nabla^2\phi = V_{\text{eff},\phi}\left(\rho, \phi\right). \tag{1.40}$$

This equation can be solved numerically by setting up a grid of scalar field values, and doing a sufficient amount of Gauss-Seidel iterations, or multigrid iterations for each time step of the particles [70]. The result is a field value at each grid point depending on the mass density in that grid cell. The field achieves the value it would have had if it did not oscillate, specifically $\phi = \pm\phi_0$ in vacuum far from galaxy clusters, and $\phi = 0$

*The variable h is used as a normalization during calculations, so that the results are valid even if the actual value of h turns out to be slightly different.

in high density areas. This approach for simulating scalar fields is used in for example [61] and [40].

To include the oscillating nature of the scalar field, one sets up a time-stepping scheme similar to the one used for solving the equation of motion for particles. One can then discretize the full equation of motion for the scalar field. Defining a new variable $q = \dot{\phi}$, and applying the leapfrog scheme, one obtains these difference equations, that can be solved step by step numerically:

$$\begin{aligned} q\left(t+\frac{1}{2}\Delta t\right) &= q\left(t\right) + \ddot{\phi}\left(t\right)\cdot\frac{1}{2}\Delta t, \\ \phi\left(t+\Delta t\right) &= \phi\left(t\right) + q\left(t+\frac{1}{2}\Delta t\right)\cdot\Delta t, \\ q\left(t+\Delta t\right) &= q\left(t+\frac{1}{2}\Delta t\right) + \ddot{\phi}\left(t+\Delta t\right)\cdot\Delta t. \end{aligned} \tag{1.41}$$

The acceleration of the field is calculated by isolating $\ddot{\phi}$ in the specific equation of motion for the field that is simulated.

This non-static approach is used by Llinares et al. in the paper [39], where they describe the method outlined above in detail, including how to choose initial conditions for the field values. A point worth mentioning is that the symmetron field is expected to oscillate faster than the average motion of dark matter particles. This is allowed in the code by letting the field evolve with multiple smaller time steps for each coarse time step of the particles. A problem with current non-static codes is that they don't allow for adaptive mesh refinement of the N-body grid.

The resulting non-static Isis code from the paper [39] is used to implement the disformal equations presented in this thesis.

Chapter 2

The disformal equations

After specifying the disformally coupled model, we will in this chapter calculate both the field equation of motion – describing how the field will evolve when coupling to matter – and the geodesic equation – describing how dark matter particles will move in this model. Before implementing these equations, we normalize the field and introduce *supercomoving variables* to make the implementation easier. For more specific details on the implementation, see Appendix D.

2.1 Specifying the disformally coupled model

The action in disformal gravity is in general given by

$$S = \int \left[\sqrt{-g} \left(\frac{R}{16\pi G} - \frac{1}{2}\phi^{,\mu}\phi_{,\mu} - V(\phi) \right) + \sqrt{-\bar{g}}\bar{\mathcal{L}}_{\mathrm{m}} \right] \mathrm{d}^4x, \tag{2.1}$$

with

$$\bar{g}_{\mu\nu} = A(\phi)\, g_{\mu\nu} + B(\phi)\, \phi_{,\mu}\phi_{,\nu}. \tag{2.2}$$

The field potential $V(\phi)$ can have many different forms, but we choose the symmetron "Mexican hat" potential given by

$$V(\phi) = -\frac{1}{2}\mu^2\phi^2 + \frac{1}{4}\lambda\phi^4 + V_0, \tag{2.3}$$

with the three free parameters μ, λ, and V_0. The specific forms of the conformal term $A(\phi)$ and the disformal term $B(\phi)$ studied in this thesis are as follows:

$$A(\phi) = 1 + \left(\frac{\phi}{M}\right)^2, \tag{2.4}$$

$$B(\phi) = B_0 \exp\left(\beta\frac{\phi}{\phi_0}\right). \tag{2.5}$$

B_0 and β are free parameters for the disformal coupling. ϕ_0 is a normalization constant chosen to be the vacuum expectation value of the field $\phi_0 \equiv \frac{\mu}{\sqrt{\lambda}}$. The symmetron mass scale M is a free parameter, deciding the interaction strength of the conformal coupling.

This specific choice of A, B, and V essentially gives a symmetron model with an additional non-symmetric disformal term described by the exponential $B(\phi)$, meaning that the model should reduce to the already well studied symmetron model when setting $B_0 = 0$. Hopefully the conformally coupled symmetron part of the equations will be dominating, and turning up the disformal part step by step will show how these parts interact.

Both the existence of a conformal term A and a disformal term B can lead to screening effects, see [64] and [25] respectively.

2.2 Assumptions

The main assumptions that will be used in this thesis are:

1. ϕ is a canonical massless field with Lagrangian density $\mathcal{L}_\phi = -\frac{1}{2}\partial^\mu\phi\partial_\mu\phi - V(\phi)$.

2. All matter is nonrelativistic shearless and pressureless matter, namely cold dark matter. This means that the energy-momentum tensor simply is given by $T_{\mathrm{m}}^{\mu\nu} = \mathrm{diag}(\rho, 0, 0, 0)$. Most observations indicate that dark matter is cold, and that it has multiple times more mass than baryonic matter. This should not be a too bad assumption for a first study.

3. We are working on large scales, and with nonrelativistic, shearless, and pressureless matter. The metric can therefore be set to the linearly perturbed flat FLRW metric, also called the conformal Newtonian gauge [71]. The line element is given by $\mathrm{d}s^2 = -(1+2\Psi)\,\mathrm{d}t^2 + a^2(t)(1-2\Psi)\left(\mathrm{d}x^2 + \mathrm{d}y^2 + \mathrm{d}z^2\right)$. Note that the time and space perturbations are assumed equal, and in the nonrelativistic limit the perturbation Ψ is equal to the Newtonian gravitational potential.

4. The Newtonian gravitational potential is negligible on the scales we are interested in, $|\Psi| \ll 1$. This means the approximation $(1 + \mathcal{O}(\Psi)) = 1$ is safe in the last step of derivations*.

5. Assuming matter moves slowly, it follows from assumption 4 that the gravitational field varies very slowly in time, namely $\left|\dot{\Psi}\right| \approx 0$. This is called the quasistatic approximation.

Notice that we do not assume the quasistatic approximation for the scalar field ϕ. This is because the symmetron field oscillates in a potential, and the non-static terms might

*This is true as long as the main volume of the scalar field is not too close to a neutron star or a black hole, where the zeroth order assumption that $1+\mathcal{O}(\Psi) = 1$ – and even the first order perturbation of the metric – will break down. As an example, let us look at the supermassive black hole at the centre of the Milky Way, with $M_{\mathrm{bh}} = 4.1 \cdot 10^6 M_\odot$ [72]. The dimensionless Newtonian potential is given by $\Psi = -G_\odot M/r$, meaning that in the extreme case – to have $(1+\Psi) = 1$ within 1 % accuracy – one needs a distance of at least $r > G_\odot M/0.01 \approx 2 \cdot 10^{-5}$ pc, which is just over 4 astronomical units. Anything smaller than solar system scale is completely irrelevant for cosmological purposes, but might of course be important to consider when doing solar system tests of modified gravity. This assumption will in addition be checked numerically in section 4.5.

contribute even in the symmetron case [39]. Moreover, the time derivatives of the field are especially important in disformal theory, where the fifth force is expected to be proportional to the double time derivative of ϕ (see equation 1.31).

2.3 The equation of motion for the scalar field

The resulting equation of motion for the field after varying the action (2.1) with respect to ϕ is in general given by

$$\mathcal{M}^{\mu\nu}\nabla_\mu\nabla_\nu\phi + \frac{A}{A-2BX}\mathcal{Q}_{\mu\nu}T^{\mu\nu} + \mathcal{V} = 0, \tag{2.6}$$

where

$$\mathcal{M}^{\mu\nu} = \mathcal{L}_{\phi,X}g^{\mu\nu} + \mathcal{L}_{\phi,XX}\phi^{,\mu}\phi^{,\nu} - \frac{B}{A-2BX}T_m^{\mu\nu}, \tag{2.7}$$

$$\mathcal{Q}_{\mu\nu} = \frac{A_{,\phi}}{2A}g_{\mu\nu} + \left(\frac{A_{,\phi}B}{A^2} - \frac{B_{,\phi}}{2A}\right)\phi_{,\mu}\phi_{,\nu}, \tag{2.8}$$

$$X \equiv -\frac{1}{2}\left(\nabla^\mu\phi\right)\left(\nabla_\mu\phi\right) = -\frac{1}{2}g^{\mu\nu}\phi_{,\mu}\phi_{,\nu}, \tag{2.9}$$

$$\mathcal{V} = \mathcal{L}_{\phi,\phi} + 2X\mathcal{L}_{\phi,X\phi}. \tag{2.10}$$

This formula is taken from the paper [25], and will be the starting point for finding a more tangible equation of motion for the specific model given here.

The assumed canonical field with $\mathcal{L}_\phi = X - V(\phi)$, means that $\mathcal{L}_{\phi,X} = 1$, $\mathcal{L}_{\phi,XX} = \mathcal{L}_{\phi,X\phi} = 0$. This simplifies the following symbols:

$$\mathcal{M}^{\mu\nu} = g^{\mu\nu} - \frac{B}{A-2BX}T_m^{\mu\nu} \tag{2.11}$$

$$\mathcal{V} = -V_{,\phi}. \tag{2.12}$$

The insertion and calculation of the specific equation of motion is done in appendix B. The resulting equation of motion for ϕ is given by

$$\begin{aligned}\left(-1+2\Psi - \frac{B}{A-2BX}\rho\right)\ddot{\phi} + \frac{1}{a^2}\left(1+2\Psi\right)\sum_{i=1,2,3}\phi_{,ii} + \frac{B}{A-2BX}\frac{\rho}{a^2}\sum_{i=1,2,3}\Psi_{,i}\phi_{,i} \\ -3H\left(1-2\Psi\right)\dot{\phi} + \frac{A}{A-2BX}\left(-\left(1+2\Psi\right)\frac{A_{,\phi}}{2A} + \left(\frac{A_{,\phi}B}{A^2} - \frac{B_{,\phi}}{2A}\right)\dot{\phi}^2\right)\rho - V_{,\phi} = 0.\end{aligned} \tag{2.13}$$

One can now further simplify the expression in equation (2.13) by assuming that $(1+\Psi) = 1$. This should drastically reduce the amount of computational operations needed in the code while still keeping enough accuracy for the purpose of this thesis. It will be useful to introduce the shorthand notation

$$\gamma^2 = \frac{B}{A-2BX}. \tag{2.14}$$

Now the equation of motion for any A, B, and V in the conformal Newtonian gauge is given by

$$\left(1+\gamma^2\rho\right)\ddot{\phi}+3H\dot{\phi}-\frac{1}{a^2}\nabla^2\phi= \tag{2.15}$$
$$\gamma^2\rho\left(\frac{A_{,\phi}\left(\phi\right)}{A\left(\phi\right)}\dot{\phi}^2-\frac{B_{,\phi}\left(\phi\right)}{2B\left(\phi\right)}\dot{\phi}^2-\frac{A_{,\phi}\left(\phi\right)}{2B\left(\phi\right)}+\frac{1}{a^2}\sum_{i=1,2,3}\Psi_{,i}\phi_{,i}\right)-V_{,\phi}\left(\phi\right).$$

2.3.1 Inserting A, B, and V

We can already now insert the expressions for A, B, and V that will be used, namely

$$A\left(\phi\right)=1+\left(\frac{\phi}{M}\right)^2, \tag{2.16}$$
$$A_{,\phi}\left(\phi\right)=2\frac{\phi}{M^2}, \tag{2.17}$$
$$B\left(\phi\right)=B_0\exp\left(\beta\frac{\phi}{\phi_0}\right), \tag{2.18}$$
$$B_{,\phi}\left(\phi\right)=\frac{\beta}{\phi_0}B\left(\phi\right), \tag{2.19}$$
$$V\left(\phi\right)=-\frac{1}{2}\mu^2\phi^2+\frac{1}{4}\lambda\phi^4+V_0, \tag{2.20}$$
$$V_{,\phi}\left(\phi\right)=-\mu^2\phi+\lambda\phi^3. \tag{2.21}$$

This means that the specific equation of motion is

$$\left(1+\gamma^2\rho\right)\ddot{\phi}+3H\dot{\phi}-\frac{1}{a^2}\nabla^2\phi=\gamma^2\rho\left(\frac{2\phi}{M^2+\phi^2}-\frac{\beta}{2\phi_0}\right)\dot{\phi}^2 \tag{2.22}$$
$$-\frac{\rho\phi}{M^2}\left(\frac{\gamma^2}{B_0\exp\left(\beta\frac{\phi}{\phi_0}\right)}\right)+\mu^2\phi-\lambda\phi^3,$$

where, fully written out, γ^2 is given by

$$\gamma^2=\frac{B_0\exp\left(\beta\frac{\phi}{\phi_0}\right)}{1+\left(\frac{\phi}{M}\right)^2+B_0\exp\left(\beta\frac{\phi}{\phi_0}\right)g^{\mu\nu}\phi_{,\mu}\phi_{,\nu}}. \tag{2.23}$$

The term $\frac{1}{a^2}\sum_{i=1,2,3}\Psi_{,i}\phi_{,i}$ from equation (2.15) is omitted for now, because this gradient is difficult to interpret analytically. The term will be kept when doing the numerical analysis later.

On this form, the equation of motion (2.22) is not very useful; it simply has too many terms to understand intuitively, and it is not optimized for insertion into the N-body code. However, one can make some predictions about the behaviour of the disformal field in three special cases.

2.3.2 Analytical considerations in three special cases

The symmetron limit

The symmetron limit is equivalent to taking $\beta = B_0 = 0$. In the term with γ^2/B_0 one must first cancel B_0 in the numerator and denominator, then insert $B_0 = 0$ everywhere else. This results in the symmetron equation of motion

$$\ddot{\phi} + 3H\dot{\phi} - \frac{1}{a^2}\nabla^2\phi = -\frac{\rho\phi}{M^2}\left(\frac{1}{1+\left(\frac{\phi}{M}\right)^2}\right) + \mu^2\phi - \lambda\phi^3. \tag{2.24}$$

When assuming $1+(\phi/M)^2 = 1$*, the equation above reduces to exactly the equation of motion that is used in the paper [39], where the symmetron model is simulated without assuming the quasistatic approximation $\ddot{\phi} = \dot{\phi} = 0$.

The low density limit

There are two predictions that can be made about the behaviour of the scalar field in the disformal case, with $B_0 \neq 0$. First and simplest is the low density limit, which is equivalent to setting $\rho = 0$ in equation (2.22). In this case the equation becomes exactly the vacuum symmetron equation of motion

$$\ddot{\phi} + 3H\dot{\phi} - \frac{1}{a^2}\nabla^2\phi = \mu^2\phi - \lambda\phi^3. \tag{2.25}$$

From this one can expect that in the void far from dense galaxy cluster, the disformal field will behave like the symmetron field. The differences between these models should be more important on small scales.

A simple way to find the vacuum expectation value ϕ_0, is to see where the field has no acceleration when assuming no velocity and no gradient. $\ddot{\phi} = \dot{\phi} = \nabla^2\phi = 0$ gives the following equation for the stationary points ϕ_{SP} of the effective potential:

$$\mu^2\phi_{\mathrm{SP}} - \lambda\phi_{\mathrm{SP}}^3 = 0. \tag{2.26}$$

One solution is $\phi_{\mathrm{SP}} = 0$, but this solution is unstable since the potential has a local maximum there. The other two solutions are the stable minima of the potential, given by $\phi_{\mathrm{SP}} = \pm\mu/\sqrt{\lambda}$. This is the reason for defining the "vacuum expectation value" of the field $\phi_0 \equiv \mu/\sqrt{\lambda}$.

The high density limit

The last special case is the high density limit, where one can assume that $\rho \to \infty$, and therefore ignore all terms without ρ in equation (2.22). After dividing by $\gamma^2\rho$ on both sides one finds

$$\ddot{\phi} = \left(\frac{2\phi}{M^2+\phi^2} - \frac{\beta}{2\phi_0}\right)\dot{\phi}^2 - \frac{\phi}{B_0 \exp\left(\beta\frac{\phi}{\phi_0}\right) M^2} \tag{2.27}$$

*This is actually a good approximation in the symmetron case, see section 4.5.

In this case, assuming $\dot{\phi}$ is small enough that one safely can take $\dot{\phi}^2 \approx 0$, one finds a stable attractor at $\phi = 0$. Unlike in the symmetron case, however, this attractor will not behave exactly like a symmetric harmonic oscillator. The terms with β makes the effective potential asymmetric.

Consider the exponential factor in the denominator of the last term of equation (2.27). For positive ϕ, the exponential will be larger than one, and the acceleration term $\ddot{\phi}$ will become smaller than if ϕ was negative. This means that at a negative displacement $\phi = -\epsilon$, there will be a stronger acceleration towards $\phi = 0$ than at a positive displacement of the same magnitude $\phi = +\epsilon$. This effect gives a net positive acceleration for the disformal field in high density areas. However, the term $-\beta\dot{\phi}^2/(2\phi_0)$ gives a net negative acceleration when the time derivative of the field is not negligible. Telling which of these effects – if any – that will dominate, is difficult at this point.

2.4 The equation of motion, arranged for the computer

2.4.1 Dimensionless definition of the field

For computational convenience, the field is normalized to the vacuum expectation value of the field,

$$\phi_0 \equiv \frac{\mu}{\sqrt{\lambda}}. \tag{2.28}$$

The new dimensionless field $\chi = \phi/\phi_0$ should keep in the range $\mathcal{O}(\pm 1)$, at least for a symmetron-dominated case when B_0 is small. We introduce the parameter a_{SSB}, defining the expansion factor at spontaneous symmetry breaking, assuming a conformally coupled field and a uniform matter distribution [39]. Furthermore, we define the density of spontaneous symmetry breaking

$$\rho_{\mathrm{SSB}} \equiv M^2\mu^2 = \frac{\rho_{0(z=0)}}{a_{\mathrm{SSB}}^3}, \tag{2.29}$$

a dimensionless symmetron coupling constant

$$\theta \equiv \frac{\phi_0 M_{\mathrm{Pl}}}{M^2}, \tag{2.30}$$

the symmetron range

$$\lambda_0 \equiv \frac{1}{\sqrt{2}\mu}, \tag{2.31}$$

and finally, the dimensionless disformal coupling constant

$$b_0 = B_0 H_0^2 M_{\mathrm{Pl}}^2. \tag{2.32}$$

$M_{\mathrm{Pl}} = 1/\sqrt{8\pi G}$ is the Planck mass in natural units. The average matter density ρ_0 at redshift zero for a flat universe, found from the Friedmann equations [73], is

$$\rho_{0(z=0)} = \Omega_0\rho_c = 3\Omega_0 H_0^2 M_{\mathrm{Pl}}^2. \tag{2.33}$$

These definitions will yield practical parameters, where θ and a_{SSB} are dimensionless and have values around 1; and λ_0 has units of length, usually around 1 Mpc [40]. All relevant parameters will be summarized and explained in subsection 3.1.

Realizing that $V_{,\phi}(\phi) = \left(\frac{\partial\chi}{\partial\phi}\right) V_{,\chi}(\chi) = \frac{1}{\phi_0} V_{,\chi}(\chi)$, then inserting $\phi = \chi\phi_0$ and dividing by ϕ_0 in the equation of motion (2.15), gives the general disformal equation of motion for the dimensionless field χ,

$$\left(1+\gamma^2\rho\right)\ddot{\chi} + 3H\dot{\chi} - \frac{1}{a^2}\nabla^2\chi = \gamma^2\rho\left(\frac{A_{,\chi}(\chi)}{A(\chi)}\dot{\chi}^2 - \frac{B_{,\chi}(\chi)}{2B(\chi)}\dot{\chi}^2 - \frac{A_{,\chi}(\chi)}{2\phi_0^2 B(\chi)}\right) - \frac{V_{,\chi}(\chi)}{\phi_0^2}. \tag{2.34}$$

Using the dimensionless system introduced here, some useful relations can be found from simple algebra, namely

$$M^2 = \frac{\rho_{0(z=0)}}{\mu^2 a_{\mathrm{SSB}}^3}, \tag{2.35}$$

$$M^2 = \frac{6\Omega_0 H_0^2 M_{\mathrm{Pl}}^2 \lambda_0^2}{a_{\mathrm{SSB}}^3}, \tag{2.36}$$

$$\lambda = \frac{\mu^2}{\phi_0^2}, \tag{2.37}$$

$$\phi_0 = \theta\frac{M^2}{M_{\mathrm{Pl}}} = \frac{6\theta\Omega_0 H_0^2 M_{\mathrm{Pl}}\lambda_0^2}{a_{\mathrm{SSB}}^3}. \tag{2.38}$$

It already seems convenient to use a constant

$$\zeta \equiv \frac{3\Omega_0 H_0^2 \lambda_0^2}{a_{\mathrm{SSB}}^3}, \tag{2.39}$$

to shorten equations. Notice specifically that this means

$$M^2 = 2M_{\mathrm{Pl}}^2\zeta. \tag{2.40}$$

With these new definitions for the dimensionless field χ, one gets the following expressions for A, B, V, and their derivatives :

$$A(\chi) = 1 + 2\theta^2\zeta\chi^2, \tag{2.41}$$

$$A_{,\chi}(\chi) = 4\theta^2\zeta\chi, \tag{2.42}$$

$$B(\chi) = \frac{b_0}{H_0^2 M_{\mathrm{Pl}}^2}\exp(\beta\chi), \tag{2.43}$$

$$B_{,\chi}(\chi) = \beta B(\chi), \tag{2.44}$$

$$V(\chi) = -\frac{1}{2}\mu^2\phi_0^2\chi^2 + \frac{1}{4}\lambda\phi_0^4\chi^4 + V_0, \tag{2.45}$$

$$V_{,\chi}(\chi) = -\frac{\phi_0^2}{2\lambda_0^2}\chi + \frac{\phi_0^2}{2\lambda_0^2}\chi^3. \tag{2.46}$$

Notice how because of the definition of μ and λ, one has in the expression for V that

$$\lambda\phi_0^4 = \mu^2\phi_0^2 = \frac{\phi_0^2}{2\lambda_0^2}. \tag{2.47}$$

The equation of motion for the dimensionless field, equation (2.34), with these expressions inserted, now becomes

$$\begin{aligned}&\left(1+\gamma^2\rho\right)\ddot{\chi} + 3H\dot{\chi} - \frac{1}{a^2}\nabla^2\chi = \\ &\gamma^2\rho\left(\frac{4\theta^2\zeta}{A\left(\phi\right)}\chi\dot{\chi}^2 - \frac{\beta}{2}\dot{\chi}^2 - \frac{1}{2\zeta B\left(\phi\right)M_{\mathrm{Pl}}^2}\chi + \frac{1}{a^2}\sum_{i=1,2,3}\Psi_{,i}\chi_{,i}\right) + \left(\chi-\chi^3\right)\frac{1}{2\lambda_0^2}.\end{aligned} \tag{2.48}$$

2.4.2 Supercomoving time

What remains before we can insert equation (2.48) into Isis/Ramses is a switch to supercomoving time – the time variable used by Ramses, defined by [74] – and to split this second order differential equation of motion into a set of two coupled first order differential equations. Supercomoving time τ is related to the cosmic time t by $\mathrm{d}\tau = \frac{1}{a^2}\mathrm{d}t$. All primes in this thesis denote derivatives with respect to supercomoving time $' \equiv \frac{\partial x}{\partial\tau}$. The transformation of time derivatives is done through the relations

$$\frac{\mathrm{d}}{\mathrm{d}t} = \frac{1}{a^2}\frac{\mathrm{d}}{\mathrm{d}\tau}, \tag{2.49}$$

$$\frac{\mathrm{d}^2}{\mathrm{d}t^2} = \frac{1}{a^4}\left(\frac{\mathrm{d}^2}{\mathrm{d}\tau^2} - 2\tilde{H}\frac{\mathrm{d}}{\mathrm{d}\tau}\right). \tag{2.50}$$

Supercomoving variables (marked with tilde) are defined by

$$\tilde{H} \equiv \frac{a'}{a} = a^2H, \tag{2.51}$$

$$\tilde{\Psi} \equiv a^2\Psi. \tag{2.52}$$

Just substituting these relations into the equation (2.48) gives

$$\begin{aligned}&\left(1+\gamma^2\rho\right)\frac{1}{a^4}\left(\frac{\mathrm{d}^2}{\mathrm{d}\tau^2}\chi - 2\tilde{H}\frac{\mathrm{d}}{\mathrm{d}\tau}\chi\right) + 3H\frac{1}{a^2}\frac{\mathrm{d}}{\mathrm{d}\tau}\chi - \frac{1}{a^2}\nabla^2\chi = \\ &\gamma^2\rho\left(\left[\frac{4\theta^2\zeta}{A}\chi - \frac{\beta}{2}\right]\left(\frac{1}{a^2}\frac{\mathrm{d}}{\mathrm{d}\tau}\chi\right)^2 - \frac{1}{2\zeta BM_{\mathrm{Pl}}^2}\chi + \frac{1}{a^4}\sum_{i=1,2,3}\tilde{\Psi}_{,i}\chi_{,i}\right) + \left(\chi-\chi^3\right)\frac{1}{2\lambda_0^2}.\end{aligned} \tag{2.53}$$

Multiplying this by a^4 and isolating χ'' on the left hand side gives

$$\begin{aligned}\chi'' =& \frac{1}{1+\gamma^2\rho} \times \Bigg\{ -3\tilde{H}\chi' + \left(1+\gamma^2\rho\right) 2\tilde{H}\chi' + a^2\nabla^2\chi \\ &+\gamma^2\rho \left(\left[\frac{4\theta^2\zeta}{A}\chi - \frac{\beta}{2}\right] \left(\chi'\right)^2 - \frac{a^4}{2\zeta B M_{\mathrm{Pl}}^2}\chi + \sum_{i=1,2,3} \tilde{\Psi}_{,i}\chi_{,i} \right) + \left(\chi - \chi^3\right) \frac{a^4}{2\lambda_0^2} \Bigg\}. \end{aligned} \tag{2.54}$$

The variable q is now introduced to represent the time derivative of the field by defining $q = a\chi'$, which results in $q' = a'\chi' + a\chi''$. This choice of q gives a cancellation of $\tilde{H}q$ in the equation for q'. We end up with this set of two first order differential equations in q and χ:

$$\chi' = \frac{q}{a} \tag{2.55}$$

$$\begin{aligned} q' =& \frac{1}{1+\gamma^2\rho} \times \Bigg\{ a^3\nabla^2\chi + \gamma^2\rho \left(3\tilde{H}q + \left[\frac{4\theta^2\zeta}{A}\chi - \frac{\beta}{2}\right] \frac{q^2}{a} + a \sum_{i=1,2,3} \tilde{\Psi}_{,i}\chi_{,i} \right) \\ &- \frac{1}{A - 2BX} \frac{a^5}{2\zeta M_{\mathrm{Pl}}^2}\rho\chi + \left(1-\chi^2\right) \frac{a^5}{2\lambda_0^2}\chi \Bigg\}. \end{aligned} \tag{2.56}$$

Here one term has been extracted from the $\gamma^2\rho$-bracket to cancel factors of B in the numerator and denominator. This system of differential equations can readily be solved by the leapfrog scheme, which is already implemented in the non-static version of Isis/Ramses [39], as shown in the subsection 1.7.4.

2.5 The geodesic equation

As already stated in section 1.6, the disformal geodesics are given by the general equation

$$\ddot{x}^\mu + \bar{\Gamma}^\mu_{\alpha\beta}\dot{x}^\alpha\dot{x}^\beta = 0. \tag{2.57}$$

Since we are studying nonrelativistic dark matter with $v \ll c$, the proper time for a particle goes as cosmic time $\mathrm{d}s = \mathrm{d}t$, and therefore $\dot{x}^0 = 1$. Neglecting quadratic terms in the velocity, the geodesic equation can be simplified to

$$\ddot{x}^i + \bar{\Gamma}^i_{00} + 2\bar{\Gamma}^i_{j0}\dot{x}^j = 0. \tag{2.58}$$

The calculations of the necessary Jordan frame Christoffel symbols $\bar{\Gamma}^i_{00}$ and $\bar{\Gamma}^i_{j0}$ are done in Appendix C.

2.5.1 The resulting geodesic equation

The full nonrelativistic equation of motion (2.58) to first order in Ψ with both Jordan frame Christoffel symbols inserted becomes

$$\begin{aligned}
&\ddot{x}^i + \frac{\Psi_{,i}}{a^2} - \frac{2}{Aa^2}\frac{\phi\phi_{,i}\dot{\phi}^2}{M^2}\gamma^2\left(1+2\Psi\right) + \frac{1}{a^2}\left(1+4\Psi\right)\frac{\phi\phi_{,i}}{M^2}\frac{1}{A-2BX} \\
&+\frac{\left(1+2\Psi\right)\phi_{,i}}{a^2}\left(\ddot{\phi} - \frac{1}{a^2}\sum_{j=1,2,3}\Psi_{,j}\phi_{,j}\right)\gamma^2 + \frac{1}{2}\frac{\left(1+2\Psi\right)}{a^2}\frac{\beta}{\phi_0}\gamma^2\dot{\phi}^2\phi_{,i} \\
+2\Bigg[&H\delta^i_j - \gamma^2\frac{1}{a^2}\frac{\phi}{AM^2}\phi_{,i}\phi_{,j}\dot{\phi}\left(1+2\Psi\right) + \frac{1}{a^2}\left(1+2\Psi\right)\phi_{,i}\left(\phi_{,j0} - H\phi_{,j} - \Psi_{,j}\dot{\phi}\right)\gamma^2 \\
&+\frac{1}{2a^2}\left(1+2\Psi\right)\frac{\beta}{\phi_0}\dot{\phi}\phi_{,i}\phi_{,j}\gamma^2 + \frac{\phi\dot{\phi}}{AM^2}\left(\delta^i_j - \frac{1}{a^2}\gamma^2\phi_{,i}\phi_{,j}\left(1+2\Psi\right)\right)\Bigg]\dot{x}^j = 0.
\end{aligned} \tag{2.59}$$

Taking the approximation $(1+2\Psi) = 1$, this results in the more compact disformal geodesic equation

$$\begin{aligned}
&\ddot{x}^i + \frac{\Psi_{,i}}{a^2} - \frac{2}{AM^2a^2}\gamma^2\phi\phi_{,i}\dot{\phi}^2 + 2\left(H + \frac{\phi\dot{\phi}}{AM^2}\right)\dot{x}^i \\
&+\frac{1}{a^2}\gamma^2\left(\ddot{\phi} - \frac{1}{a^2}\sum_{k=1,2,3}\Psi_{,k}\phi_{,k} + \frac{1}{2}\frac{\beta}{\phi_0}\dot{\phi}^2\right)\phi_{,i} \\
&+2\frac{1}{a^2}\gamma^2\left(\dot{\phi}_{,j} - H\phi_{,j} - \Psi_{,j}\dot{\phi} + \frac{\beta}{2\phi_0}\dot{\phi}\phi_{,j}\right)\phi_{,i}\dot{x}^j \\
&+\frac{1}{M^2a^2}\frac{1}{A-2BX}\phi\phi_{,i} - 4\gamma^2\frac{\phi}{a^2AM^2}\phi_{,i}\phi_{,j}\dot{\phi}\dot{x}^j = 0.
\end{aligned} \tag{2.60}$$

This equation fully describes how nonrelativistic particles move through curved spacetime in disformal symmetron gravity*. However, just like for the equation of motion, it is difficult to say anything about the expression intuitively, and it is not yet ready for implementation into the code; it still needs a switch to the dimensionless field and supercomoving time variables. One can at this stage recognize the acceleration terms associated with perturbed FLRW geodesics in standard gravity, namely

$$\ddot{x}^i + \frac{\Psi_{,i}}{a^2} + 2H\dot{x}^i = 0, \tag{2.61}$$

where the second term is the standard acceleration due to Newtonian gravity, and the third term is the Hubble friction. All the other terms in equation (2.60) are due to the disformal theory of gravity.

*As long as they are not close to a black hole or a neutron star, of course.

2.5.2 Changing to supercomoving time and the dimensionless field definition

Switching to supercomoving time $\mathrm{d}\tau = \frac{1}{a^2}\mathrm{d}t$, the geodesic equation becomes,

$$\begin{aligned}\frac{1}{a^4}\left(\frac{\mathrm{d}^2}{\mathrm{d}\tau^2} - 2\tilde{H}\frac{\mathrm{d}}{\mathrm{d}\tau}\right)x^i + \frac{\tilde{\Psi}_{,i}}{a^4} - \frac{2}{AM^2a^6}\gamma^2\phi\phi_{,i}\left(\frac{\mathrm{d}\phi}{\mathrm{d}\tau}\right)^2 + \frac{2}{a^4}\left(\tilde{H} + \frac{\phi}{AM^2}\frac{\mathrm{d}\phi}{\mathrm{d}\tau}\right)\frac{\mathrm{d}x^i}{\mathrm{d}\tau} \\ + \frac{1}{a^6}\gamma^2\left(\left(\frac{\mathrm{d}^2}{\mathrm{d}\tau^2} - 2\tilde{H}\frac{\mathrm{d}}{\mathrm{d}\tau}\right)\phi - \sum_{k=1,2,3}\tilde{\Psi}_{,k}\phi_{,k} + \frac{1}{2}\frac{\beta}{\phi_0}\left(\frac{\mathrm{d}\phi}{\mathrm{d}\tau}\right)^2\right)\phi_{,i} \\ + \frac{2}{a^6}\gamma^2\left(\frac{\mathrm{d}\phi_{,j}}{\mathrm{d}\tau} - \tilde{H}\phi_{,j} - \frac{1}{a^2}\tilde{\Psi}_{,j}\frac{\mathrm{d}\phi}{\mathrm{d}\tau} + \frac{\beta}{2\phi_0}\frac{\mathrm{d}\phi}{\mathrm{d}\tau}\phi_{,j}\right)\phi_{,i}\frac{\mathrm{d}x^j}{\mathrm{d}\tau} \\ + \frac{1}{M^2a^2}\frac{1}{A-2BX}\phi\phi_{,i} - 4\gamma^2\frac{\phi}{a^6AM^2}\phi_{,i}\phi_{,j}\frac{\mathrm{d}\phi}{\mathrm{d}\tau}\frac{\mathrm{d}x^j}{\mathrm{d}\tau} = 0.\end{aligned} \tag{2.62}$$

Simplifying this equation and grouping together similar terms, one finds

$$\begin{aligned}x^{i\prime\prime} + \tilde{\Psi}_{,i} + \frac{2\phi}{AM^2}\phi' x^{i\prime} + \frac{a^2}{M^2}\frac{1}{A-2BX}\phi\phi_{,i} \\ + \left\{\frac{\gamma^2}{a^2}\left(\phi'' - 2\tilde{H}\phi' - \sum_{k=1,2,3}\tilde{\Psi}_{,k}\phi_{,k} - \frac{2}{AM^2}\phi\left(\phi'\right)^2 + \frac{\beta}{2\phi_0}\left(\phi'\right)^2\right)\right\}\phi_{,i} \\ + \frac{2}{a^2}\gamma^2\left(\phi'_{,j} - \tilde{H}\phi_{,j} - \frac{1}{a^2}\tilde{\Psi}_{,j}\phi' + \frac{\beta}{2\phi_0}\phi'\phi_{,j} - \frac{2\phi}{AM^2}\phi_{,j}\phi'\right)\phi_{,i}x^{j\prime} = 0.\end{aligned} \tag{2.63}$$

Notice that the supercomoving coordinates automatically incorporate the Hubble friction; in general relativity the supercomoving version of equation (2.61) would simply read $x^{i\prime\prime} = -\tilde{\Psi}_{,i}$.

Using the definition for the dimensionless field $\chi = \phi/\phi_0$, $\chi'' = \frac{1}{a}\left(q' - \tilde{H}q\right)$ and $\chi' = q/a$, leads to the following equation for particle motion:

$$\begin{aligned}x^{i\prime\prime} + \tilde{\Psi}_{,i} + \frac{4\zeta\theta^2}{1+2\zeta\theta^2\chi^2}\frac{1}{a}\chi q x^{i\prime} + 2\theta^2\zeta\frac{a^2}{A-2BX}\chi\chi_{,i} \\ + 2\theta^2\zeta\left\{\frac{2\zeta\gamma^2M_{\mathrm{Pl}}^2}{a^4}\left(a\left[q' - 3\tilde{H}q - a\sum_{k=1,2,3}\tilde{\Psi}_{,k}\chi_{,k}\right] + \left(\beta - \frac{4}{A}\theta^2\chi\right)\zeta q^2\right)\right\}\chi_{,i} \\ + \frac{8\theta^2\zeta^2}{a^3}\left(\gamma^2M_{\mathrm{Pl}}^2\right)\left(q_{,j} - a\tilde{H}\chi_{,j} + \left[\frac{\beta}{2}\chi_{,j} - \frac{1}{a^2}\tilde{\Psi}_{,j} - \frac{4}{A}\theta^2\zeta\chi\chi_{,j}\right]q\right)\chi_{,i}x^{j\prime} = 0.\end{aligned} \tag{2.64}$$

2.5.3 Fifth force for a stationary cold dark matter particle

It would be possible to implement the full equation (2.64) into an N-body code. However, this would both use a lot of computing power, and the results would be difficult to interpret due to the vast amount of terms that could give different effects. As a starting point for exploring disformal gravity we therefore choose to only study the disformal effects when ignoring all damping terms proportional to x'. This is equivalent to assuming that the massive cold dark matter particles move very slowly through the cosmic grid*.

To isolate the effect of the fifth force on a particle, the standard gravity term can be separated from the fifth force terms,

$$x^{i\prime\prime} = -\tilde{\Psi}_{,i} + x^{\prime\prime i}_{\text{fifth}}. \tag{2.65}$$

The resulting acceleration in supercomoving time, due to the fifth force of disformal gravity, is given by

$$x^{\prime\prime i}_{\text{fifth}} = -\frac{2\theta^2\zeta}{A + B\cdot(\partial\phi)^2}\times \left\{ a^2\chi + \frac{2\zeta}{a^4}\frac{b_0\exp(\beta\chi)}{H_0^2}\left(a\left[q' - 3\tilde{H}q - a\sum_{k=1,2,3}\tilde{\Psi}_{,k}\chi_{,k}\right] + \left[\beta - \frac{4\theta^2\chi}{A}\right]\zeta q^2\right)\right\}\chi_{,i}. \tag{2.66}$$

Where the relation

$$\gamma^2 M_{\text{Pl}}^2 = \frac{b_0\exp(\beta\chi)}{H_0^2(A - 2BX)} \tag{2.67}$$

has been inserted. This expression for the fifth force is relatively simple to implement numerically, and if the particle velocities are small, this should be very close to the true fifth force due to the disformally coupled scalar field.

*This might not be a too bad approximation, as will be shown in section 5.4

Chapter 3

Parameters and algorithms used

In addition to implementing the disformal equations into Isis/Ramses, one must use a couple of other programs and scripts both for creating the initial particle distribution, and for analysing the final data. Here follows a short description of all parameters, software, and algorithms used in this study of disformal gravity.

3.1 Parameters

In all data preparations, simulations, and analyses, certain cosmological parameters are needed. All cosmological parameters used in this work are extracted from the Planck 2013 data best fit [9], and can be found in table 3.1.

The free model parameters are given and explained in table 3.2 on the following page. All model parameters except λ_0 are dimensionless. λ_0 and $a_{\rm SSB}$ are equivalent to the same parameters in symmetron papers like [39], and θ in this thesis is equivalent to what is often called β in these papers.

Cosmological Parameter	Value used
Matter density parameter Ω_m	0.3175
Dark energy density parameter Ω_Λ	0.6825
Hubble expansion factor H_0	67.11 km/s/Mpc
Hubble coefficient h	0.6711
Spectral index n_s	0.9624
Cluster abundance normalization σ_8	0.8344

Table 3.1: Cosmological parameters used in the simulations.

Symbol	Interpretation	Values used
θ	Strength factor for the fifth force	1
b_0	Disformal coupling strength	0, 1, 2
β	Disformal exponential factor	0, 1, 2
λ_0	Symmetron potential range	1 Mpc
a_{SSB}	Expansion factor of spontaneous symmetry breaking, assuming a uniform universe	0.5

Table 3.2: Model specific parameters for the disformal equations.

3.2 Initial particle and field distribution

The software GRAFIC1 from the package GRAFIC-2 is used to generate initial particle distribution from Gaussian random fields. The procedure is described in [75]. Note that all parameters used here are found by assuming standard gravity and ΛCDM when they are extracted from Planck data, and the same assumptions are used when GRAFIC computes the initial particle distributions. This is not a big problem because the early universe is screened, and should follow the evolution of ΛCDM closely. Consequently, the resulting particle distribution at early redshifts should stay unchanged. GRAFIC1 finds the transfer function $T(k)$ from an approximate analytical fit to the parameters chosen, and normalizes the power spectrum to σ_8. The random seed number 123456789 was used for GRAFIC to find the specific particle distributions used in this thesis.

The mass of each particle is simply $M = \rho_0 \cdot V_{\mathrm{box}}/N_{\mathrm{particles}}$, where ρ_0 is the average matter density at redshift zero, V_{box} is the volume of the simulation box, and $N_{\mathrm{particles}}$ is the amount of particles in the simulated volume. We let the measure for the box length $L_{\mathrm{Mpc}/h}$ (which is actually given in Mpc$/h$) be dimensionless. The particle number is typically given as a cubed number, $N_{\mathrm{particles}} = (N_{\mathrm{1d}})^3$. The average matter density in a flat universe is $\rho_0 = \Omega_m \rho_c$, which leads to a particle mass given by

$$M_{\mathrm{particle}} = \Omega_m \frac{3H_0^2}{8\pi G} \left(\frac{L_{\mathrm{Mpc}/h}}{h \cdot N_{\mathrm{1d}}} \,\mathrm{Mpc} \right)^3 . \tag{3.1}$$

Inserting all parameters and constants here gives the numerical value

$$M_{\mathrm{particle}} = 8.812 \cdot 10^{10} \cdot \left(\frac{L_{\mathrm{Mpc}/h}}{N_{\mathrm{1d}}} \right)^3 M_\odot/h, \tag{3.2}$$

for the mass of each particle in the simulation. In practice this means that every point particle is comparable to a small galaxy in a typical simulation, with one particle per Mpc$/h$ of the grid.

The initial value of the dimensionless scalar field χ at the early time $a \approx 4 \cdot 10^{-2}$, was set to some small value drawn from a uniform random distribution with $\chi_0 \in [-10^{-13}, 10^{-13}]$. The scalar field was assigned a random, independent value from this distribution at each separate grid point. This procedure is tested in section 4.1 and found to be acceptable.

3.3 Finding the time average of the field

At any given point in space, the symmetron field oscillates noticeably over time [39]. It is therefore necessary to do a time smoothing of the scalar field χ over multiple oscillations to achieve a mean field value at any point*. We choose the start of the time smoothing to be at expansion factor $a = 0.995$. The time average of χ^2 was also calculated, so that the standard deviation of the field value at any point could be found by using the formula

$$\sigma_\chi = \sqrt{\langle \chi^2 \rangle - \langle \chi \rangle^2}. \tag{3.3}$$

The lookback time to $a = 0.995$ is about 10^8 years, and it might be argued that this is a too long time for smoothing. Matter moving at peculiar velocities of 10^4 km/s could have moved a whole Mpc during this time. This is enough to move a particle from one grid box to another. We wanted to capture enough oscillations of the scalar field for a statistically significant average, and in section 5.4 we will show that the velocity of most particles are below 10^3 km/s. Haloes should therefore not be able to move more than a fraction of the grid resolution during this time.

3.4 Field profile and fifth force at redshift zero

The ROCKSTAR halo finder – described in [76] – is used to find the most massive dark matter halo in the redshift zero output from RAMSES/ISIS. A script plots the radial profile of the scalar field, where r is the distance from the centre of this halo. The script divides the distance from 0 to 20 Mpc/h into evenly spaced bins, and places each grid box in one of those bins according to its distance to the centre of the halo. For each bin i, the average of all n_i time averaged field values $\langle \chi \rangle$ at the same distance r_i from the halo centre is computed. The average of the standard deviation σ_χ of all the boxes in the bin is also found. This results in an average field value and an average field dispersion around the massive halo, as a function of distance from the halo centre.

Similarly, another script plots the absolute value of the acceleration due to the fifth force around the most massive halo at redshift zero, see equation (2.66).

*Otherwise, one could not have compared the redshift zero fields of two simulations, since the scalar field could have been in different phases of the oscillation in the two simulations.

The distances r are normalized to the *virial radius* of the halo. The virial radius is found in ROCKSTAR, and is defined by the radius from the halo centre within which the average density is 200 times the background density ρ_0. In mathematical terms, the definition of the virial radius r_{vir} is

$$\frac{\sum M}{\frac{4}{3}\pi r_{\text{vir}}^3} = 200\rho_0.$$

3.5 Halo mass function and power spectrum

The cumulative mass function is found by first sorting all haloes from the ROCKSTAR output by their virial mass, then numerize them from highest to lowest mass. The halo number is then plotted against the mass of that halo. This results in a graph with mass M on the x-axis, where the y-axis indicates how many haloes that exist with $M_{\text{halo}} \geq M$.

In this study, a C code is used for finding the power spectrum of the final density distribution. The code takes the Fourier transform of the density field to find $P(k)$, and corrects it for discreteness errors with the method described in [77].

Chapter 4

Cosmological tests

4.1 The importance of the initial field values

We were concerned that the amplitude of the initial field would have an impact on the final evolution of the scalar field. To check whether this was the case, the simulation was run without the fifth force geodesics, only including the equations of motion for the field. The simulation had 64^3 particles in a 64 Mpc/h box. The most massive halo was found to have a virial mass of $1.2 \cdot 10^{14}\, M_\odot/h$. The scalar field around this halo was compared for the cases where the field had initial values from the random uniform distribution $\chi_0 \in [-\varepsilon, \varepsilon]$, with $\varepsilon = 10^{-5}$, 10^{-7}, 10^{-10}, 10^{-13}, 10^{-15}, and 10^{-17}. As seen from figure 4.1, the field value at redshift zero does not significantly depend on the initial values of the field. For this reason it is safe to keep $\varepsilon = 10^{-13}$, and to use a uniform distribution (and not for instance a Gaussian distribution).

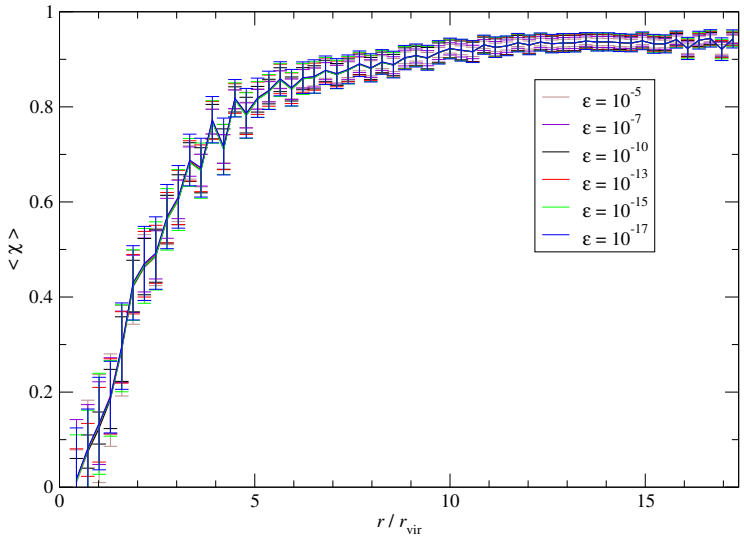

Figure 4.1: The figure shows the time averaged field profiles around a massive halo. The initial field values are drawn from a uniform distribution, $\chi_0 \in [-\varepsilon, \varepsilon]$.

4.2 Comparing the field evolution in the symmetron limit to the evolution in the symmetron code

Setting the disformal parameters such that $b_0 = \beta = 0$, $\theta = 1$, $\lambda_0 = 1\,\mathrm{Mpc}$, and $a_{\mathrm{SSB}} = 0.5$ turns off the disformal coupling, so that the model is equivalent to the symmetron model. The intent is to compare the simulation to a symmetron simulation with the code used in the paper [39], using the same parameters. Both codes are given the same initial particle distribution.

The comparison simulation consists of 128^3 particles in a box with side lengths of 64 Mpc/h. The field profiles for the two codes around the same massive halo (with virial mass $M = 2.5 \cdot 10^{14} M_\odot/h$) are very similar, with about 0.5 % difference in the centre of the halo, and less than 0.1 % difference outside one virial radius. See figure 4.2. This indicates that the symmetron part of the implemented field equation of motion is correct, and there should be no bugs related to this part.

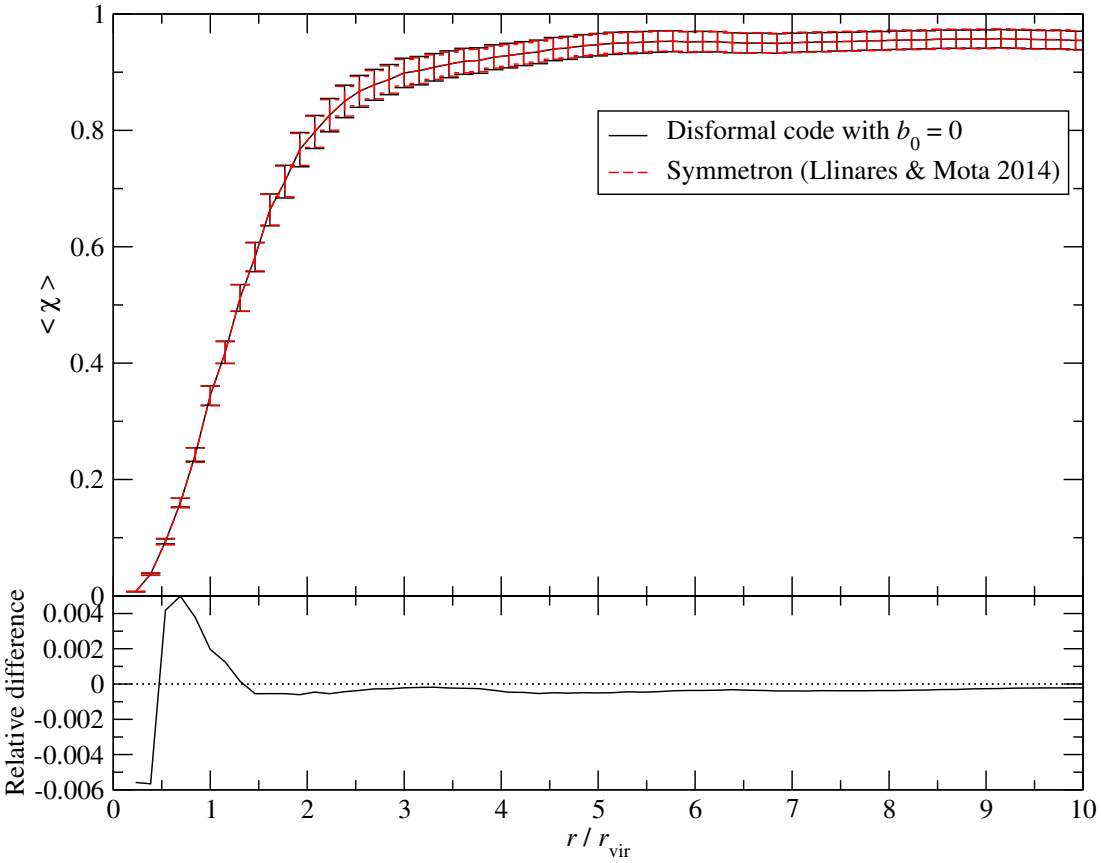

Figure 4.2: The figure shows the average field profile around a massive halo, for the symmetron code from [39] (red, dashed) and the disformal code with the disformal part turned off (black, solid). The lower panel of the graph shows the relative difference between the curves, which is less than 0.6 %.

4.3 Comparing the power spectrum in the symmetron limit to the symmetron code

After turning on the fifth forces, the power spectrum of the disformal code should be compared to the results from the symmetron code. The power spectra for the two different codes with the same parameters overlap very well. The relative difference between them is well below 0.35 % in all the simulated scales, as shown in figure 4.3. The simulations consisted of 128^3 particles in a box with side lengths of 64 Mpc/h. The initial conditions were identical.

A detail worth mentioning at this point is that the code from this study uses about three times more computing time than the symmetron code for a similarly sized simulation. This is of course both due to the fact that the disformal model is more complex* and due to the conservative use of simplifications. This leads to much more involved expressions for the equation of motion for the field and the fifth force geodesics – equations (2.55) and (2.66) respectively – than the corresponding equations used in the symmetron code [39].

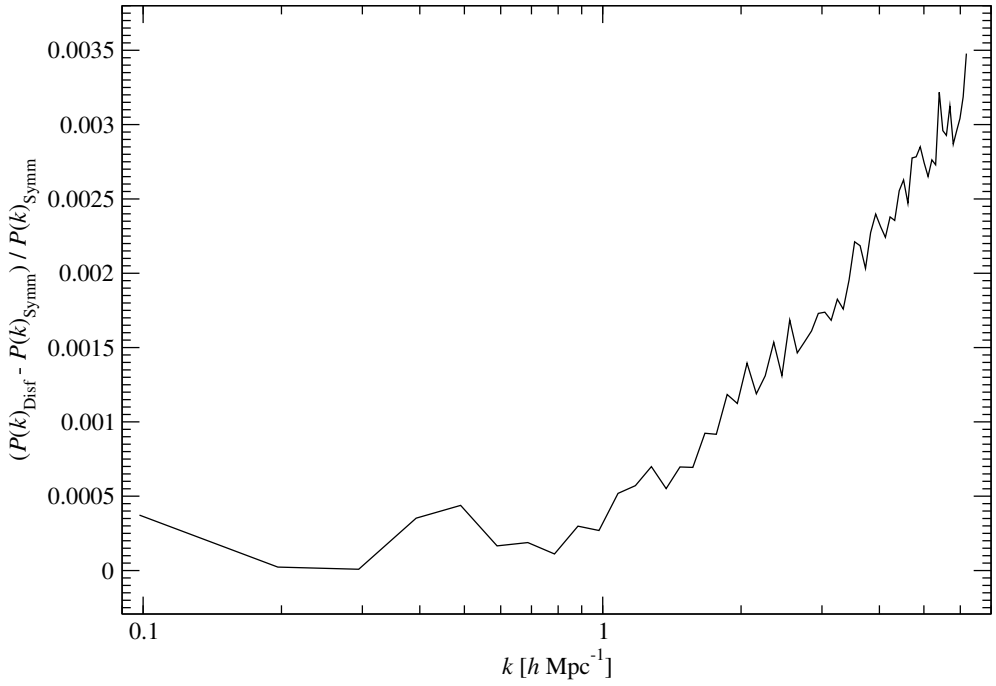

Figure 4.3: The figure shows the relative difference between the matter power spectra $P(k)$ for the disformal code, and from the symmetron code [39].

*When $b_0 = \beta = 0$, the disformal code still calculates all the terms with these factors included, even though the result is zero.

4.4 Errors in the power spectrum due to the lack of AMR

The disformal code presented here, and the non-static symmetron code from [39], both do not have refinements in their particle grids during a simulation. The great advantage of an N-body code like RAMSES is that it supports adaptive mesh refinement. However, grid refinement has proven to be very difficult to implement when including the time derivatives of the scalar fields. For the moment we unfortunately have to run simulations without refinements*. This of course leads to incorrect particle movements on small scales, which can be seen in the power specra from general relativity, shown in figure 4.4. In this plot, RAMSES was run assuming ΛCDM; once with, and once without grid refinements. It is evident that the refinements are important already around $k > 1h\,\mathrm{Mpc}^{-1}$, at smaller scales than this the error rises to above 10 %. This is for a grid of 128^3 cells in a 64 Mpc/h box, so one can expect that a grid of 256^3 cells with the same box size will give a valid power spectrum up to $k \approx 2h\,\mathrm{Mpc}^{-1}$.

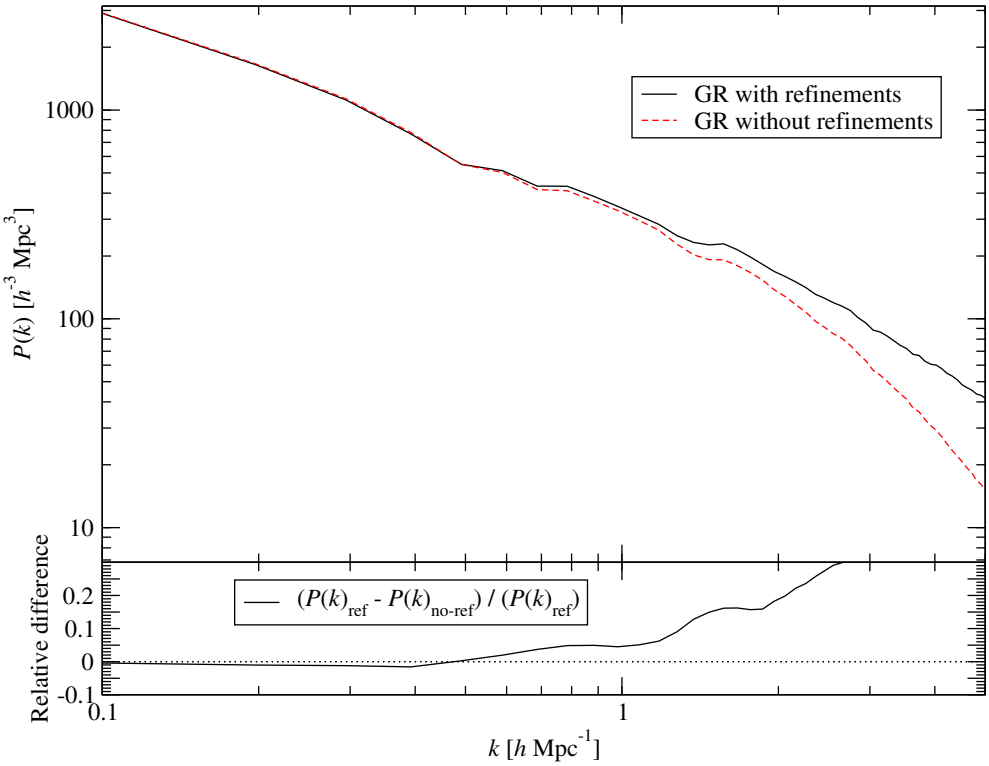

Figure 4.4: The figure shows the resulting matter power spectrum for ΛCDM. The black line, $P\,(k)_{\mathrm{no-ref}}$ results from a grid without refinements, and the red dashed line, $P\,(k)_{\mathrm{ref}}$ results from using AMR. The relative difference between $P\,(k)_{\mathrm{ref}}$ and $P\,(k)_{\mathrm{no-ref}}$ is plotted in the bottom panel.

*Implementing AMR in non-static simulations of scalar fields could be a nice mission for a PhD...

4.5 Testing some assumptions

At the end of a simulation with 128^3 particles and 64 Mpc/h box length, the code was set to output the maximum absolute value that the Newtonian potential Ψ has had in any of the grid cells, at any time; and also the value of $|\Psi|$ averaged over all values in the grid and all time steps. On average, the dimensionless Ψ had a value of around 10^{-6}, while the maximum value was about $5 \cdot 10^{-5}$, both of which are much less than 1. This means that the assumption that $(1 + \Psi) = 1$ is sufficiently accurate for this thesis, where an error of less than 1 % is considered good.

Dark matter haloes do not move very fast, and are the only things that could significantly change Ψ over time. This indicates that $\left|\dot{\Psi}\right|$ is also small, but we did not measure this explicitly, because RAMSES does not track the value of $\dot{\Psi}$.

The relative size of the term $\sum_{i=1,2,3} \Psi_{,i}\chi_{,i}$ is interesting. This term appears both in the equation of motion for the scalar field (2.54), and in the expression for the fifth force (2.66). At first the plan was to not include this term in the equations, but with no rigorous reason to neglect it, a test had to be performed. The result was that the term is on average small – a factor of 10^{-4} compared to the other terms in the equation of motion – but it does in some cases become dominant in the equation and should therefore *not* be omitted.

Additionally, we found that $1/A = 1$ is a good assumption in the symmetron case. To find this, we used the disformal code with symmetron parameters (i.e. $b_0 = \beta = 0$), using 128^3 particles in a box with side lengths 64 Mpc/h. We ran the code twice, but the second time we modified the equation of motion such that $1 + \left(\frac{\phi}{M}\right)^2 \to 1$ in the denominator of the symmetron equation of motion (2.24). This approximation is used in the symmetron code to which we are comparing [39], but it is not used in the final version of the disformal code. The field profile changes less than 10^{-4} % with this approximation, as seen in figure 4.5 on the next page. The effect is too small to account for the 0.5 % difference in the field profiles presented in section 4.2.

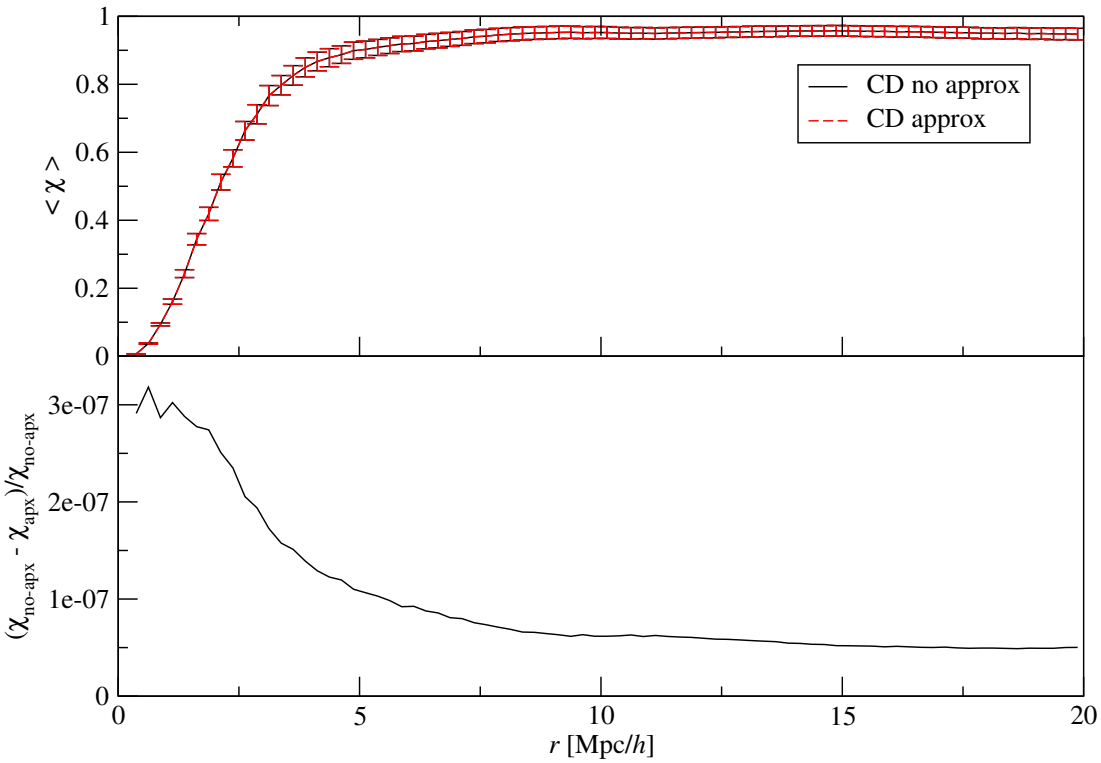

Figure 4.5: The figure shows the field profile around a massive halo, with the approximation $\frac{1}{A} = 1$ (red, dashed) and without the approximation $\frac{1}{A} = 1$ (black, solid). The field profiles overlap almost completely. The bottom panel shows the relative difference. CD is short for the conformal-only disformal code.

Chapter 5

Results of the cosmological simulations

5.1 Description of the different simulations

In this chapter, the largest simulations with this code are presented, specifically 256^3 particles in a box with side lengths 64 Mpc/h. The same initial particle distribution will always be used. Five different runs are to be compared. Table 5.1 shows the model parameters used in these simulations.

	b_0	β
Standard gravity	-	-
Symmetron-like	0	0
Disformal A	1	1
Disformal B	2	2
Disformal C	1	0

Table 5.1: Parameters for the five simulations.

Disformal A has what we consider to be standard parameters. Disformal B has an amplified disformal part due to increased b_0 and β. Disformal C has $\beta = 0$, effectively setting $B(\phi) =$ constant. Both Disformal A and Disformal B have an asymmetric $B(\phi)$ when $\phi \to -\phi$ (see the discussion about the high density limit in subsection 2.3.2). The Symmetron-like simulation is a simulation done with the disformal code, but with the disformal part of the equations turned off by setting $b_0 = \beta = 0$.

Of course, the parameter space for this disformal model must be more thoroughly explored in future papers. However, results from these simulations should serve as an indication of the effects of the disformal term on the formation of structure.

All simulations in this study have a flat ΛCDM background cosmology with $\Omega_m = 0.3175$, $\Omega_\Lambda = 0.6825$, and $H_0 = 67.11$ km/s/Mpc, the parameters presented in section 3.1. All results shown in this section are for redshift zero ($a = 1$).

5.2 Power spectrum

Figure 5.1 shows the relative difference of the power spectra compared to standard ΛCDM. The most relevant scales are $k \in [0.1, 2]\ h\mathrm{Mpc}^{-1}$ because larger scales than about $k = 0.1h\mathrm{Mpc}^{-1}$ can't be measured well in a box of only 64 Mpc/h, and smaller scales than $k = 2h\mathrm{Mpc}^{-1}$ become unprecise due to the grid resolution (as explained in subsection 4.4). Disformal B – the simulation with the strongest disformal part – results in the power spectrum which is on average closest to GR on all scales, but the decrease in power is especially visible on smaller scales (i.e. large k in figure 5.1).

All four models for modified gravity increase the power spectrum by 0.5 to 5 percent relative to the one expected from ΛCDM for the safe scales $k \in [0.1, 2]\ h\mathrm{Mpc}^{-1}$. At large scales, the power spectrum of all the four modified gravity simulations approach ΛCDM. From these data, the increase in power compared to ΛCDM is approximately proportional to k for small scales $k > 2h\mathrm{Mpc}^{-1}$. This statement should be investigated further when grid refinements are implemented in the non-static Isis code.

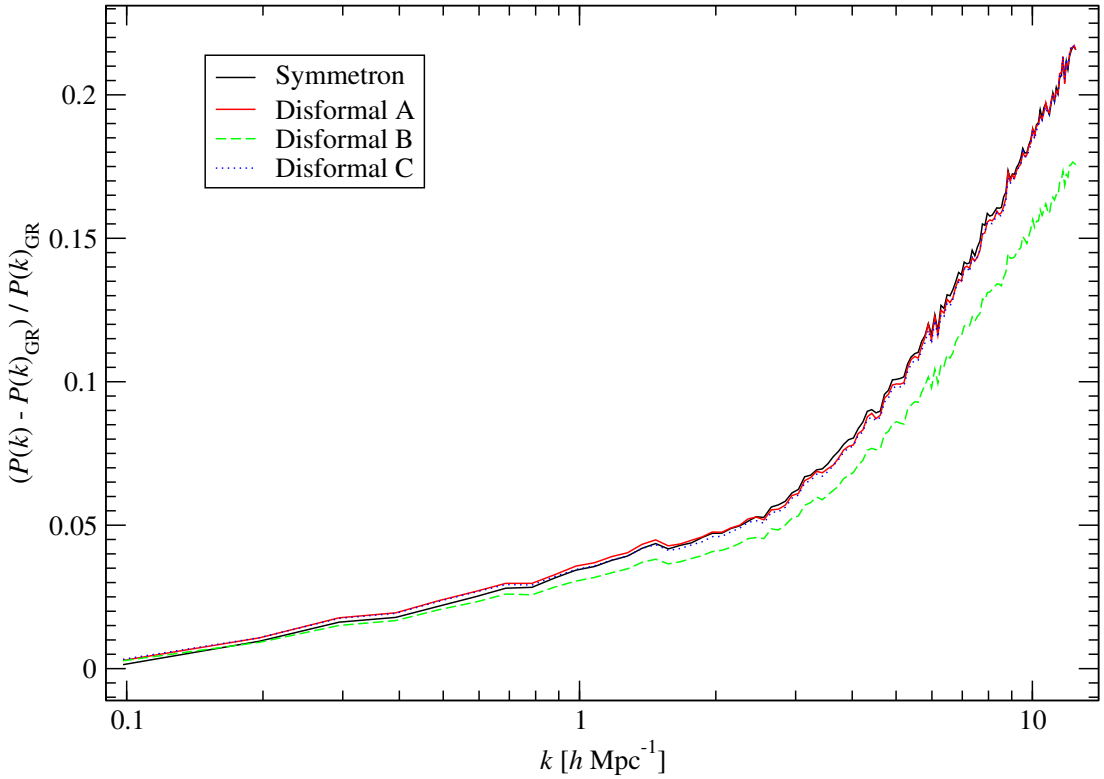

Figure 5.1: The figure shows the relative difference to GR of the matter power spectra $P(k)$ resulting from the four models of modified gravity. The difference is computed relative to the power spectrum resulting from the ΛCDM simulation ($P(k)_{\mathrm{GR}}$).

5.3 Halo mass function

Figure 5.2 shows the halo mass functions found for each of the five simulations. All modified models investigated here have an increase in the number of haloes compared to GR, but especially haloes smaller than $10^{12} M_{\odot}/h$ are about 20 to 35 percent more frequent, depending on model and halo mass. The change in the halo mass function and the power spectrum are observable ways to distinguish between the models presented here, and to constrain parameters.

It is interesting to notice that an increase in the strength of the disformal term (as in Disformal B) reduces the number of smaller haloes slightly. In other words, the disformal term can mask some of the increase in both the mass function and the power spectrum introduced by the symmetron field.

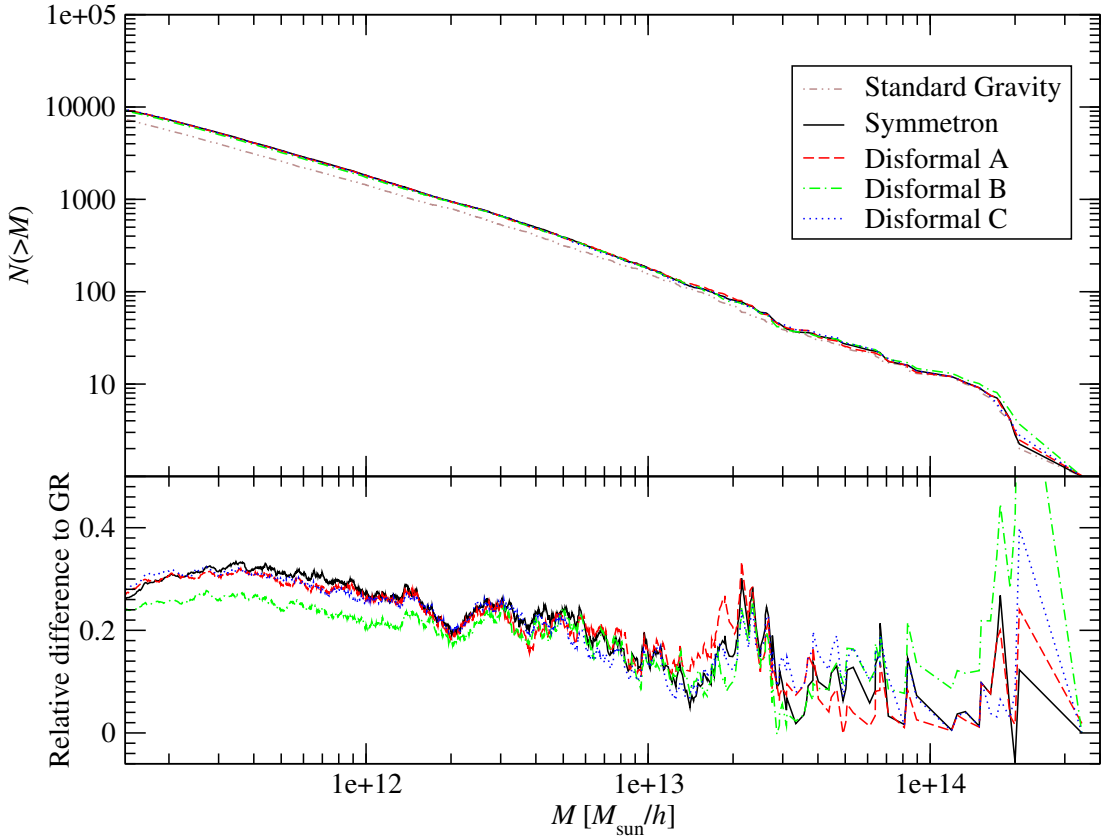

Figure 5.2: The top plot shows the total amount of haloes with virial mass larger than M, for each of the five simulations. The relative difference of the four modified models compared to GR is shown in the bottom plot.

5.4 Velocity histograms

The decrease in the power spectrum and mass function on small scales could be a result of warm dark matter*. To check if the disformal coupling actually increases the temperature of the dark matter particles, we plotted the velocity histogram of the particles, which is shown in figure 5.3.

It is evident from the plot that the strong disformal terms do *not* heat the dark matter significantly compared to the symmetron terms alone, hence the reduction in power and mass function must be a result of another mechanism.

As a side note, since $\dot{x} \ll c$, it is now more plausible to state that $x' \approx 0$ is a decent approximation for the geodesic equation, which we applied in subsection 2.5.3.

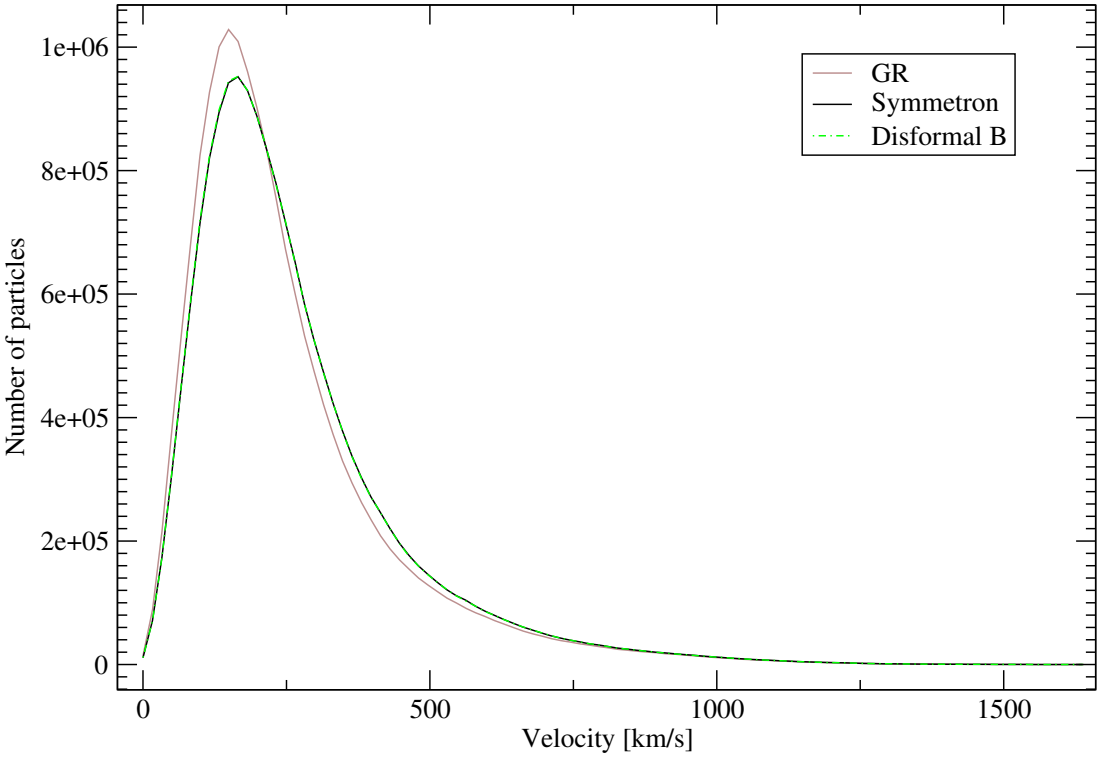

Figure 5.3: The figure shows the velocity histograms for the simulations general relativity (black), Symmetron (red), and Disformal B (green). Like Disformal B, all of the disformal models had a velocity histogram almost identical to the symmetron model. This is why Disformal A and Disformal C are not plotted.

*D. F. Mota, personal communication.

5.5 Halo choice for the field profiles

In each of the simulations, the position of the most massive halo (sorted by the virial mass found by ROCKSTAR) was identified in the redshift zero matter distribution. The most massive halo was found to have the same coordinates in all of the simulations, and had a mass of about $3.45 \cdot 10^{14} M_\odot/h \approx 5.1 \cdot 10^{14} M_\odot$ (equivalent to 10^{45} kg). To put this into perspective, the mass of this halo is about 100 times the estimated virial mass of the Local Group [78]. The variance in the halo mass was not more than 2 % between the different simulations, with the lowest virial mass of $3.42 \cdot 10^{14} M_\odot/h$ in Disformal B and the highest virial mass of $3.47 \cdot 10^{14} M_\odot/h$ in Disformal A. Because the simulations used identical initial conditions, we are certain that these haloes are actually the same halo, forming under different models for gravity.

Figure 5.4 shows the density profile in the dark matter distribution centered around this halo. The density plotted here is taken from the simulation Disformal A, but the density profile from the other simulations overlapped this one almost perfectly. The dark matter density in the core of the halo is very high, and at one virial radius the density has dropped to about 100 times the background density. The density falls to the background value at about three virial radii, or 5 Mpc/h.

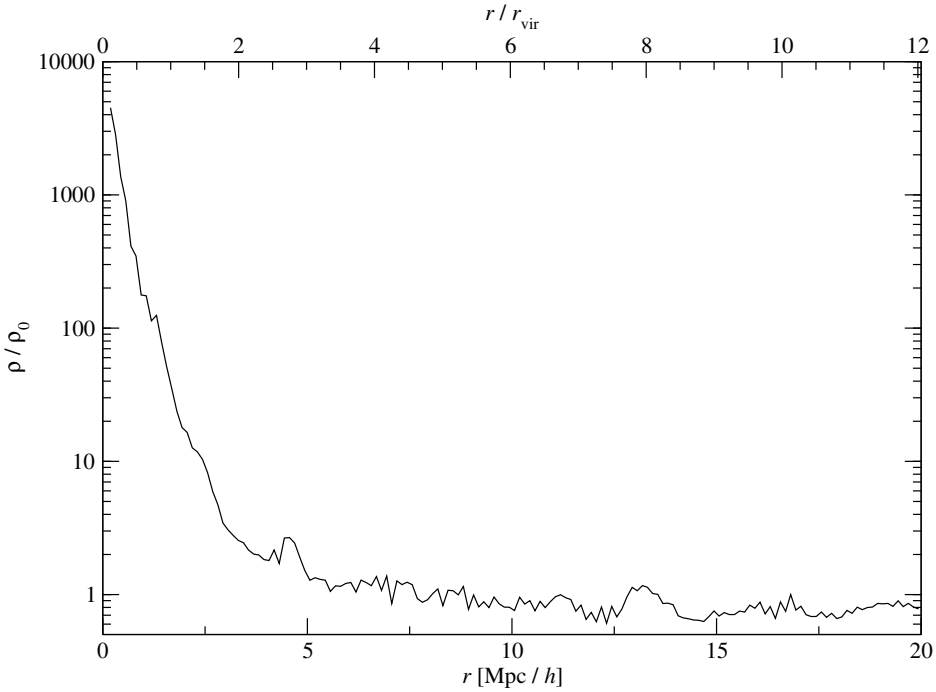

Figure 5.4: The average dark matter density at a radius r from the centre of the most massive dark matter halo in the simulations. Real distances are given in Mpc/h along the bottom x-axis, while distances normalized to the virial radius of the halo are given along the top x-axis. This density profile did not change visibly for the different simulated models.

5.6 Field profiles

All field profiles here are measured around the halo with virial mass of $3.45 \cdot 10^{14} M_\odot/h$ described in the previous section.

In all simulations except Disformal B, the field fell to the negative value in the whole 64 Mpc/h box, with an average field value* of about -0.95. Disformal B fell to the positive value of the symmetron potential and ended at an average of about $+0.95$. Very few grid cells had another sign for the field than the average in the disformal simulations, and most of these oddities are probably in the centre of massive haloes, where the disformal term leads to oscillations around zero, as we will shortly see. The symmetron simulation with no disformal term had no cells with a positive field value. No domain walls – interfaces between areas with different sign of the scalar field – were found in any of the simulations.

To plot the field profiles more comparably, all the field values were inverted (i.e. $\chi \to -\chi$) in the data from the Symmetron, Disformal A, and Disformal C simulations, before plotting the field profiles of all four models. This plot is shown in the top panel of figure 5.5 on the facing page. Without the mentioned inversion, the relevant field profile plots would have started at $\chi \approx 0$ at the centre, and fallen down to $\chi \approx -0.95$ far from the halo.

The shape of the field profiles are as expected for the symmetron model; the field is close to 0 in high density regions due to the conformal coupling to matter, and goes towards the vacuum expectation value, $\pm\phi_0$, in the regions far from the halo. The shape of the profiles for the disformal models are surprisingly similar to the symmetron field profile.

A very interesting result regarding the field profiles, is the amplitude of oscillations of the field – or equivalently, the dispersion σ_χ of the field values – which is plotted in the lower panel of figure 5.5. The well studied symmetron is supposed to have a field value approaching zero in high density regions, and will also end up being almost completely at rest there. This is because the conformal-only equation of motion gives an acceleration proportional to the field value χ. Densities where $\rho > \rho_{\text{SSB}}$ gives a stable minimum point at $\chi = 0$, and inside the overdensity the field will not oscillate far away from this value. The disformal models, however, have multiple other terms in the acceleration of the field not proportional to χ. These terms are instead proportional to some power of the fields time derivative, or even to its spatial derivatives. This could lead to a positive feedback loop in high density regions, explaining the oscillations in the centre of the halo in figure 5.5. Such oscillations should lead to increased fifth forces, see equation (2.66). The fifth forces will be explored further in the next section.

*This average is taken first over all time steps since $a = 0.995$ in each grid cell, then averaged over all grid cells.

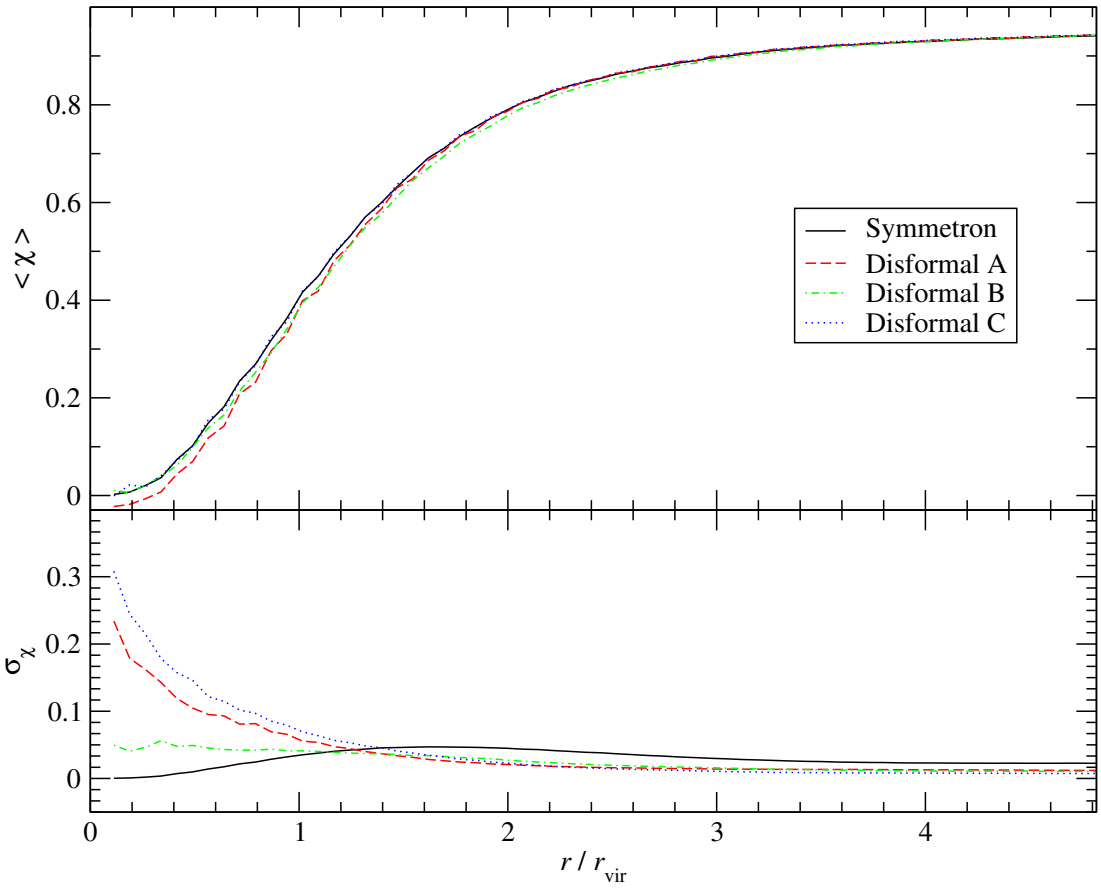

Figure 5.5: The top panel shows the average field profile $\langle\chi\rangle$ at distance r from the centre of the halo, for all four simulations of modified gravity. The Symmetron, Disformal A and Disformal C actually have negative field values, but for them $-\langle\chi\rangle$ is shown instead, such that the plotted field appears positive for all models. The bottom panel shows the average standard deviation of the field.

5.7 Fifth forces

The magnitude of the fifth force acceleration for all four modified gravity simulations is shown in figure 5.6. It is important to note that this is the *instantaneous* fifth force acceleration, not an average over time. This means that the plots of the different simulations are not necessarily comparable; if the scalar fields are in different phases, the amplitudes of the fifth forces could vary accordingly.

As expected from the increased oscillations of the field in $r < r_{\text{vir}}$, we see an increase in the fifth force compared to the symmetron model in these regions. Interestingly, all simulations have maximum fifth forces around one virial radius from the centre of the massive halo, approximately where the spatial gradient of the field is largest. All models have a reduction of the fifth force towards the centre of the halo. The fifth forces in Disformal A and especially Disformal C do not become exactly zero close to $r = 0$. This could indicate the existence of measurable fifth forces inside galaxy clusters, but the effect of this is difficult to study precisely with the current grid resolution.

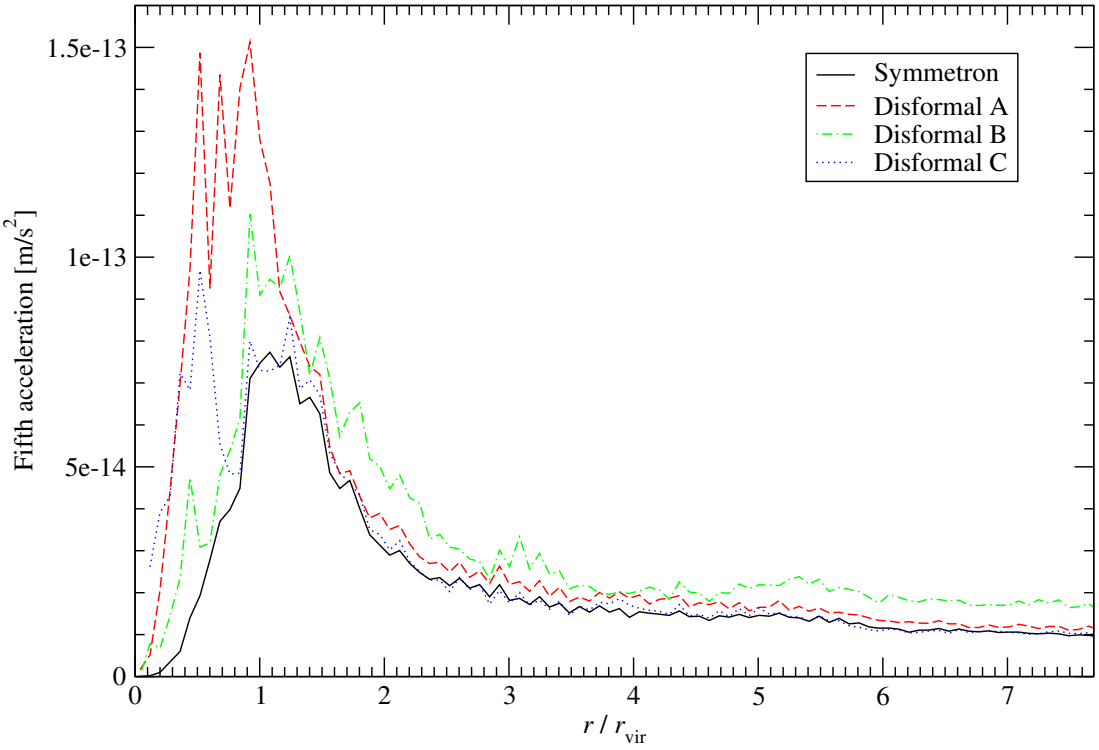

Figure 5.6: The figure shows the absolute value of the average fifth force (per mass) at distance r from the centre of the same halo, for all four modified models of gravity. This is a snapshot at exactly $a = 1$.

5.8 Disformal screening condition

The disformal screening mechanisms should be active when $B\rho \gtrsim 10$*. For this reason, it is interesting to plot the value of the dimensionless combination $B\rho$ at different distances from the massive halo. This is done in figure 5.7. The condition $B\rho \gtrsim 10$ is true approximately within one virial radius of the halo centre for the simulations Disformal A and Disformal C. More interestingly, because the field fell to the positive value in the run Disformal B, and because of the strong disformal parameters $\beta = b_0 = 2$, it follows that $B\rho \gtrsim 10$ even in low density areas of this simulation. The disformal screening mechanism should according to this be active *everywhere* in Disformal B.

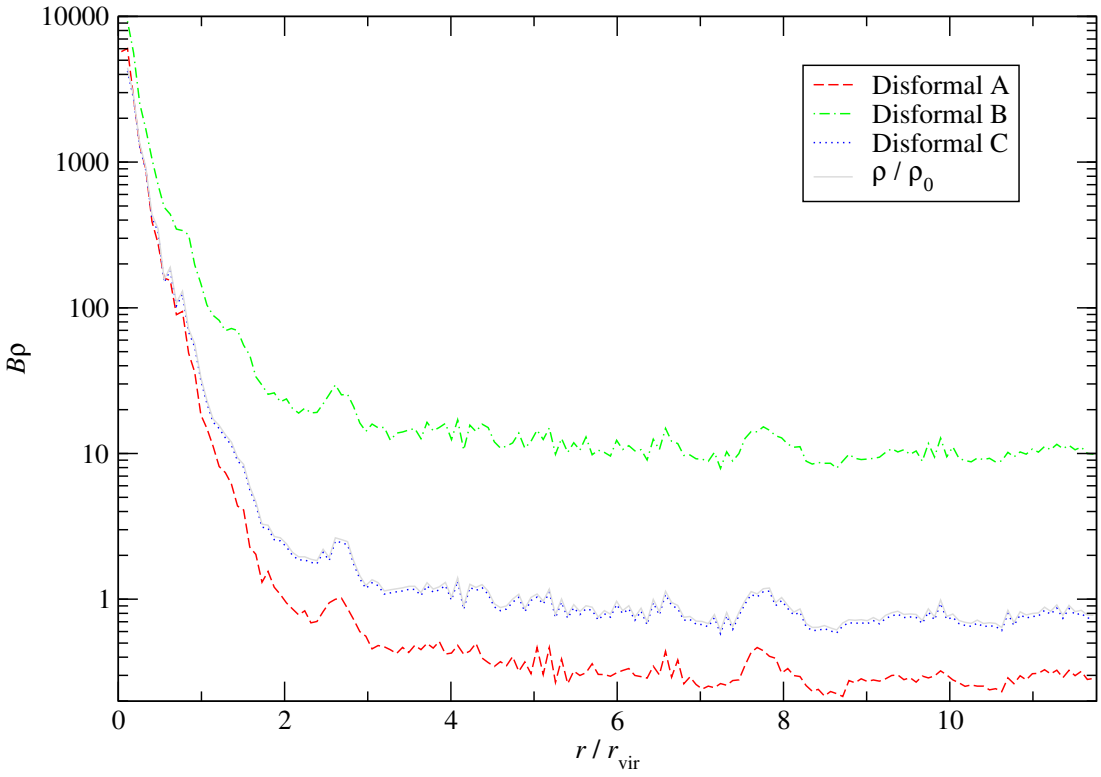

Figure 5.7: The figure shows the average value of the combination $B\rho$ at a distance r from the centre of the massive halo, for all three disformal models. The density contrast ρ/ρ_0 is also plotted (the grey line, overlapping $B\rho$ from Disformal C).

*M. Zumalacárregui, personal communication.

Chapter 6

Conclusions

6.1 Interpretations of the results

The symmetron model alone is known to increase clustering, especially on small scales, thus raising both the power spectrum and the mass function compared to ΛCDM [62]. The main result of this thesis is that adding a disformal term in the coupling between the Jordan and Einstein frame metrics, can prevent some of this symmetron clustering. The fact that the disformal terms counteract small scale clustering confirms similar findings on linear scales in a recent paper [38]. In our study, the decrease in clustering was only observed in one of the simulations, specifically the one with the strongest disformal coupling.

Velocity histograms of the dark matter particles showed a slight heating of the particles in all the modified gravity simulations compared to general relativity, but the addition of a disformal term did not heat the dark matter more than the symmetron alone. This implies that the reduction in small scale clustering is not due to a heating of the dark matter.

The reason why this reduction is seen in the specific simulation Disformal B – and not in the other disformal runs – is difficult to explain from the small amount of simulations done in this study. Part of the reason may be related to the fact that the field in Disformal B fell down to the positive potential minimum, instead of the negative like in Disformal A and Disformal C. This gives a significant increase in the dominance of the asymmetric disformal term $B = B_0 \exp(\beta\chi)$, and results in the condition $B\rho \gtrsim 10$ being fulfilled, even in voids where the density is below the average density. The mathematical reason for this increase is as follows: With $\beta = 2$, the exponential $\exp(\beta\chi)$ has the value $e^2 \approx 7.4$ if the field is at the positive minimum, and the value $e^{-2} \approx 0.14$ if the field is at the negative minimum of the potential. Consequently, the disformal term B becomes over 50 times larger – even under similar physical conditions – just because the field falls to one potential minimum instead of the other.

If the hypothesis presented in section 5.8 is correct, the disformal screening mechanism is active in areas where $B\rho \gtrsim 10$. This mechanism could play an important role in reducing the fifth forces on all scales of Disformal B, compared to the conformally

coupled symmetron. However, if the disformal screening is active, it is strange that the absolute values of the fifth forces in the massive halo were found to be larger in the disformal models than in the symmetron model. A possibility here is to consider the fact that the direction of the disformal fifth force is expected to oscillate. Specifically the fifth force will oscillate with the time derivatives of the field, as seen from equation (2.66). In this way, the absolute value of the fifth force can be larger than in the symmetron case, even though the time-averaged effect on the particle distribution is smaller. A problem with this interpretation is that large instantaneous fifth forces – even if the direction is oscillating – should be measurable, which could lead to strict constraints on the parameter space.

The increased oscillations of the field in high density regions found in section 5.6 are highly peculiar. A naive interpretation of the high density limit of the equation of motion – given by equation (2.27) – is that as long as the field starts out being at rest close to the stationary point at $\phi = 0$, it has no reason to increase the amplitude of its oscillations in high density areas. Just like in the symmetron model, the field should therefore not oscillate inside of haloes. The data presented here *do* show increased field oscillations in the centre of the haloes, and the result is an increased amplitude of the fifth force in these regions. A hypothesis that can explain the increased oscillations in the disformal model goes as follows*: The equation of motion for the scalar field (2.22) is a slightly complicated wave equation, and the factor of $(1 + \gamma^2\rho)$ in front of $\ddot{\phi}$ can be regarded as $1/c_s^2$. Here c_s is the *speed of waves* propagating in the field, comparable to the speed of sound for propagating sound waves. With increasing $\gamma^2\rho$ (or equivalently, increasing $B\rho$), the wave speed decreases. This in turn means that any wave that enters an overdensity with a large $B\rho$ will slow down, and the wave energy will effectively be trapped inside the halo, possibly increasing the amplitude of the field oscillations there. Further analysis must be done to confirm this hypothesis.

A possible connection between the increased fifth forces and the reduction in small scale power, could be that the disformal fifth forces prevent clustering by pushing particles away from dense areas. If this is the case, another unanswered question arises: There is no significant reduction in power for Disformal A, which had larger oscillations and stronger fifth forces than Disformal B, at least around the massive halo presented in sections 5.6 and 5.7. A potential reason for this is that different terms in the fifth forces could be responsible for separate effects. Some disformal terms might oscillate with the field and vary in direction and magnitude without significantly affecting the particle distribution over time; these terms might contribute more to the total fifth force in Disformal A and Disformal C. Other terms might be smaller, but systematically push particles away from overdensities. These terms could for some reason be more dominant in Disformal B. Further research on the connection between the field oscillations and the fifth forces is needed to investigate this claim.

*C. Llinares, personal communication.

6.2 Discussion and way forward

When implementing the dark matter geodesics, we ignored all terms proportional to the particle velocities x'. This was done to reduce the complexity of the model, but there is no good physical motivation for this simplification, except that the dark matter particles were expected to move relatively slowly. These terms could be important for the fifth forces and the evolution of structure in the universe. We have left for future work to study the effects of the omitted terms.

In this study, only the instantaneous absolute values of the fifth forces were analysed. Preferably, the fifth forces should be collected over time to create animated vector maps, granting the possibility to investigate whether the fifth forces are oscillating, and what the average impact of them are. This would provide valuable information for studying the effectivity of the disformal screening mechanisms.

The specific model chosen in this study has a disformal term $B = B_0 \exp(\beta\phi/\phi_0)$, which is asymmetric under the transformation $\phi \to -\phi$. Both the symmetron potential and the conformal coupling term are symmetric under the same transformation, implying that the model does not behave differently if the field falls down to $\phi = \phi_0$ or $\phi = -\phi_0$ when the disformal term is turned off. The disformal term however, will be large if ϕ is positive and smaller if ϕ is negative. The concern is that with the few simulations we could do here, only one had a field that fell to the positive minimum. Incidentally, this was the only simulation where we saw a significant decrease in small scale clustering; hence, we cannot know if the results were caused by the positive minimum, or from the choice of parameters without conducting multiple new simulations. The effect of the asymmetric disformal term is very interesting, and should be studied further to find observational signatures of this disformal model. To avoid the uncertainty mentioned above, other, symmetric forms for the disformal term could be considered, for instance $B = B_0 \exp(\beta |\phi| / \phi_0)$, or even just a polynomial $B = B_0 + B_1 (\phi/\phi_0)^2$.

We only considered four different sets of disformal parameters in this thesis. N-body simulations of sufficient resolution are very computationally intensive, so a detailed exploration of the parameter space of b_0, β, λ_0, θ, and a_{SSB} must be done by other means. Dynamical system methods have been used for other disformal models before [33], and such methods could be used to find viable parameters for this model which satisfy observational constraints. The parameters can later be tested with N-body simulations to show specific power-spectra, mass functions, and fifth forces. For each set of parameters investigated, there should also be done more simulations with different initial particle distributions. This will result in more statistically significant results, and offer a possibility to study the importance of the sign of the field in better detail.

A rather important philosophical subject regarding this study is that in the field equations, the cosmological constant Λ is replaced with the potential displacement of the scalar field potential, V_0. In this work, V_0 was set to the same numerical value as the measured $\Lambda/8\pi G$, simply to achieve a similar background evolution to the one that is found using ΛCDM. There is still a fine-tuning problem; there is no physical reason why V_0 has exactly this value. Finding a model where the correct value of $\Lambda/8\pi G$ occurs naturally in the field equation would be the holy grail to researchers in dark energy.

The initial particle distribution is computed assuming ΛCDM. Strictly speaking, one should use a modified version of GRAFIC that takes disformal gravity into account when computing the particle distribution. Moreover, the analysis of the Planck data should be done with extreme caution so as to not assume ΛCDM when extracting cosmological parameters. In this thesis, these problems are omitted by assuming that the universe has a large-scale and early time evolution which is indistinguishable from ΛCDM; therefore the error introduced when using GRAFIC and Planck data out-of-the-box is considered negligible. This statement should be investigated more rigorously.

When computing the gravitational potential, RAMSES only solves the Poisson equation from general relativity,

$$\nabla^2\Psi = 4\pi G\rho_{\mathrm{m}}. \tag{6.1}$$

However, to be completely accurate there should be more terms on the right hand side of this equation, including the energy density of the field. This fact might lead to interesting effects on the particle distribution, but in this thesis these effects are assumed small. Furthermore, the simulations presented in this thesis only considered dark matter particles, and included no hydrodynamics or baryon physics. In future works, interacting baryons should be included for more realistic particle movements and galaxy formation.

The lack of grid refinement (AMR) is a big disadvantage when studying particle distributions in the nonlinear regime. We hope to be able to implement refinements in the non-static ISIS/RAMSES code at a later time. This will simultaneously allow for a larger total box size and higher resolution in high density regions with the same amount of CPU hours. A higher resolution around high density haloes will of course lead to more correct particle movement on small scales, and hence a more precise power spectrum and halo mass function. In a larger simulation box, with side lengths of 256 or 512 Mpc/h, the formation of superclusters will be possible, such superclusters might influence the field evolution.

Larger simulations will also increase the probability to find domain walls, where the scalar field value falls to opposite signs in two neighbouring regions after the symmetry breaking. Such domain walls in the symmetron model were found to have interesting properties [65, 66], and could lead to significant effects in the disformal model, where the derivatives of the field are even more important than in the symmetron case. It must be noted that even though no domain walls were found in the final output of our simulations, they could have formed at earlier times and collapsed before $z = 0$. Such a collapse releases significant amounts of energy in the form of waves in the scalar field.

We use the leapfrog algorithm for stepping the field χ and its time derivative q forward in time. However, the value of q is used when calculating the acceleration of the field q', as seen in equation (2.55). This can be a slight problem, because the leapfrog scheme is designed to be a stable second order algorithm if the acceleration is *velocity-independent* [68]. The error made by including an asynchronous velocity q in the calculation of the acceleration q' is probably not too large, so the algorithm is still more accurate than a simple Euler integration. In future work, it should nevertheless be considered to use other integration schemes for the scalar field – like the fourth order

Runge-Kutta – such schemes work well, even if q' depends on q. Since RAMSES uses the leapfrog scheme for integrating particle positions as well, the same problem will arise if one in the future is to include velocity-dependent fifth forces in the geodesic equation.

As a concluding remark, the dynamics of the disformal model studied here were found to be very rich and the results open many doors for future research in disformally coupled theories. Both the reduction in small scale clustering, and the increase of oscillations in the centre of haloes are new phenomena that will be interesting to investigate further.

Appendices

Appendix A

Useful relations

A.1 Definitions used for the disformal field

$$
\begin{aligned}
\gamma^2 &\equiv \frac{B}{A-2BX} \\
\zeta &\equiv \frac{3\Omega_0 H_0^2 \lambda_0^2}{a_{\mathrm{SSB}}^3} \\
\chi &\equiv \phi/\phi_0 \\
\phi_0 &\equiv \frac{\mu}{\sqrt{\lambda}} = \theta \frac{M^2}{M_{\mathrm{Pl}}} = 2\theta\zeta M_{\mathrm{Pl}} \\
A(\chi) &= 1 + 2\zeta\theta^2\chi^2 \\
B(\chi) &= \frac{b_0}{H_0^2 M_{\mathrm{Pl}}^2} \exp(\beta\chi) \\
X &\equiv -\frac{1}{2} g^{\mu\nu}\phi_{,\mu}\phi_{,\nu} \\
X(\chi) &= -2\theta^2\zeta^2 M_{\mathrm{Pl}}^2 g^{\mu\nu}\chi_{,\mu}\chi_{,\nu} \\
M^2 &= \frac{\rho_{0(z=0)}}{\mu^2 a_{\mathrm{SSB}}^3} = 2M_{\mathrm{Pl}}^2\zeta \\
\gamma^2 M_{\mathrm{Pl}}^2 &= \frac{b_0 \exp(\beta\chi)}{H_0^2 (A-2BX)} \\
B\rho &= \frac{3\Omega_0}{a^3} b_0 \eta \exp(\beta\chi)
\end{aligned}
$$

A.2 Cosmological relations

$$
\begin{aligned}
M_{\mathrm{Pl}} &\equiv 1/\sqrt{8\pi G} \\
\rho_{0(z=0)} &= \Omega_0 \rho_c = 3\Omega_0 H_0^2 M_{\mathrm{Pl}}^2 \\
\rho &= \frac{3H_0^2\Omega_0}{a^3} M_{\mathrm{Pl}}^2 \eta \\
\eta &= \frac{\rho}{\rho_0}
\end{aligned}
$$

A.3 Supercomoving time, and related variables

$$
\begin{aligned}
\mathrm{d}\tau &= \frac{1}{a^2}\mathrm{d}t \\
\frac{\mathrm{d}}{\mathrm{d}t} &= \frac{1}{a^2}\frac{\mathrm{d}}{\mathrm{d}\tau} \\
\frac{\mathrm{d}^2}{\mathrm{d}t^2} &= \frac{1}{a^4}\left(\frac{\mathrm{d}^2}{\mathrm{d}\tau^2} - 2\tilde{H}\frac{\mathrm{d}}{\mathrm{d}\tau}\right) \\
\tilde{H} &\equiv \frac{1}{a}\frac{\mathrm{d}a}{\mathrm{d}\tau} = a^2 H \\
\tilde{\Psi} &= a^2 \Psi \\
q &\equiv a\chi'
\end{aligned}
$$

A.4 Curvature: covariant derivatives, Christoffel symbols, and the Ricci scalar

$$
\begin{aligned}
\nabla_\mu x^\nu &= x^\nu{}_{,\mu} + \Gamma^\nu_{\mu\lambda} x^\lambda \\
\nabla_\mu \omega_\nu &= \omega_{\nu,\mu} - \Gamma^\lambda_{\mu\nu}\omega_\lambda \\
\nabla_\mu \phi &= \phi_{,\mu} \\
\nabla_\mu \phi_{,\nu} &= \nabla_\nu \phi_{,\mu} \\
\Gamma^\lambda_{\mu\nu} &= \frac{1}{2} g^{\sigma\rho}\left(g_{\nu\rho,\mu} + g_{\rho\mu,\nu} - g_{\mu\nu,\rho}\right) \\
R^\rho{}_{\sigma\mu\nu} &= \Gamma^\rho{}_{\nu\sigma,\mu} - \Gamma^\rho{}_{\mu\sigma,\nu} + \Gamma^\rho_{\mu\lambda}\Gamma^\lambda{}_{\nu\sigma} - \Gamma^\rho_{\nu\lambda}\Gamma^\lambda{}_{\mu\sigma} \\
R_{\mu\nu} &= R^\lambda{}_{\mu\lambda\nu} \\
R &= g^{\mu\nu} R_{\mu\nu}
\end{aligned}
$$

A.5 The Einstein frame metric, and some Christoffel symbols in the Conformal Newtonian gauge

$$
\begin{aligned}
g^{00} &= -\left(1-2\Psi\right) \\
g^{ii} &= \frac{1}{a^2}\left(1+2\Psi\right) \\
g_{00} &= -\left(1+2\Psi\right) \\
g_{ii} &= a^2\left(1-2\Psi\right) \\
\Gamma^i_{j0} &= H\delta^i_j \\
\Gamma^i_{00} &= \frac{\Psi_{,i}}{a^2} \\
\Gamma^0_{i0} &= \left(1-2\Psi\right)\Psi_{,i} \approx \Psi_{,i} \\
\Gamma^0_{00} &= 2\dot{\Psi} \approx 0
\end{aligned}
$$

A.6 Special expressions to first order

In most of this thesis the Newtonian potential Ψ is taken only to first order, meaning it is useful to know some common first order approximations. The two most common are:

$$
\begin{aligned}
\frac{1}{1+a\Psi} &= 1 - a\Psi + (a\Psi)^2 - (a\Psi)^3 + \ldots \approx 1 - a\Psi \\
\left(1+a\Psi\right)^2 &= 1 + 2a\Psi + (a\Psi)^2 \approx 1 + 2a\Psi
\end{aligned}
$$

Here, a is some real number. Furthermore, a general multiplication of two first order terms is to first order given by

$$
\left(1+a\Psi\right)\left(1+b\Psi\right) = 1 + a\Psi + b\Psi + ab\Psi^2 \approx 1 + \left(a+b\right)\Psi.
$$

Appendix B

Calculation of the disformal field equation of motion

The general equation of motion for the scalar field is given by [25]:

$$\mathcal{M}^{\mu\nu}\nabla_\mu\nabla_\nu\phi + \frac{A}{A-2BX}\mathcal{Q}_{\mu\nu}T^{\mu\nu} + \mathcal{V} = 0, \tag{B.1}$$

with

$$\mathcal{M}^{\mu\nu} = \mathcal{L}_{\phi,X}g^{\mu\nu} + \mathcal{L}_{\phi,XX}\phi^{,\mu}\phi^{,\nu} - \frac{B}{A-2BX}T_m^{\mu\nu}, \tag{B.2}$$

$$\mathcal{Q}_{\mu\nu} = \frac{A_{,\phi}}{2A}g_{\mu\nu} + \left(\frac{A_{,\phi}B}{A^2} - \frac{B_{,\phi}}{2A}\right)\phi_{,\mu}\phi_{,\nu}, \tag{B.3}$$

$$X \equiv -\frac{1}{2}\left(\nabla^\mu\phi\right)\left(\nabla_\mu\phi\right) = -\frac{1}{2}g^{\mu\nu}\phi_{,\mu}\phi_{,\nu}, \tag{B.4}$$

$$\mathcal{V} = \mathcal{L}_{\phi,\phi} + 2X\mathcal{L}_{\phi,X\phi}. \tag{B.5}$$

From the line element $\mathrm{d}s^2$, one can read out the metric tensor

$$g_{\mu\nu} = \mathrm{diag}\left(-\left(1+2\Psi\right), a^2\left(t\right)\left(1-2\Psi\right), a^2\left(t\right)\left(1-2\Psi\right), a^2\left(t\right)\left(1-2\Psi\right)\right). \tag{B.6}$$

The inverse metric tensor is given by

$$g^{\mu\nu} = \mathrm{diag}\left(-\left(1-2\Psi\right), \frac{1}{a^2\left(t\right)}\left(1+2\Psi\right), \frac{1}{a^2\left(t\right)}\left(1+2\Psi\right), \frac{1}{a^2\left(t\right)}\left(1+2\Psi\right)\right). \tag{B.7}$$

This is found trivially since $g_{\mu\nu}$ is diagonal, thus $g^{\mu\mu} = 1/g_{\mu\mu}$.

The only contributing part of the energy-momentum tensor is $T^{00} = \rho$ (i.e. the dark matter density). This means that $\mathcal{M}^{\mu\nu}$ is diagonal, so we only need to calculate the diagonal elements of $\nabla_\mu\nabla_\nu\phi$. For calculating the first term of equation (B.1), one therefore needs the quantity

$$\nabla_\mu\nabla_\mu\phi = \nabla_\mu\left(\phi_{,\mu}\right) = \phi_{,\mu\mu} - \Gamma^\nu_{\mu\mu}\phi_{,\nu}, \tag{B.8}$$

where repeated lower indices do not indicate a summation, but simply means any single index; 0, 1, 2 or 3.

Because $\Psi \ll 1$, one can always discard terms of higher order in Ψ than $\mathcal{O}\left(\Psi^1\right)$.

Using the definition

$$\Gamma^{\mu}_{\alpha\beta} = \frac{1}{2} g^{\mu\nu} \left(g_{\nu\alpha,\beta} + g_{\nu\beta,\alpha} - g_{\alpha\beta,\nu} \right), \tag{B.9}$$

the 00 index of the first term, $\nabla_0 \nabla_0 \phi = \nabla_0 \phi_{,0}$ is given by

$$\nabla_0 \nabla_0 \phi = \ddot{\phi} - \frac{1}{2} g^{\mu\nu} \left(g_{\nu 0,0} + g_{\nu 0,0} - g_{00,\nu} \right) \phi_{,\mu}. \tag{B.10}$$

The only terms from $g^{\mu\nu}$ that will contribute here are the ones where $\mu = \nu$, and the only non-zero term from $g_{\nu 0,0}$ has $\nu = 0$, therefore

$$\nabla_0 \nabla_0 \phi = \ddot{\phi} - \frac{1}{2} \left(g^{00} g_{00,0} \phi_{,0} + g^{00} g_{00,0} \phi_{,0} - g^{\mu\nu} g_{00,\nu} \phi_{,\mu} \right) \tag{B.11}$$

$$\nabla_0 \nabla_0 \phi = \ddot{\phi} - \frac{1}{2} \left(g^{00} g_{00,0} \phi_{,0} - \sum_{i=1,2,3} g^{ii} g_{00,i} \phi_{,i} \right). \tag{B.12}$$

However, $g_{00,0} = -2\dot{\Psi} \approx 0$. Moreover $g^{ii} = (1 + 2\Psi)/a^2$ and $g_{00,i} = -2\Psi_{,i}$. Only terms to the first order in Ψ are kept, and the quantity $\Psi \Psi_{,i}$ is assumed negligible.

Doing this for all the possible indices in the first term will result in

$$\nabla_0 \nabla_0 \phi = \ddot{\phi} - \frac{1}{a^2} \sum_{i=1,2,3} \Psi_{,i} \phi_{,i}, \tag{B.13}$$

$$\begin{aligned} \nabla_1 \nabla_1 \phi &= \phi_{,11} - \frac{1}{2} \left(g^{11} g_{11,1} \phi_{,1} - g^{00} g_{11,0} \phi_{,0} - g^{22} g_{11,2} \phi_{,2} - g^{33} g_{11,3} \phi_{,3} \right) \\ &= \phi_{,11} - a^2 H \left(1 - 4\Psi\right) \dot{\phi} + \Psi_{,1} \phi_{,1} - \Psi_{,2} \phi_{,2} - \Psi_{,3} \phi_{,3}, \end{aligned} \tag{B.14}$$

$$\nabla_2 \nabla_2 \phi = \phi_{,22} - a^2 H \left(1 - 4\Psi\right) \dot{\phi} + \Psi_{,2} \phi_{,2} - \Psi_{,1} \phi_{,1} - \Psi_{,3} \phi_{,3}, \tag{B.15}$$

$$\nabla_3 \nabla_3 \phi = \phi_{,33} - a^2 H \left(1 - 4\Psi\right) \dot{\phi} + \Psi_{,3} \phi_{,3} - \Psi_{,1} \phi_{,1} - \Psi_{,2} \phi_{,2}. \tag{B.16}$$

Here a dot symbolizes a derivative with respect to cosmic time $t = x_0$. The sum $\sum_{i=1,2,3} \left(g^{ii}\right) \nabla_i \nabla_i \phi$ can be found by first realizing that $g^{ii} = (1 + 2\Psi)/a^2$ for all i, such that g^{ii} can be taken outside of the sum. The remaining sum is given by

$$\sum_{i=1,2,3} \nabla_i \nabla_i \phi = \sum_{i=1,2,3} \left(\phi_{,ii} - \Psi_{,i} \phi_{,i} \right) - 3a^2 H \left(1 - 4\Psi\right) \dot{\phi}. \tag{B.17}$$

Remember that $(1 + 2\Psi)(1 - 4\Psi) = 1 - 2\Psi$ to first order in Ψ.

To finalize the expansion of the first term, one must insert the diagonal $\mathcal{M}^{\mu\nu}$, and separate the expression in time terms and the space terms.

$$\left(g^{\mu\nu} - \frac{B}{A-2BX}T^{\mu\nu}\right)\nabla_\mu\nabla_\nu\phi$$
$$= \left(g^{00} - \frac{B}{A-2BX}T^{00}\right)\nabla_0\nabla_0\phi + \sum_{i=1,2,3}\left(g^{ii}\right)\nabla_i\nabla_i\phi \tag{B.18}$$
$$= \left(-\left(1-2\Psi\right) - \frac{B}{A-2BX}\rho\right)\left(\ddot{\phi} - \frac{1}{a^2}\sum_{i=1,2,3}\Psi_{,i}\phi_{,i}\right)$$
$$+ \frac{1}{a^2}\left(1+2\Psi\right)\sum_{i=1,2,3}\left(\phi_{,ii} - \Psi_{,i}\phi_{,i}\right) - 3H\left(1-2\Psi\right)\dot{\phi} \tag{B.19}$$

Multiplying this out, the resulting expression for the first term becomes

$$\left(g^{\mu\nu} - \frac{B}{A-2BX}T^{\mu\nu}\right)\nabla_\mu\nabla_\nu\phi$$
$$= \left(-1+2\Psi - \frac{B}{A-2BX}\rho\right)\ddot{\phi} + \left(\frac{B}{A-2BX}\rho\right)\frac{1}{a^2}\sum_{i=1,2,3}\Psi_{,i}\phi_{,i}$$
$$+ \frac{1}{a^2}\sum_{i=1,2,3}\Psi_{,i}\phi_{,i} - \frac{2\Psi}{a^2}\sum_{i=1,2,3}\Psi_{,i}\phi_{,i}$$
$$+ \frac{1}{a^2}\left(1+2\Psi\right)\sum_{i=1,2,3}\phi_{,ii} - \frac{1}{a^2}\sum_{i=1,2,3}\Psi_{,i}\phi_{,i} - \frac{2\Psi}{a^2}\sum_{i=1,2,3}\Psi_{,i}\phi_{,i}$$
$$- 3H\left(1-2\Psi\right)\dot{\phi} \tag{B.20}$$
$$= \left(-1+2\Psi - \frac{B}{A-2BX}\rho\right)\ddot{\phi} + \frac{1}{a^2}\left(1+2\Psi\right)\sum_{i=1,2,3}\phi_{,ii}$$
$$- 4\Psi\frac{1}{a^2}\sum_{i=1,2,3}\Psi_{,i}\phi_{,i} + \frac{B}{A-2BX}\frac{\rho}{a^2}\sum_{i=1,2,3}\Psi_{,i}\phi_{,i}$$
$$- 3H\left(1-2\Psi\right)\dot{\phi}. \tag{B.21}$$

Using this, and again assuming that $\Psi\Psi_{,i} \approx 0$, the complete field equation to first order in Ψ can now be written out as

$$\left(-1+2\Psi - \frac{B}{A-2BX}\rho\right)\ddot{\phi} + \frac{1}{a^2}\left(1+2\Psi\right)\sum_{i=1,2,3}\phi_{,ii} + \frac{B}{A-2BX}\frac{\rho}{a^2}\sum_{i=1,2,3}\Psi_{,i}\phi_{,i}$$
$$-3H\left(1-2\Psi\right)\dot{\phi} + \frac{A}{A-2BX}\left(-\left(1+2\Psi\right)\frac{A_{,\phi}}{2A} + \left(\frac{A_{,\phi}B}{A^2} - \frac{B_{,\phi}}{2A}\right)\dot{\phi}^2\right)\rho - V_{,\phi} = 0. \tag{B.22}$$

Appendix C

Calculations of the Jordan frame Christoffel symbols

To find the necessary barred Christoffel symbols, the following equation is used [58]:

$$\bar{\Gamma}^{\mu}_{\alpha\beta} = \Gamma^{\mu}_{\alpha\beta} + \frac{1}{2}\bar{g}^{\mu\nu}\left[\nabla_{\alpha}\bar{g}_{\beta\nu} + \nabla_{\beta}\bar{g}_{\alpha\nu} - \nabla_{\nu}\bar{g}_{\alpha\beta}\right]. \tag{C.1}$$

The covariant derivative of the Jordan frame metric must be calculated. Writing out $\nabla_{\alpha}\bar{g}_{\mu\nu}$ gives

$$\nabla_{\alpha}\left(Ag_{\mu\nu} + B\phi_{,\mu}\phi_{,\nu}\right) = g_{\mu\nu}\left(\nabla_{\alpha}A\right) + A\left(\nabla_{\alpha}g_{\mu\nu}\right) + B\left(\nabla_{\alpha}\phi_{,\mu}\phi_{,\nu}\right) + \phi_{,\mu}\phi_{,\nu}\left(\nabla_{\alpha}B\right). \tag{C.2}$$

The Einstein frame connections $\Gamma^{\mu}_{\alpha\beta}$ are chosen such that $\nabla_{\alpha}g_{\mu\nu}$ vanishes [46]. Furthermore, the expressions for A and B are scalar quantities, thus the covariant derivative acting on them is equivalent to a partial derivative. The simplified expression used to find the covariant derivatives is therefore

$$\nabla_{\alpha}\bar{g}_{\mu\nu} = g_{\mu\nu}A_{,\alpha} + B\left(\nabla_{\alpha}\phi_{,\mu}\phi_{,\nu}\right) + \phi_{,\mu}\phi_{,\nu}B_{,\alpha}. \tag{C.3}$$

Two of the Jordan frame Christoffel symbols need to be found to achieve the expression for $\ddot{x}^{i}$, namely $\bar{\Gamma}^{i}_{00}$ and $\bar{\Gamma}^{i}_{j0}$. Both of these will be calculated here, by using equation (C.1) with the relevant indices, followed by inserting the necessary version of equation (C.3).

C.1 The inverse Jordan frame metric with proof

The Jordan frame metric in disformal theories is $\bar{g}_{\mu\nu} = Ag_{\mu\nu} + B\phi_{,\mu}\phi_{,\nu}$, but one also needs the inverse of this metric, $\bar{g}^{\mu\nu}$ – which is given in [58] – to calculate the geodesics. The expression is

$$\begin{aligned}\bar{g}^{\mu\nu} &= \frac{1}{A}\left(g^{\mu\nu} - \frac{Bg^{\mu\alpha}g^{\nu\beta}\phi_{,\alpha}\phi_{,\beta}}{A + Bg^{\sigma\lambda}\phi_{,\sigma}\phi_{,\lambda}}\right) \\ &\equiv \frac{1}{A}\left(g^{\mu\nu} - \frac{B\phi^{,\mu}\phi^{,\nu}}{A - 2BX}\right). \end{aligned} \tag{C.4}$$

A short proof that this is the correct form for $\bar{g}^{\mu\nu}$ can be done by contracting the Jordan frame metric with its inverse,

$$\begin{aligned}&\bar{g}^{\lambda\sigma}\bar{g}_{\sigma\nu} \\ =&\frac{1}{A}\left(g^{\lambda\sigma} - \frac{Bg^{\lambda\alpha}g^{\sigma\beta}\phi_{,\alpha}\phi_{,\beta}}{A + Bg^{\rho\tau}\phi_{,\rho}\phi_{,\tau}}\right)\left(Ag_{\sigma\nu} + B\phi_{,\sigma}\phi_{,\nu}\right) \\ =&\left(\delta^{\lambda}_{\nu} - \frac{Bg^{\lambda\alpha}g^{\sigma\beta}\phi_{,\alpha}\phi_{,\beta}}{A + Bg^{\rho\tau}\phi_{,\rho}\phi_{,\tau}}g_{\sigma\nu} + \frac{B}{A}\phi_{,\sigma}\phi_{,\nu}g^{\lambda\sigma} - \frac{B}{A}\phi_{,\sigma}\phi_{,\nu}\frac{Bg^{\lambda\alpha}g^{\sigma\beta}\phi_{,\alpha}\phi_{,\beta}}{A + Bg^{\rho\tau}\phi_{,\rho}\phi_{,\tau}}\right) \\ =&\left(\delta^{\lambda}_{\nu} + \frac{-Bg^{\lambda\alpha}g^{\sigma\beta}\phi_{,\alpha}\phi_{,\beta}g_{\sigma\nu} + \frac{B}{A}\phi_{,\sigma}\phi_{,\nu}g^{\lambda\sigma}\left(A + Bg^{\alpha\beta}\phi_{,\alpha}\phi_{,\beta}\right) - \frac{B^2}{A}\phi_{,\sigma}\phi_{,\nu}g^{\lambda\alpha}g^{\sigma\beta}\phi_{,\alpha}\phi_{,\beta}}{A + Bg^{\rho\tau}\phi_{,\rho}\phi_{,\tau}}\right) \\ =&\left(\delta^{\lambda}_{\nu} + \frac{-Bg^{\lambda\alpha}\phi_{,\alpha}\phi_{,\nu} + B\phi_{,\sigma}\phi_{,\nu}g^{\lambda\sigma} + \frac{B^2}{A}\phi_{,\sigma}\phi_{,\nu}g^{\lambda\sigma}g^{\alpha\beta}\phi_{,\alpha}\phi_{,\beta} - \frac{B^2}{A}\phi_{,\sigma}\phi_{,\nu}g^{\lambda\alpha}g^{\sigma\beta}\phi_{,\alpha}\phi_{,\beta}}{A + Bg^{\rho\tau}\phi_{,\rho}\phi_{,\tau}}\right)\end{aligned} \tag{C.5}$$

Indices that are summed over in a term are dummy indices, and can be renamed. Therefore all the terms in the fraction above cancel out, and we are left with $\bar{g}^{\lambda\sigma}\bar{g}_{\sigma\nu} = \delta^{\lambda}_{\nu}$, which is the definition of a tensor and its inverse.

C.2 Finding the $i00$ component:

$$\begin{aligned}&\bar{\Gamma}^{i}_{00} \\ =&\Gamma^{i}_{00} + \frac{1}{2}\bar{g}^{i\nu}\left[\nabla_0\bar{g}_{0\nu} + \nabla_0\bar{g}_{0\nu} - \nabla_\nu\bar{g}_{00}\right] \\ =&\Gamma^{i}_{00} + \frac{1}{2}\bar{g}^{i\nu}\left[2g_{0\nu}A_{,0} + 2B\left(\nabla_0\phi_{,0}\phi_{,\nu}\right) + 2\phi_{,0}\phi_{,\nu}B_{,0} - g_{00}A_{,\nu} - B\left(\nabla_\nu\phi_{,0}\phi_{,0}\right) - \phi_{,0}\phi_{,0}B_{,\nu}\right] \\ =&\Gamma^{i}_{00} + \bar{g}^{i0}g_{00}A_{,0} + \frac{1}{2}\bar{g}^{i\nu}\left[-g_{00}A_{,\nu} + 2B\phi_{,\nu}\nabla_0\phi_{,0} + 2\phi_{,0}\phi_{,\nu}B_{,0} - \phi_{,0}\phi_{,0}B_{,\nu}\right].\end{aligned} \tag{C.6}$$

Where in the last step we used the relation $\nabla_0\phi_{,\nu} = \nabla_\nu\phi_{,0}$* to find that

$$\begin{aligned}2\nabla_0\left(\phi_{,0}\phi_{,\nu}\right) - \nabla_\nu\left(\phi_{,0}\phi_{,0}\right) &= 2\phi_{,\nu}\nabla_0\phi_{,0} + 2\phi_{,0}\nabla_0\phi_{,\nu} - 2\phi_{,0}\nabla_\nu\phi_{,0} \\ &= 2\phi_{,\nu}\nabla_0\phi_{,0}.\end{aligned} \tag{C.7}$$

*The relation can be seen from the fact that $\nabla_\mu\nabla_\nu\phi = \nabla_\mu\phi_{,\nu} = \phi_{,\mu\nu} - \Gamma^{\lambda}_{\mu\nu}\phi_{,\lambda}$. Because partial derivatives commute, and because the Christoffel symbols are symmetric in the two lower indices, one finds that $\nabla_\mu\phi_{,\nu} = \phi_{,\nu\mu} - \Gamma^{\lambda}_{\nu\mu}\phi_{,\lambda} = \nabla_\nu\phi_{,\mu}$.

Inserting the first order expressions for the Einstein frame metric, one can write out all six terms of equation (C.6).

The first term is

$$\begin{aligned}\Gamma^i_{00} &= \frac{1}{2}g^{i\nu}\left(g_{\nu 0,0}+g_{\nu 0,0}-g_{00,\nu}\right)\\ &= -\frac{1}{2}g^{ii}g_{00,i}\\ &= \frac{\Psi_{,i}}{a^2}.\end{aligned} \tag{C.8}$$

Here it was used that $\nu = i$ is the only nonzero contribution from $g^{i\nu}$, and therefore it follows that $g_{\nu 0,0} = g_{i0,0} = 0$. This is a common trick that will be applied in the following calculations.

The second term is

$$\begin{aligned}\bar{g}^{i0}g_{00}A_{,0} &= \left(\frac{g^{i0}}{A}g_{00}A_{,0}-\frac{1}{A}\frac{B\phi^{,i}\phi^{,0}}{A-2BX}g_{00}A_{,0}\right)\\ &= \frac{1}{A}\frac{B\phi^{,i}\phi^{,0}A_{,0}}{A-2BX}\left(1+2\Psi\right).\end{aligned} \tag{C.9}$$

The third term is

$$\begin{aligned}-\frac{1}{2}\bar{g}^{i\nu}g_{00}A_{,\nu} &= \frac{1}{2}\left(\frac{g^{i\nu}}{A}A_{,\nu}-\frac{1}{A}\frac{B\phi^{,i}\phi^{,\nu}}{A-2BX}A_{,\nu}\right)\left(1+2\Psi\right)\\ &= \frac{1}{2}\frac{(1+4\Psi)}{a^2A}A_{,i}-\left(1+2\Psi\right)\frac{1}{2A}\frac{BA_{,\nu}\phi^{,\nu}\phi^{,i}}{A-2BX}.\end{aligned} \tag{C.10}$$

The fourth term is

$$\begin{aligned}\frac{1}{2}\bar{g}^{i\nu}2B\phi_{,\nu}\nabla_0\phi_{,0} =& B\left(\frac{g^{i\nu}}{A}-\frac{1}{A}\frac{B\phi^{,i}\phi^{,\nu}}{A-2BX}\right)\left(\phi_{,\nu}\nabla_0\phi_{,0}\right)\\ =& B\left(\frac{(1+2\Psi)}{a^2A}\left(\phi_{,i}\nabla_0\phi_{,0}\right)-\frac{1}{A}\frac{B\phi^{,i}\phi^{,\nu}\phi_{,\nu}\nabla_0\phi_{,0}}{A-2BX}\right)\\ =& \frac{B\left(1+2\Psi\right)}{a^2}\frac{1}{A}\left(1+\frac{2BX}{A-2BX}\right)\left(\phi_{,i}\nabla_0\phi_{,0}\right).\end{aligned} \tag{C.11}$$

Now follows an intermediate step using the definition of the covariant time derivative, resulting in the relation

$$\nabla_0\phi_{,0} = \ddot{\phi}-\frac{1}{a^2}\sum_{j=1,2,3}\Psi_{,j}\phi_{,j}, \tag{C.12}$$

which means that the fourth term can be written

$$\frac{B\left(1+2\Psi\right)}{a^2}\frac{1}{A}\left(1+\frac{2BX}{A-2BX}\right)\phi_{,i}\left(\ddot{\phi}-\frac{1}{a^2}\sum_{j=1,2,3}\Psi_{,j}\phi_{,j}\right). \tag{C.13}$$

The fifth term is

$$\begin{aligned}\frac{1}{2}\bar{g}^{i\nu}2\phi_{,0}\phi_{,\nu}B_{,0} &= \left(\frac{g^{i\nu}}{A}-\frac{1}{A}\frac{B\phi^{,i}\phi^{,\nu}}{A-2BX}\right)\phi_{,0}\phi_{,\nu}B_{,0}\\ &= \left(\frac{\left(1+2\Psi\right)}{a^2A}\phi_{,0}\phi_{,i}B_{,0}+\frac{1}{A}\frac{2Bg^{ii}\phi_{,i}\phi_{,0}XB_{,0}}{A-2BX}\right)\\ &= \frac{\left(1+2\Psi\right)}{a^2}\frac{1}{A}\left(1+\frac{2BX}{A-2BX}\right)\phi_{,0}\phi_{,i}B_{,0}.\end{aligned} \tag{C.14}$$

Finally, the sixth term of $\bar{\Gamma}^i_{00}$ is given by

$$\begin{aligned}-\frac{1}{2}\bar{g}^{i\nu}\phi_{,0}\phi_{,0}B_{,\nu} &= -\frac{1}{2}\left(\frac{g^{i\nu}}{A}-\frac{1}{A}\frac{B\phi^{,i}\phi^{,\nu}}{A-2BX}\right)\phi_{,0}\phi_{,0}B_{,\nu}\\ &= -\frac{1}{2}\frac{\left(1+2\Psi\right)\phi_{,0}\phi_{,0}B_{,i}}{a^2A}+\frac{1}{2A}\frac{B\phi^{,i}\phi^{,\nu}\phi_{,0}\phi_{,0}B_{,\nu}}{A-2BX}.\end{aligned} \tag{C.15}$$

C.2.1 Inserting derivatives of A and B, and lowering the indices.

The expressions for the partial derivatives of A and B are given by

$$A_{,0}=\frac{\partial A}{\partial\phi}\dot{\phi}=2\frac{\phi\dot{\phi}}{M^2}, \tag{C.16}$$

$$A_{,i}=\frac{\partial A}{\partial\phi}\phi_{,i}=2\frac{\phi\phi_{,i}}{M^2}, \tag{C.17}$$

$$B_{,\nu}=\frac{\partial B}{\partial\phi}\phi_{,\nu}=\frac{\beta}{\phi_0}B\phi_{,\nu}. \tag{C.18}$$

All derivatives of physical vectors are covariant, therefore all derivative indices that are not summed over, must be lowered. This is done through the inverse metric, specifically

$$\phi^{,i}=g^{ij}\phi_{,j}=\frac{1}{a^2}\left(1+2\Psi\right)\phi_{,i}, \tag{C.19}$$

$$\phi^{,0}=g^{00}\phi_{,0}=-\left(1-2\Psi\right)\dot{\phi}. \tag{C.20}$$

The final expression for the third term is now

$$-\frac{1}{2}\bar{g}^{i\nu}g_{00}A_{,\nu} = \frac{1}{2}\frac{(1+4\Psi)}{a^2A}A_{,i} - (1+2\Psi)\frac{1}{2A}\frac{BA_{,\nu}\phi^{,\nu}\phi^{,i}}{A-2BX},$$
$$= \frac{1}{a^2}(1+4\Psi)\frac{\phi\phi_{,i}}{M^2}\frac{1}{A}\left(1+\frac{2BX}{A-2BX}\right). \tag{C.21}$$

Moreover, the sixth term is given by

$$-\frac{1}{2}\bar{g}^{i\nu}\phi_{,0}\phi_{,0}B_{,\nu} = -\frac{1}{2}\frac{(1+2\Psi)\,\phi_{,0}\phi_{,0}B_{,i}}{a^2A} + \frac{1}{2A}\frac{B\phi^{,i}\phi^{,\nu}\phi_{,0}\phi_{,0}B_{,\nu}}{A-2BX},$$
$$= -\frac{1}{2a^2}(1+2\Psi)\frac{\beta}{\phi_0}B\phi_{,0}\phi_{,0}\phi_{,i}\frac{1}{A}\left(1+\frac{2BX}{A-2BX}\right). \tag{C.22}$$

It seems that this familiar combination appears in many terms:

$$\frac{B}{A}\left(1+\frac{2BX}{A-2BX}\right) = \frac{B}{A}\left(\frac{A-2BX+2BX}{A-2BX}\right) = \frac{B}{A-2BX} \equiv \gamma^2. \tag{C.23}$$

Combining all the terms and simplifying gives the final expression for $\bar{\Gamma}^i_{00}$:

$$\bar{\Gamma}^i_{00} = \frac{\Psi_{,i}}{a^2} - \frac{2}{a^2A}\frac{\phi\phi_{,i}\dot{\phi}^2}{M^2}\gamma^2(1+2\Psi) + \frac{1}{a^2}(1+4\Psi)\frac{\phi\phi_{,i}}{M^2}\frac{1}{A-2BX}$$
$$+ \frac{(1+2\Psi)}{a^2}\gamma^2\phi_{,i}\left(\ddot{\phi} - \frac{1}{a^2}\sum_{j=1,2,3}\Psi_{,j}\phi_{,j}\right)$$
$$+ \frac{1}{2}\frac{(1+2\Psi)}{a^2}\frac{\beta}{\phi_0}\gamma^2\dot{\phi}^2\phi_{,i}. \tag{C.24}$$

C.3 Finding the $ij0$ component:

$$\begin{aligned}\bar{\Gamma}^i_{j0} =& \Gamma^i_{j0} + \frac{1}{2}\bar{g}^{i\nu}\left[\nabla_j\bar{g}_{0\nu} + \nabla_0\bar{g}_{j\nu} - \nabla_\nu\bar{g}_{j0}\right],\\ =& \Gamma^i_{j0} + \frac{1}{2}\bar{g}^{i\nu}\left[g_{0\nu}A_{,j} + B\phi_{,\nu}\nabla_j\phi_{,0} + B\phi_{,0}\nabla_j\phi_{,\nu} + \phi_{,0}\phi_{,\nu}B_{,j}\right.\\ &+ g_{j\nu}A_{,0} + B\phi_{,\nu}\nabla_0\phi_{,j} + B\phi_{,j}\nabla_0\phi_{,\nu} + \phi_{,j}\phi_{,\nu}B_{,0}\\ &\left.-g_{j0}A_{,\nu} - B\phi_{,0}\nabla_\nu\phi_{,j} - B\phi_{,j}\nabla_\nu\phi_{,0} - \phi_{,j}\phi_{,0}B_{,\nu}\right],\\ =& \Gamma^i_{j0} + \frac{1}{2}\bar{g}^{i\nu}\left[g_{0\nu}A_{,j} + 2B\phi_{,\nu}\nabla_j\phi_{,0} + B'\phi_{,0}\phi_{,\nu}\phi_{,j} + g_{j\nu}A_{,0}\right],\end{aligned} \tag{C.25}$$

where many terms cancelled out. Again, one can write out all five remaining terms, where the first term is simply

$$\Gamma^i_{j0} = \frac{1}{2}g^{i\nu}\left(g_{\nu j,0} + g_{\nu 0,j} - g_{j0,\nu}\right)$$
$$= \frac{1}{2}g^{ii}g_{ij,0}$$
$$= H\delta^i_j. \tag{C.26}$$

The second term is

$$\begin{aligned}\frac{1}{2}\bar{g}^{i\nu}g_{0\nu}A_{,j} &= \frac{1}{2A}\left(\frac{B\phi^{,i}\phi^{,0}}{A-2BX}\right)(1+2\Psi)\,A_{,\phi}\phi_{,j} \\ &= -\gamma^2\frac{1}{a^2}\frac{\phi}{AM^2}\phi_{,i}\phi_{,j}\dot{\phi}\,(1+2\Psi)\,. \end{aligned} \tag{C.27}$$

The third term, using the same logic as for the sixth term of $\bar{\Gamma}^i_{00}$, is

$$\frac{1}{2}\bar{g}^{i\nu}2B\phi_{,\nu}\nabla_j\phi_{,0} = \frac{1}{a^2}\,(1+2\Psi)\,\phi_{,i}\nabla_j\phi_{,0}\gamma^2. \tag{C.28}$$

The fourth term is

$$\frac{1}{2}\bar{g}^{i\nu}B_{,\phi}\phi_{,0}\phi_{,\nu}\phi_{,j} = \frac{1}{2a^2}\,(1+2\Psi)\,\frac{\beta}{\phi_0}\dot{\phi}\phi_{,i}\phi_{,j}\gamma^2. \tag{C.29}$$

Lastly, the fifth term is

$$\begin{aligned}\frac{1}{2}\bar{g}^{i\nu}g_{j\nu}A_{,0} &= \frac{1}{2}\bar{g}^{ij}g_{jj}A_{,\phi}\phi_{,0} \\ &= \frac{1}{2A}\left(\delta^i_j\frac{1}{a^2}\,(1+2\Psi) - \frac{B\phi^{,i}\phi^{,j}}{A-2BX}\right)a^2\,(1-2\Psi)\,A_{,\phi}\phi_{,0} \\ &= \frac{\phi\dot{\phi}}{AM^2}\left(\delta^i_j - \frac{1}{a^2}\gamma^2\phi_{,i}\phi_{,j}\,(1+2\Psi)\right). \end{aligned} \tag{C.30}$$

One can further insert

$$\begin{aligned}\nabla_j\phi_{,0} &= \phi_{,j0} - \Gamma^\nu_{j0}\phi_{,\nu} \\ &= \phi_{,j0} - H\phi_{,j} - \Psi_{,j}\dot{\phi}. \end{aligned} \tag{C.31}$$

This is because $\Gamma^\nu_{j0}\phi_{,\nu} = \Gamma^i_{j0}\phi_{,i} + \Gamma^0_{j0}\phi_{,0}$. We have already found that $\Gamma^i_{j0}\phi_{,i} = H\phi_{,j}$, and can now find Γ^0_{j0}, given by

$$\begin{aligned}\Gamma^0_{j0} &= \frac{1}{2}g^{0\nu}\left(g_{\nu j,0} + g_{\nu 0,j} - g_{j0,\nu}\right), \\ &= \frac{1}{2}g^{00}g_{00,j}, \\ &= (1-2\Psi)\,\Psi_{,j} \approx \Psi_{,j}. \end{aligned} \tag{C.32}$$

When piecing all of this together, one arrives at the expression

$$\begin{aligned}\bar{\Gamma}^i_{j0} =& H\delta^i_j - \gamma^2\frac{1}{a^2}\frac{\phi}{AM^2}\phi_{,i}\phi_{,j}\dot{\phi}\,(1+2\Psi) + \frac{1}{a^2}\,(1+2\Psi)\,\phi_{,i}\left(\phi_{,j0} - H\phi_{,j} - \Psi_{,j}\dot{\phi}\right)\gamma^2 \\ &+ \frac{1}{2a^2}\,(1+2\Psi)\,\frac{\beta}{\phi_0}\dot{\phi}\phi_{,i}\phi_{,j}\gamma^2 + \frac{\phi\dot{\phi}}{AM^2}\left(\delta^i_j - \frac{1}{a^2}\gamma^2\phi_{,i}\phi_{,j}\,(1+2\Psi)\right). \end{aligned} \tag{C.33}$$

Appendix D

Implementation details

The equations introduced in the chapter 2 are readable by humans, but computers do not understand the Einstein summation notation. Additionally, all instances of the Planck mass $M_{\rm Pl}$ must be cancelled by hand before inserting the equations into the code, because this number is far away from $\mathcal{O}(1)$, which would reduce the precision of the calculations drastically. RAMSES uses internal units where $c \neq 1$, thus one must use dimensional analysis to regain these factors.

The conformal factor A is supposed to be dimensionless. From section 2.4.1, this factor is given by

$$A = 1 + \frac{2}{c^2}\zeta\theta^2\chi^2, \tag{D.1}$$

where a factor of c^2 is now inserted because the units of ζ are velocity squared*. The result is a dimensionless A, which can be implemented without problems.

One term used both in the equation of motion for the scalar field and in the geodesics is $-2BX$. Written out this term reads

$$\frac{b_0}{H_0^2 M_{\rm Pl}^2} \exp\left(\beta\chi\right) g^{\mu\nu}\phi_{,\mu}\phi_{,\nu}. \tag{D.2}$$

Using the definition for the dimensionless field,

$$\phi = 2\theta M_{\rm Pl}\zeta\chi, \tag{D.3}$$

one finds that the Planck mass indeed cancels out, and one ends up with (still with $c = 1$)

$$-2BX = 4b_0\left(\frac{\zeta\theta}{H_0}\right)^2 \exp\left(\beta\chi\right) g^{\mu\nu}\chi_{,\mu}\chi_{,\nu}. \tag{D.4}$$

*$\zeta \equiv \frac{3\Omega_0 H_0^2 \lambda_0^2}{a_{\rm SSB}^3}$, where H_0 carries units of inverse time, and λ_0 has units of length. The other symbols are dimensionless, hence $[\zeta] = \left[c^2\right]$.

Deciding that the derivatives $\chi_{,\mu}$ have units of inverse length, $g^{\mu\nu}\chi_{,\mu}\chi_{,\nu}$ can be written out as

$$g^{\mu\nu}\chi_{,\mu}\chi_{,\nu} = -\frac{1}{c^2}\left(1-2\Psi\right)\left(\dot{\chi}\right)^2 + \sum_{i=123}\frac{1}{a^2\left(t\right)}\left(1+2\Psi\right)\left(\chi_{,i}\right)^2, \tag{D.5}$$

$$\approx -\frac{q^2}{a^6c^2} + \frac{1}{a^2\left(t\right)}\sum_{i=123}\left(\chi_{,i}\right)^2. \tag{D.6}$$

The fact that $\dot{\chi} = x'/a^2 = q/a^3$ was utilized, and in the last step it was assumed that $\Psi \ll 1$. Now, since the units of ζ are velocity squared, $1/H_0$ has units of time, and $g^{\mu\nu}\chi_{,\mu}\chi_{,\nu}$ has units of inverse length squared, the correct dimensionless form of $-2BX$ is given by

$$-2BX = \frac{4b_0}{c^2}\left(\frac{\zeta\theta}{H_0}\right)^2\exp\left(\beta\chi\right)\left\{-\frac{q^2}{a^6c^2} + \frac{1}{a^2\left(t\right)}\sum_{i=123}\left(\chi_{,i}\right)^2\right\}. \tag{D.7}$$

The density ρ can be written as

$$\rho = \frac{\rho_{0(z=0)}}{a^3}\eta = \frac{3H_0^2\Omega_0}{a^3}M_{\mathrm{Pl}}^2\eta, \tag{D.8}$$

where η is the density contrast $\eta = \rho/\rho_0$. This means that the factor $\gamma^2\rho$ can be written out without the Planck mass, namely

$$\gamma^2\rho = \frac{b_0\exp\left(\beta\chi\right)}{A-2BX}\cdot\frac{3\Omega_0}{a^3}\eta. \tag{D.9}$$

Here, the Planck mass cancelled because the choice of the dimensionless definition of b_0. Similarly, the factor $\gamma^2M_{\mathrm{Pl}}^2$ that appears in the geodesic equation can be rewritten as

$$\gamma^2M_{\mathrm{Pl}}^2 = \frac{b_0\exp\left(\beta\chi\right)}{H_0^2\left(A-2BX\right)}. \tag{D.10}$$

Some parts of the equation of motion (2.55) can be rewritten. By remembering that q' should have units of inverse time squared, one finds the term in square brackets to be

$$\left[\frac{4\theta^2\zeta}{Ac^2}\chi - \frac{\beta}{2}\right] = \frac{4\theta^2\zeta\chi}{c^2+2\zeta\theta^2\chi^2} - \frac{\beta}{2}. \tag{D.11}$$

Furthermore, inserting the expression (D.8) for ρ, the term with $\rho\chi$ in the equation of motion (2.55) can be written as

$$\frac{1}{A-2BX}\frac{a^5}{2\zeta M_{\mathrm{Pl}}^2}c^2\rho\chi = \frac{1}{A-2BX}\frac{a^5c^2}{2\lambda_0^2}\frac{a_{\mathrm{SSB}}^3}{a^3}\eta\chi. \tag{D.12}$$

This means that the last two terms of the equation of motion for the scalar field (2.55) can be written together, specifically

$$-\frac{1}{A-2BX}\frac{a^5}{2\zeta M_{\mathrm{Pl}}^2}c^2\rho\chi+\left(\chi-\chi^3\right)\frac{c^2a^5}{2\lambda_0^2}=\left(1-\frac{1}{A-2BX}\frac{a_{\mathrm{SSB}}^3}{a^3}\eta-\chi^2\right)\chi\frac{c^2a^5}{2\lambda_0^2}. \tag{D.13}$$

These terms give rise to a symmetron-like behaviour of the effective potential when $b_0 = 0$. Notice the similarity to the symmetron equation of motion used in the paper [39].

Bibliography

[1] A. Einstein. Die Feldgleichungen der Gravitation. *Sitzungsberichte der Königlich Preußischen Akademie der Wissenschaften (Berlin), Seite 844-847.*, pages 844–847, 1915.

[2] A. Einstein. Kosmologische Betrachtungen zur allgemeinen Relativitätstheorie. *Sitzungsberichte der Königlich Preußischen Akademie der Wissenschaften (Berlin), Seite 142-152.*, pages 142–152, 1917.

[3] E. Hubble. A Relation between Distance and Radial Velocity among Extra-Galactic Nebulae. *Proceedings of the National Academy of Science*, 15:168–173, March 1929.

[4] A. G. Lemaître. Contributions to a British Association Discussion on the Evolution of the Universe. *Nature*, 128:704–706, October 1931.

[5] A. A. Penzias and R. W. Wilson. A Measurement of Excess Antenna Temperature at 4080 Mc/s. *ApJ*, 142:419–421, July 1965.

[6] A. G. Riess et al. Observational Evidence from Supernovae for an Accelerating Universe and a Cosmological Constant. *AJ*, 116:1009–1038, September 1998.

[7] S. Perlmutter et al. Measurements of Ω and Λ from 42 High-Redshift Supernovae. *ApJ*, 517:565–586, June 1999.

[8] F. Zwicky. Die Rotverschiebung von extragalaktischen Nebeln. *Helvetica Physica Acta*, 6:110–127, 1933.

[9] Planck Collaboration et al. Planck 2013 results. XVI. Cosmological parameters. *arXiv:1303.5076 [astro-ph.CO]*, March 2013.

[10] M. Tegmark et al. Cosmological constraints from the SDSS luminous red galaxies. *Phys. Rev. D*, 74(12):123507, December 2006.

[11] Planck Collaboration et al. Planck 2013 results. XV. CMB power spectra and likelihood. *A&A*, 571:A15, November 2014.

[12] S. Weinberg. The cosmological constant problem. *Reviews of Modern Physics*, 61:1–23, January 1989.

[13] E. Cremmer, S. Ferrara, C. Kounnas, and D. V. Nanopoulos. Naturally vanishing cosmological constant in N=1 supergravity. *Physics Letters B*, 133:61–66, December 1983.

[14] T. Clifton, P. G. Ferreira, A. Padilla, and C. Skordis. Modified gravity and cosmology. *Phys. Rep.*, 513:1–189, March 2012.

[15] S. Reynaud and M.-T. Jaekel. Tests of general relativity in the Solar System. In E. Arimondo, W. Ertmer, W. P. Schleich, and E. M. Rasel, editors, *Atom Optics and Space Physics*, page 203, 2009.

[16] Austin Joyce, Bhuvnesh Jain, Justin Khoury, and Mark Trodden. Beyond the Cosmological Standard Model. 2014.

[17] V. Springel et al. Simulations of the formation, evolution and clustering of galaxies and quasars. *Nature*, 435:629–636, June 2005.

[18] D. J. Eisenstein et al. SDSS-III: Massive Spectroscopic Surveys of the Distant Universe, the Milky Way, and Extra-Solar Planetary Systems. *AJ*, 142:72, September 2011.

[19] M. Boylan-Kolchin, J. S. Bullock, and M. Kaplinghat. The Milky Way's bright satellites as an apparent failure of ΛCDM. *MNRAS*, 422:1203–1218, May 2012.

[20] B. Moore, S. Ghigna, F. Governato, G. Lake, T. Quinn, J. Stadel, and P. Tozzi. Dark Matter Substructure within Galactic Halos. *ApJ*, 524:L19–L22, October 1999.

[21] A. Del Popolo, J. A. S. Lima, J. C. Fabris, and D. C. Rodrigues. A unified solution to the small scale problems of the ΛCDM model. *J. Cosmology Astropart. Phys.*, 4:21, April 2014.

[22] Nemanja Kaloper. Disformal inflation. *Phys.Lett.*, B583:1–13, 2004.

[23] Tomi S. Koivisto. Disformal quintessence. 2008.

[24] M. Zumalacárregui, T.S. Koivisto, D.F. Mota, and P. Ruiz-Lapuente. Disformal Scalar Fields and the Dark Sector of the Universe. *JCAP*, 1005:038, 2010.

[25] T. S. Koivisto, D. F. Mota, and M. Zumalacárregui. Screening Modifications of Gravity Through Disformally Coupled Fields. *Physical Review Letters*, 109(24):241102, December 2012.

[26] Carsten van de Bruck, Jack Morrice, and Susan Vu. Constraints on Nonconformal Couplings from the Properties of the Cosmic Microwave Background Radiation. *Phys.Rev.Lett.*, 111:161302, 2013.

[27] Philippe Brax, Clare Burrage, Anne-Christine Davis, and Giulia Gubitosi. Cosmological Tests of the Disformal Coupling to Radiation. *JCAP*, 1311:001, 2013.

[28] Dario Bettoni and Stefano Liberati. Disformal invariance of second order scalar-tensor theories: Framing the Horndeski action. *Phys.Rev.*, D88(8):084020, 2013.

[29] J. Neveu, V. Ruhlmann-Kleider, P. Astier, M. BesanÃ§on, A. Conley, et al. First experimental constraints on the disformally coupled Galileon model. *Astron.Astrophys.*, 569:A90, 2014.

[30] Philippe Brax and Clare Burrage. Constraining Disformally Coupled Scalar Fields. *Phys.Rev.*, D90(10):104009, 2014.

[31] Nathalie Deruelle and Josephine Rua. Disformal transformations, veiled General Relativity and Mimetic Gravity. *JCAP*, 1409:002, 2014.

[32] Shinji Tsujikawa. Disformal invariance of cosmological perturbations in a generalized class of Horndeski theories. 2014.

[33] Jeremy Sakstein. Disformal Theories of Gravity: From the Solar System to Cosmology. *JCAP*, 1412(12):012, 2014.

[34] M. Zumalacárregui and J. García-Bellido. Transforming gravity: From derivative couplings to matter to second-order scalar-tensor theories beyond the Horndeski Lagrangian. *Phys. Rev. D*, 89(6):064046, March 2014.

[35] D. Bettoni and M. Zumalacárregui. Shaken, not stirred: kinetic mixing in scalar-tensor theories of gravity. *ArXiv e-prints*, February 2015.

[36] Jeremy Sakstein. Towards Viable Cosmological Models of Disformal Theories of Gravity. *Phys.Rev.*, D91(2):024036, 2015.

[37] Tomi S. Koivisto and Federico R. Urban. Disformal vectors and anisotropies on a warped braneHulluilla on Halvat Huvit. *JCAP*, 1503(03):003, 2015.

[38] C. van de Bruck and J. Morrice. Disformal couplings and the dark sector of the universe. *J. Cosmology Astropart. Phys.*, 4:36, April 2015.

[39] C. Llinares and D. F. Mota. Cosmological simulations of screened modified gravity out of the static approximation: Effects on matter distribution. *Phys. Rev. D*, 89(8):084023, April 2014.

[40] C. Llinares, D. F. Mota, and H. A. Winther. ISIS: a new N-body cosmological code with scalar fields based on RAMSES. Code presentation and application to the shapes of clusters. *A&A*, 562:A78, February 2014.

[41] R. Teyssier. Cosmological hydrodynamics with adaptive mesh refinement. A new high resolution code called RAMSES. *A&A*, 385:337–364, April 2002.

[42] T. Guillet and R. Teyssier. A simple multigrid scheme for solving the Poisson equation with arbitrary domain boundaries. *Journal of Computational Physics*, 230:4756–4771, June 2011.

[43] M. Blanton and the Sloan Digital Sky Survey. Sdss galaxy map, 2013. `http://www.sdss3.org/science/gallery_sdss_pie2.php`.

[44] V. Springel et al. The millennium simulation project, 2005. `http://www.mpa-garching.mpg.de/galform/virgo/millennium/index.shtml`.

[45] S. Dodelson. *Modern cosmology*. 2003.

[46] S. M. Carroll. *Spacetime and geometry. An introduction to general relativity*. 2004.

[47] C. G. Gray. Principle of least action. 4(12):8291, 2009. revision #142580.

[48] H. Weyl. Eine neue Erweiterung der Relativitätstheorie. *Annalen der Physik*, 364:101–133, 1919.

[49] R. Utiyama and B. S. DeWitt. Renormalization of a Classical Gravitational Field Interacting with Quantized Matter Fields. *Journal of Mathematical Physics*, 3:608–618, July 1962.

[50] M. Milgrom. A modification of the Newtonian dynamics as a possible alternative to the hidden mass hypothesis. *ApJ*, 270:365–370, July 1983.

[51] G. W. Angus, B. Famaey, and H. S. Zhao. Can MOND take a bullet? Analytical comparisons of three versions of MOND beyond spherical symmetry. *MNRAS*, 371:138–146, September 2006.

[52] B. Famaey and S. S. McGaugh. Modified Newtonian Dynamics (MOND): Observational Phenomenology and Relativistic Extensions. *Living Reviews in Relativity*, 15:10, September 2012.

[53] A. A. Starobinsky. A new type of isotropic cosmological models without singularity. *Physics Letters B*, 91:99–102, March 1980.

[54] G. W. Horndeski. Second-Order Scalar-Tensor Field Equations in a Four-Dimensional Space. *International Journal of Theoretical Physics*, 10:363–384, September 1974.

[55] P. W. Higgs. Spontaneous Symmetry Breakdown without Massless Bosons. *Physical Review*, 145:1156–1163, May 1966.

[56] S. Chatrchyan et al. Observation of a new boson with mass near 125 GeV in pp collisions at sqrt(s) =7 and 8 TeV. *Journal of High Energy Physics*, 6:81, June 2013.

[57] L. Amendola and S. Tsujikawa. *Dark Energy: Theory and Observations*. 2010.

[58] M. Zumalacárregui, T. S. Koivisto, and D. F. Mota. DBI Galileons in the Einstein frame: Local gravity and cosmology. *Phys. Rev. D*, 87(8):083010, April 2013.

[59] K. Hinterbichler, J. Khoury, A. Levy, and A. Matas. Symmetron cosmology. *Phys. Rev. D*, 84(10):103521, November 2011.

[60] P. Brax, C. van de Bruck, A.-C. Davis, B. Li, B. Schmauch, and D. J. Shaw. Linear growth of structure in the symmetron model. *Phys. Rev. D*, 84(12):123524, December 2011.

[61] A.-C. Davis, B. Li, D. F. Mota, and H. A. Winther. Structure Formation in the Symmetron Model. *ApJ*, 748:61, March 2012.

[62] P. Brax, A.-C. Davis, B. Li, H. A. Winther, and G.-B. Zhao. Systematic simulations of modified gravity: symmetron and dilaton models. *J. Cosmology Astropart. Phys.*, 10:2, October 2012.

[63] C. Llinares and D. F. Mota. Releasing Scalar Fields: Cosmological Simulations of Scalar-Tensor Theories for Gravity Beyond the Static Approximation. *Physical Review Letters*, 110(16):161101, April 2013.

[64] K. Hinterbichler and J. Khoury. Screening Long-Range Forces through Local Symmetry Restoration. *Physical Review Letters*, 104(23):231301, June 2010.

[65] C. Llinares and L. Pogosian. Domain walls coupled to matter: The symmetron example. *Phys. Rev. D*, 90(12):124041, December 2014.

[66] J. A. Pearson. Simulating the symmetron: Domain walls and symmetry-restoring impurities. *Phys. Rev. D*, 90(12):125011, December 2014.

[67] I. Newton and P. Frost. *Newton's Principia: Sections I. II. III.* Macmillan and Company, 1863.

[68] P. Young. Physics 115/242 computational physics lecture notes: The leapfrog method and other "symplectic" algorithms for integrating newton's laws of motion, April 2014. `http://young.physics.ucsc.edu/115/leapfrog.pdf`.

[69] V. Springel. The cosmological simulation code GADGET-2. *MNRAS*, 364:1105–1134, December 2005.

[70] William H. Press, Saul A. Teukolsky, William T. Vetterling, and Brian P. Flannery. *Numerical Recipes in FORTRAN; The Art of Scientific Computing.* Cambridge University Press, New York, NY, USA, 2nd edition, 1993.

[71] V. F. Mukhanov, H. A. Feldman, and R. H. Brandenberger. Theory of cosmological perturbations. *Phys. Rep.*, 215:203–333, June 1992.

[72] A. M. Ghez, S. Salim, N. N. Weinberg, J. R. Lu, T. Do, J. K. Dunn, K. Matthews, M. R. Morris, S. Yelda, E. E. Becklin, T. Kremenek, M. Milosavljevic, and J. Naiman. Measuring Distance and Properties of the Milky Way's Central Supermassive Black Hole with Stellar Orbits. *ApJ*, 689:1044–1062, December 2008.

[73] A. Friedmann. Über die Krümmung des Raumes. *Zeitschrift fur Physik*, 10:377–386, 1922.

[74] H. Martel and P. R. Shapiro. A convenient set of comoving cosmological variables and their application. *MNRAS*, 297:467–485, June 1998.

[75] E. Bertschinger. Multiscale Gaussian Random Fields and Their Application to Cosmological Simulations. *ApJS*, 137:1–20, November 2001.

[76] P. S. Behroozi, R. H. Wechsler, and H.-Y. Wu. The ROCKSTAR Phase-space Temporal Halo Finder and the Velocity Offsets of Cluster Cores. *ApJ*, 762:109, January 2013.

[77] Y. P. Jing. Correcting for the Alias Effect When Measuring the Power Spectrum Using a Fast Fourier Transform. *ApJ*, 620:559–563, February 2005.

[78] Y.-S. Li and S. D. M. White. Masses for the Local Group and the Milky Way. *MNRAS*, 384:1459–1468, March 2008.